The University of Alberta
Printing Department
Edmonton, Alberta

THE UNIVERSITY OF ALBERTA

A QUALITATIVE CONSIDERATION OF THE POST-BUCKLING PROBLEM FOR THE AXIALLY LOADED CIRCULAR CYLINDRICAL SHELL

by

JOSEPH M. CHUDOBIAK

A THESIS

SUBMITTED TO THE FACULTY OF GRADUATE STUDIES

IN PARTIAL FULFILMENT OF THE REQUIREMENTS FOR THE DEGREE

OF DOCTOR OF PHILOSOPHY

DEPARTMENT OF MECHANICAL ENGINEERING

EDMONTON ALBERTA

DATE:.....

UNIVERSITY OF ALBERTA

FACULTY OF GRADUATE STUDIES

The undersigned certify that they have read, and recommend to the Faculty of Graduate Studies for acceptance, a thesis entitled "A QUALITATIVE CONSIDERATION OF THE POST-BUCKLING PROBLEM FOR THE AXIALLY LOADED CIRCULAR CYLINDRICAL SHELL" submitted by JOSEPH M. CHUDOBIAK in partial fulfilment of the requirements for the degree of Doctor of Philosophy.

ABSTRACT

It is the purpose of this study to consider the post-buckling behavior of an axially compressed thin circular cylindrical shell. To this end, a simple model of the post-buckling configuration has been devised. The model required the consideration of three parameters and minimization with respect to two parameters. The model is shown to produce results comparable to current, more elaborate, investigations. As with the current solutions to the problem, the results of the analysis presented in this thesis are strictly qualitative.

ACKNOWLEDGMENTS

The author wishes to thank Dr. J. S. Kennedy for having undertaken the supervision of this thesis. He also gratefully acknowledges the financial support for this research by the National Research Council and by the University of Alberta.

Members of the Mechanical Engineering Shop staff who participated in the investigation were P. Arnold, P. A. Bradbury, R. Marak, and A. Smart.

The drafting in this thesis was done by Gerard de Vries and was of great value to the author. Mr. de Vries freely rendered this service and on numerous occasions curtailed his own research in order to aid the author.

In conclusion, appreciation is expressed to J. W. Craven (Chief Metallurgist, Dominion Foundries and Steel, Limited, Hamilton, Ontario) who kindly provided a quantity of tin plate for the construction of test cylinders.

TABLE OF CONTENTS

LIST OF TABLES

LIST OF FIGURES

LIST OF FIGURES (con't)

LIST OF FIGURES (con't)

NOMENCLATURE

y, x	represent circumferential and axial co-ordinates in Chapter 1, co-ordinates based on the middle surface redefined to represent axial and circumferential co-ordinates in Chapters 2, 3, and 4
z	co-ordinate normal to middle surface
X, Y, Z	basic orthogonal cartesian co-ordinate frame
t	shell thickness
R	middle surface radius of initial cylinder
R_e	radius of edge spiral
R_M	radius of middle spiral
E, ν	Young's modulus and Poisson's ratio
$\sigma R/Et$	nondimensional axial stress (load)
n	number of buckles circumferentially
T_{ij}	macroscopic stress tensor components (membrane)
$M_{\alpha\beta}$	macroscopic stress tensor components (bending)
u, v, w	axial, tangential, and radial components of displacement vector with respect to the undeformed middle surface
e_x, e_y, e_{xy}	middle plane strain components, non tensor definition of e_{xy} in Chapter 1, tensor definition in Chapters 2, 3, and 4
κ_x, κ_y, κ_{xy}	changes of curvature
F	stress function

Donnell (7, 1934) displacement format:

$$w = \frac{t}{\sqrt{[12(1 - \nu^2)]}} \left(W \sin \frac{2\pi x}{L_x} \sin \frac{2\pi y}{L_y} + A \cos \frac{4\pi x}{L_x} \right)$$

L_x axial wave length

L_y circumferential wave length

l_x $L_x/2$

l_y $L_y/2$

μ l_y/l_x

von Kármán and Tsien (8, 1941) displacement format:

$$\frac{w}{R} = \left(f_0 + \frac{f_1}{4}\right) + \frac{f_1}{2}\left(\cos \mu \frac{nx}{R} \cos \frac{ny}{R} + \frac{1}{4} \cos 2\mu \frac{nx}{R} + \frac{1}{4} \cos \frac{2ny}{R}\right) + \frac{f_2}{4}\left(\cos 2\mu \frac{nx}{R} + \cos \frac{2ny}{R}\right)$$

Michielsen (18, 1948) displacement format:

$$\frac{w}{R} = g_0 + g_1 \cos \frac{mx}{R} \cos \frac{ny}{R} + g_2 \left(\cos \frac{2mx}{R} + \cos \frac{2ny}{R}\right)$$

m μn

Kempner (10, 1954) displacement format:

$$w = at \left(\cos \frac{\pi x}{l_x} \cos \frac{\pi y}{l_y} + b \cos \frac{2\pi x}{l_x} + c \cos \frac{2\pi y}{l_y} + d\right)$$

Hoff, Madsen, and Mayers (12, 1966) displacement format:

$$w = \frac{R}{n^2} \sum_i \sum_j A_{ij} \cos i \frac{\pi x}{l_x} \cos j \frac{\pi y}{l_y} \qquad i + j = \text{even}$$

Madsen and Hoff (27, 1965) displacement format:

$$w = \sum_{i=0} A_{i,i} \cos \frac{i\pi x}{l_x} \cos \frac{i\pi y}{l_y} + \sum_{i=1} A_{2i,0} \cos \frac{2i\pi x}{l_x}$$

V potential energy

U_B, U_M bending and membrane elastic energy

U $U_B + U_M$

η	n^2t/R
σ_{ij}	stress tensor components
e	unit axial shortening
ϕ	parameter in equation of spiral
Δ	π/n
B_0	circumferential buckle width (see Fig. 20), $B_0 = 2\pi R/n$
L_0	buckle half length axially (see Fig. 20), $L_0 = BB_0$
B	$1/2\mu$
L	side spiral width, $L = 2R_e\Delta$
c	$R_e = cR$
M	see Fig. 19
N	see Eq. 2.3.2b
$\overline{G}_{01}$, $\overline{G}_{02}$, $\overline{G}_{03}$	base vectors on deformed middle surface
$\overline{G}_1$, $\overline{G}_2$, $\overline{G}_3$	base vectors off deformed middle surface
$G_{\alpha\beta}$, $g_{\alpha\beta}$	final and initial metric tensor components
$\underline{i}$, $\underline{j}$, $\underline{K}$	orthogonal cartesian reference frame base vectors
r	ϕ/Δ
Ψ	middle spiral angle of turning

CHAPTER 1

INTRODUCTION AND DISCUSSION OF THE LITERATURE

1.1 Introduction

This thesis will consider the problem of determining the elastic post-buckling behavior of a thin circular cylindrical shell under axial load, a problem first defined in its present form by von Kármán and Tsien in 1941. It can be shown that the mathematical model of von Kármán and Tsien is governed by two nonlinear partial differential equations, the derivation of which is based on a neglecting of the nonlinear reference to the tangential displacement components in the geometric relations. The desirable procedure in effecting a solution would be to solve these differential equations subject to the imposed boundary conditions and other constraints, but this has not yet proven possible. Von Kármán and Tsien initiated a consideration of the solution through the principle of virtual work. Many investigators have since continued the approach of von Kármán and Tsien, and the essential difference between their work and that of von Kármán and Tsien has been the addition of more parameters. This extension of the number of parameters from the three von Kármán and Tsien used to twenty or more has been made possible through the use of modern electronic computers.

Nearly thirty years have passed since von Kármán and Tsien's basic work, yet it cannot be stated that substantial progress has been made. The post-buckling load has been lowered by successive investigators, but a less often discussed fact is that the theoretical geometrical results deviate considerably from the experimental geometry. The use of additional parameters has by now resulted in a post-buckling load which is less than the experimental result. This would seem to indicate a major theoretical difficulty in the procedures used in present investigations of this problem, for one expects that a prescribed continuous form of buckled shell would be stiffer than the actual buckled shell, and should therefore result in an upper bound to the post-buckling load. Until such time as these problems, the discrepancy between the theoretical and experimental geometry and the theoretical and experimental loads, have been resolved, the theoretical results cannot be said to be a firm foundation for design; rather, the designer must have recourse to experimental data.

Because of the poor agreement between experiment and theory, it was felt that a simpler, less involved, analysis could be found which would at least achieve results comparable to those of the present theory and would, hopefully, yield results closer to the experimental values. To this end, a simple model of the post-buckling configuration has been devised. This model required the consideration of three parameters and minimization with respect to two parameters. The model is shown to produce results comparable to the current, more elaborate, investigations. As with the existing solutions to the problem of post-buckling, the results of the analysis given in this thesis are qualitative and are not suitable for design.

1.2 Discussion of the Literature

Before undertaking a discussion of the literature on the subject of post-buckling, it is useful to examine the experimental observations concerning the post-buckling configuration of a thin circular cylindrical shell under axial load. Some necessary notations are:

σ = axial compressive stress;

R/t = radius to thickness ratio;

E = Young's modulus;

$\sigma R/Et$ = nondimensional axial stress;

n = number of waves in the circumferential direction.

The experimental observations are, in part, as follows:

1) The cylinder buckles from a uniformly compressed small-deflection configuration to a large-deflection state (termed the "post-buckling configuration"). The actual failing stress varies greatly, and is probably dependent upon such factors as initial imperfections and eccentricity of load application. Upon buckling, the load drops greatly to a value termed the "post-buckling load".

2) The large-deflection configuration is composed of diamond-shaped patterns; the diamonds are approximately square, and commonly occur as shown in Figs. 1 and 2.

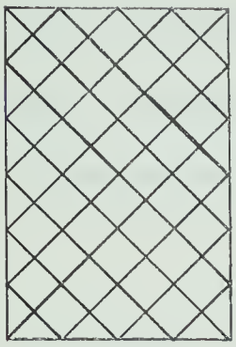

Fig. 1
Ideal Buckle

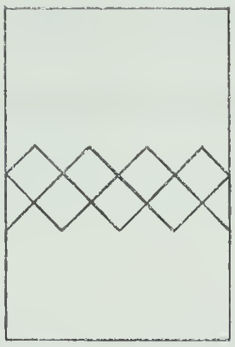

Fig. 2a
Tier Buckle

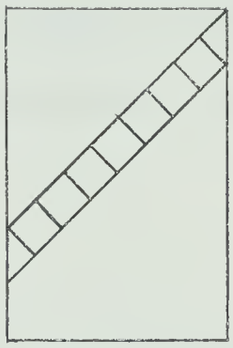

Fig. 2b
Helical Buckle

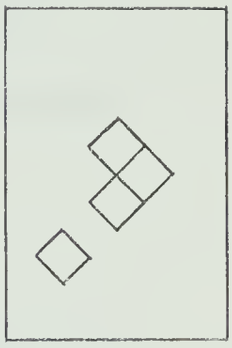

Fig. 2c
Random Buckle

The "Ideal", shown in Fig. 1, seldom occurs in tests but it serves as the simplest mathematical model.

3) Buckling usually occurs over only a part of the shell and is predominantly inwards. Figure 3, which is from de Neufville (1), gives an indication of the buckle size and shows that n increases as R/t increases.

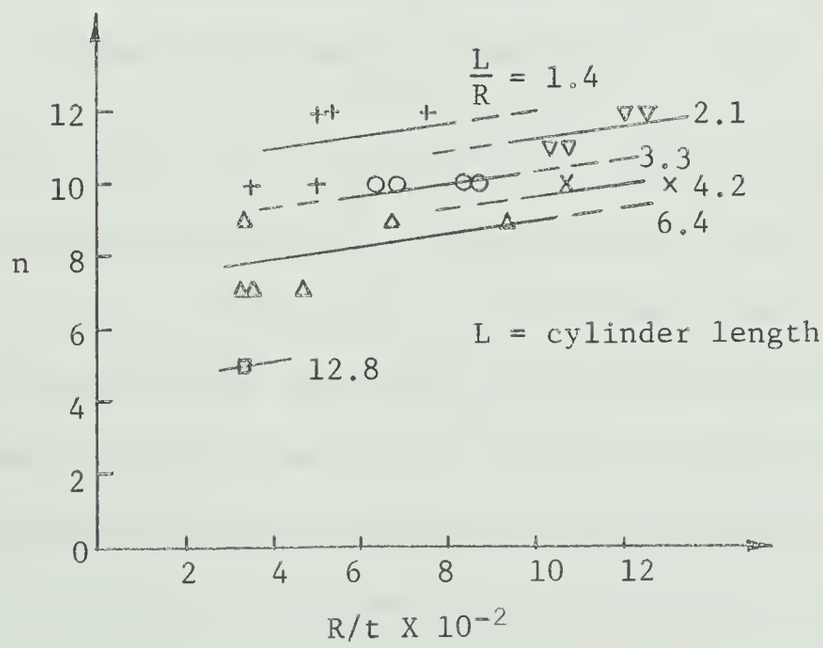

Fig. 3 Variation of n with R/t

4) The nondimensional buckling load depends upon R/t in that it decreases as R/t increases. This fact is illustrated in Fig. 4 taken from Weingarten, Morgan, and Seide (2). The wide scatter of the experimental results is evident.

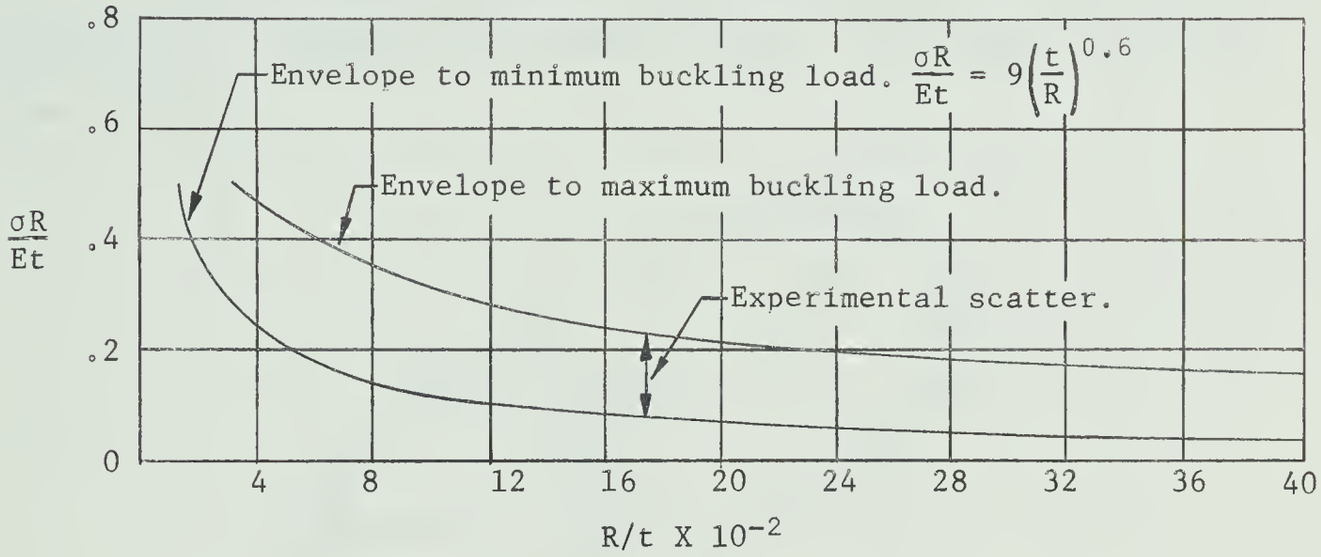

Fig. 4 Variation of Experimental Buckling Load with R/t

5) The post-buckling configuration can be made largely elastic by a suitable combination of material and R/t ratio.

This chapter will now consider in turn the most pertinent theoretical papers dealing with "large-deflection" and "post-buckling" theories of circular cylindrical thin shells under axial load. Only those papers dealing with the static equilibrium behavior, as opposed to the dynamic behavior [see Yao (3), Yao (4), Bieniek, Fan, and Lackman (5), Roth and Klosner (6)], are discussed. The papers reviewed are Donnell (7, 1934), von Kármán and Tsien (8, 1941), Donnell and

Wan (9, 1950), Kempner (10, 1954), Almroth (11, 1963), Hoff, Madsen, and Mayers (12, 1966), Uemura (13, 1963), and Pogorelov (14, 1962). Reference will also be made to the works of Yoshimura (15, 1951), Jones (16, 1966), and Madsen and Hoff (27, 1965).

In reviewing the papers, the co-ordinates and components of displacement of a point on the middle surface of the shell will be as shown in Fig. 5.

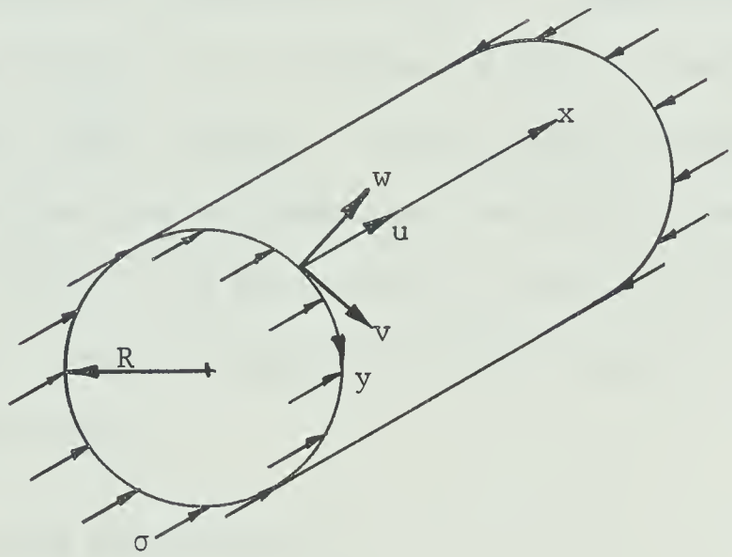

Fig. 5 Co-ordinates and Components of Displacement

Classical buckling theory [see, for instance, Pogorelov (14)] shows that

$$\sigma R/Et \doteq 0.60.$$

The fact that experiments failed to confirm this relationship led to the need to extend the classical theory. The basic extensions to date are those of Donnell (7, 1934), who introduced the application of non-linear large-deflection theory plus the effect of initial imperfections; and of von Kármán and Tsien (8, 1941), who introduced the concept of

a large-deflection post-buckling state. The papers published since 1941 largely differ from these in the extent of mathematical computation.

1.2.1. Donnell (7, 1934)

As previously mentioned, experiments do not confirm the classical buckling load; indeed, experimental failure stresses range from approximately 0.6 to 0.1 of the classical value. The extreme variation of results is indicated in Fig. 4. Donnell attempted to explain this variation by the existence of initial imperfections which increased rapidly under loading. It was assumed that the load-carrying capacity was reduced upon attainment of the yield stress at the most highly stressed point. His procedure is as follows and is included for completeness, since it contains the basic equations of large-deflection shell theory.

Following Donnell, let

w_1 = initial displacement,

w_2 = final displacement,

$w = w_2 - w_1$ = displacement due to load,

and assume that

$$w \propto w_1;$$

so that

$$w_1 = \frac{K - 1}{2} w \quad \text{and} \quad w_2 = \frac{K + 1}{2} w \quad .$$

The unit strains in terms of the displacements are:

$$e_x = \frac{\partial u}{\partial x} + \frac{K}{2}\left(\frac{\partial w}{\partial x}\right)^2 \quad ,$$

$$e_y = \frac{\partial v}{\partial y} - \frac{w}{R} + \frac{K}{2}\left(\frac{\partial w}{\partial y}\right)^2 ,$$

$$e_{xy} = \frac{\partial u}{\partial y} + \frac{\partial v}{\partial x} + K\frac{\partial w}{\partial x}\frac{\partial w}{\partial y} ;$$

and the changes in curvature are:

$$\kappa_x = \frac{\partial^2 w}{\partial x^2} ,$$

$$\kappa_y = \frac{\partial^2 w}{\partial y^2} ,$$

and

$$\kappa_{xy} = \frac{\partial^2 w}{\partial x \partial y} .$$

The nonlinear terms in w lead to the terminology "large-deflection". The absence of nonlinear terms in u and v should be noted.

The stress resultants are defined by:

$$T_x = \frac{Et}{1-\nu^2}\left(e_x + \nu e_y\right) ,$$

$$T_y = \frac{Et}{1-\nu^2}\left(e_y + \nu e_x\right) ,$$

$$T_{xy} = \frac{Et}{2(1+\nu)} e_{xy} ,$$

$$M_x = \frac{Et^3}{12(1-\nu^2)}\left(\kappa_x + \nu\kappa_y\right) ,$$

$$M_y = \frac{Et^3}{12(1-\nu^2)}\left(\kappa_y + \nu\kappa_x\right) ,$$

and

$$M_{xy} = \frac{Et^3}{12(1+\nu)} \kappa_{xy} ;$$

and the transverse shears are defined by the equilibrium equations.

The macroscopic equations of equilibrium (i.e., the equilibrium equations in terms of the macroscopic stress tensors) number six, Donnell assumed that the equations

$$\Sigma F_x = 0 \quad ,$$

and

$$\Sigma F_y = 0 \quad ,$$

could be approximated by

$$\frac{\partial T_x}{\partial x} + \frac{\partial T_{xy}}{\partial y} = 0 \quad ,$$

and

$$\frac{\partial T_{yx}}{\partial x} + \frac{\partial T_y}{\partial y} = 0 \quad .$$

These equations become identities with the introduction of a stress function, F, such that

$$T_x = \frac{Et^2}{d} \frac{\partial^2 F}{\partial y^2} \quad ,$$

$$T_y = \frac{Et^2}{d} \frac{\partial^2 F}{\partial x^2} \quad ,$$

and

$$T_{xy} = -\frac{Et^2}{d} \frac{\partial^2 F}{\partial x \partial y} \quad ;$$

where

$$d = \left(12(1 - \nu^2)\right)^{\frac{1}{2}} \quad .$$

By eliminating u and v from the strain-displacement relations, the following constraint on e_x, e_y and e_{xy} is obtained:

$$\frac{\partial^2 e_x}{\partial y^2} + \frac{\partial^2 e_y}{\partial x^2} - \frac{\partial^2 e_{xy}}{\partial x \partial y} = -\frac{1}{R} \frac{\partial^2 w}{\partial x^2} + K \left[\left(\frac{\partial^2 w}{\partial x \partial y} \right)^2 - \frac{\partial^2 w}{\partial x^2} \frac{\partial^2 w}{\partial y^2} \right] \quad ,$$

which, if one notes that

$$e_x = \frac{t}{d} \left(\frac{\partial^2 F}{\partial y^2} - \nu \frac{\partial^2 F}{\partial x^2} \right) \quad ,$$

$$e_y = \frac{t}{d}\left(\frac{\partial^2 F}{\partial x^2} - \nu \frac{\partial^2 F}{\partial y^2}\right) ,$$

and

$$e_{xy} = -\frac{2(1+\nu)t}{d} \frac{\partial^2 F}{\partial x \partial y} ,$$

becomes

$$\frac{t}{d} \nabla^4 F = \frac{1}{R} \frac{\partial^2 w}{\partial x^2} + K \left[\left(\frac{\partial^2 w}{\partial x \partial y}\right)^2 - \frac{\partial^2 w}{\partial x^2} \frac{\partial^2 w}{\partial y^2}\right] . \quad (1.2.1.1)$$

Donnell assumed w and used this equation to determine F.

For w Donnell assumed

$$w = \frac{t}{d}\left(W \sin \frac{2\pi x}{L_x} \sin \frac{2\pi y}{L_y} + A \cos \frac{4\pi x}{L_x}\right) , \quad (1.2.1.2)$$

where

L_x = axial wave length

and

L_y = circumferential wave length.

The first term in Eq. 1.2.1.2 is the classical solution and the second term is designed to reduce the large deflection stresses. This assumed form of w introduces the four unknowns W, A, L_x, and L_y into the problem.

Returning to Eq. 1.2.1.1, the assumed form of w would indicate that a particular solution for F is of the form

$$F = B \sin \frac{2\pi x}{L_x} \sin \frac{2\pi y}{L_y} + C \cos \frac{4\pi y}{L_y} . \quad (1.2.1.3)$$

Substitution of Eqs. 1.2.1.2, and 1.2.1.3 into Eq. 1.2.1.1 yields

$$B = B(W, A) \quad (1.2.1.4a)$$

and

$$C = C(W, A) \quad . \tag{1.2.1.4b}$$

The complementary solution of Eq. 1.2.1.1 is taken to be

$$F = -\frac{\sigma y^2}{2}$$

which corresponds to a uniform axial compression.

The unknown A is determined from the condition of loading that

$$\oint T_y dy = 0 \quad . \tag{1.2.1.5}$$

To determine W, Donnell employed the virtual work equation

$$\frac{\partial V}{\partial W} = 0 \quad , \tag{1.2.1.6}$$

where the potential energy, V, is defined by

$$V = U - \int_{S_T} T_i U_i dS \quad ,$$

U being the elastic energy, S_T the surface of prescribed loading, T_i the components of prescribed loading, and U_i being the displacement components on S_T.

Equation 1.2.1.6 yields

$$P = \frac{\frac{(X + S)^2}{X} + \frac{X}{(X + S)^2} + KXW(W + W_1)\left(\frac{1}{16} + S^2\right)}{\frac{(W + W_1)}{W} + \frac{K^2 S^2 W}{8}(2W + W_1)} \quad , \tag{1.2.1.7}$$

where

$$X = \frac{4\pi^2}{d}\frac{Rt}{L_x^2} \quad , \qquad S = \frac{4\pi^2}{d}\frac{Rt}{L_y^2} \quad ,$$

and

$$P = \frac{1}{d}\frac{\sigma R}{Et} \quad .$$

Equation 1.2.1.7 yields P in terms of W, W_1, X, and S. It should be noted that the quantity W_1, the amplitude of the initial imperfection, appears in this equation for P because K is a function of W.

This follows from the relation

$$w_1 = \left(\frac{W_1}{W} \right) w = \frac{(K - 1)}{2} w \quad .$$

Now, if σ (i.e., P) is prescribed and X, S, and W_1 are known then Eq. 1.2.1.7 defines W.

However, Donnell wished to include the restriction that yielding occurred at critical points on the cylinder. He employed the von Mises yield criterion for plane stress which is

$$\sigma_x^2 - \sigma_x \sigma_y + \sigma_y^2 + 3\sigma_{xy}^2 = Y^2 \quad .$$

Taking

$$\sigma_x = \frac{T_x}{t} + \frac{12M_x}{t^3} \frac{t}{2} \quad , \qquad \sigma_y = \frac{T_y}{t} + \frac{12M_y}{t^3} \frac{t}{2} \quad ,$$

and

$$\sigma_{xy} = \frac{T_{xy}}{t} + \frac{12M_{xy}}{t^3} \frac{t}{2} \quad ,$$

this yield criterion becomes

$$P_y^2 = P^2 + PKXW^2 \left(0.25 + \frac{3(2 - \nu)S}{d} \right) + 3XSW^2 \left(\frac{X}{(X + S)^2} + \frac{6(1 - \nu)}{d} \right)^2$$
$$+ (KXW)^2 \left(\frac{1}{64} + \frac{3(2 - \nu)S}{8d} + \frac{9(1 - \nu - \nu^2)S^2}{d^2} \right) \quad ; \quad (1.2.1.8)$$

where

$$P_y = \frac{dYR}{Et} \quad .$$

Substitution of the expression for P from Eq. 1.2.1.7 into Eq. 1.2.1.8 leads to an equation for W, and the critical value of P may then be obtained. Donnell assigned L_x, L_y, and W so that his theory approximated his experimental results (the procedure being described in detail in Donnell's paper). Donnell's basic results are contained in Fig. 6a, b, and c.

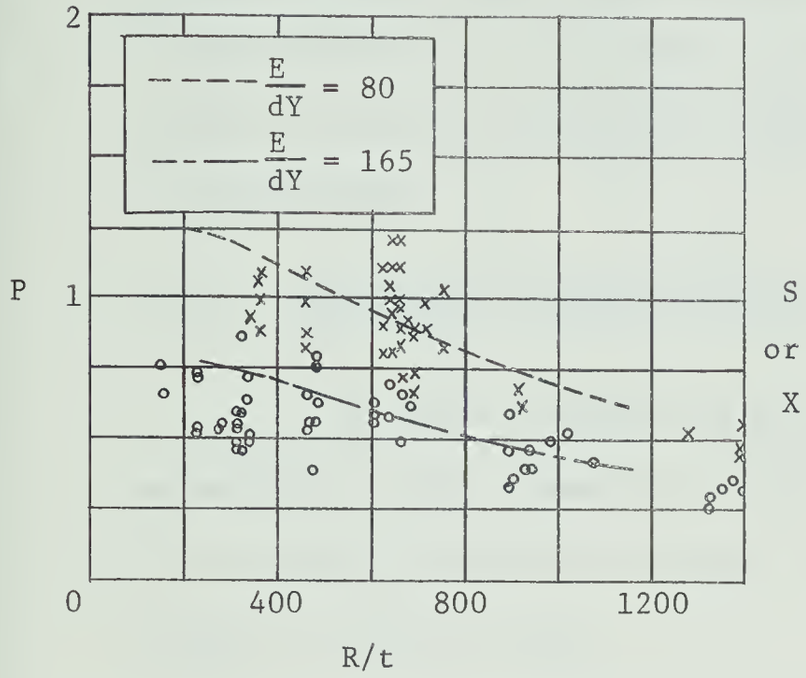

Fig. 6a Theory Approximation to Test Results

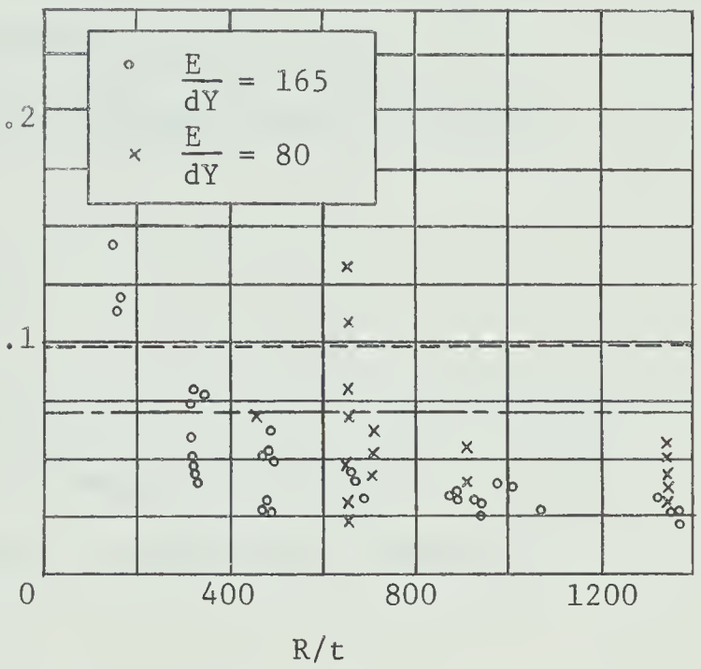

Rig. 6b Values of X and S Assumed in Theory

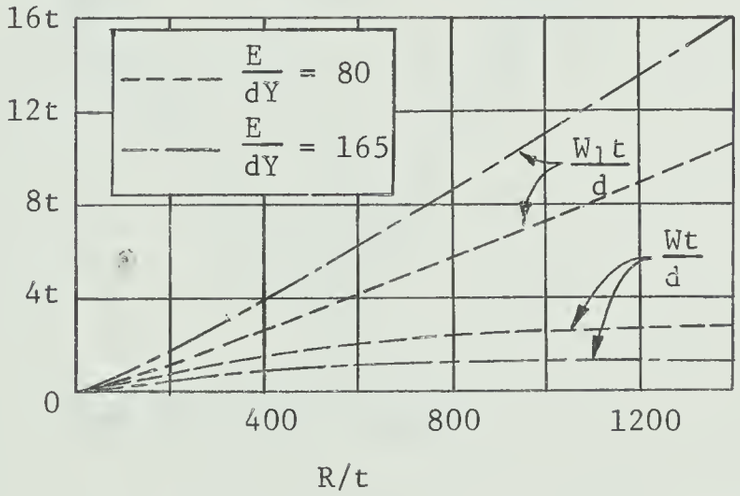

Fig. 6c Values of W_1 Needed to Duplicate Experiments

Donnell did not show that

$$\delta^2 V = 0 \quad ,$$

which would seem to be a necessary condition at the buckling configuration.

Von Kármán (17) noted that the initial amplitudes of Fig. 6c are excessive

and would be easily visible. Experiments indicate that buckling proceeds without these large initial deflections. Von Kármán further noted that in very thin shells, the failure does not appear to be plastic, since the deflections completely disappear when the applied load is removed.

1.2.2. von Kármán and Tsien (8, 1941)

In 1939 von Kármán and Tsien (17), in a study of the stability of spherical shells loaded by external pressure, introduced the concept of the post-buckling load to shell theory. Considering a spherical segment as shown in Fig. 7,

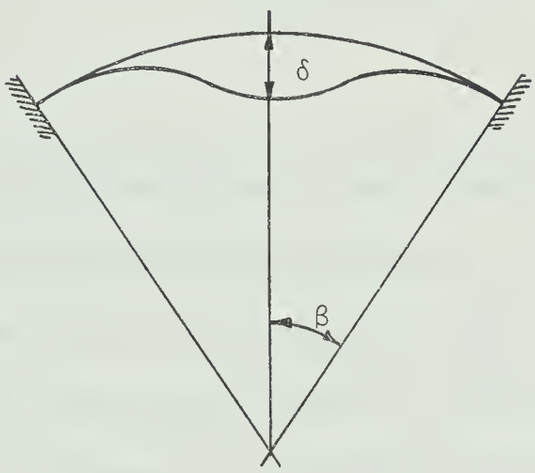

Fig. 7 Spherical Shell Segment

von Kármán and Tsien found, by large-deflection procedures, that load-deflection curves of the nature indicated in Fig. 8 were possible.

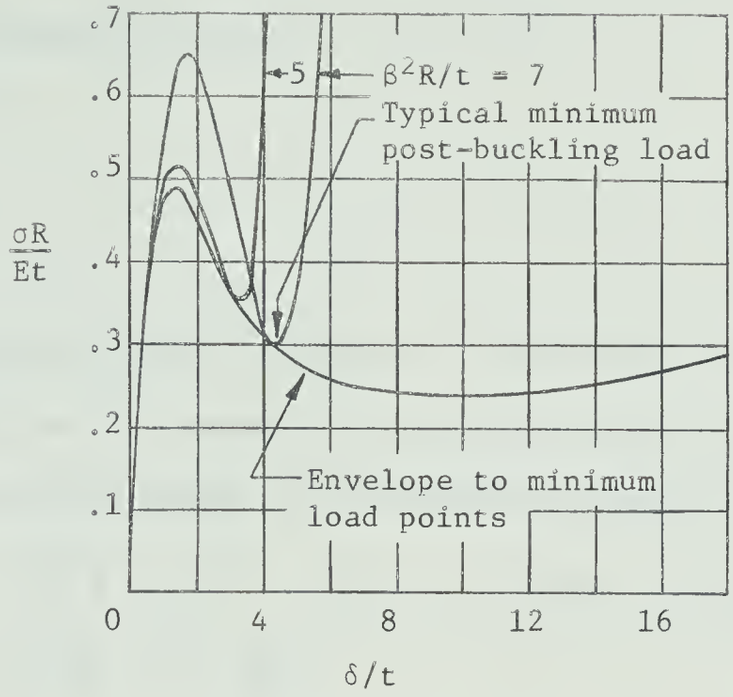

Fig. 8 Illustration of Post-buckling Load

The envelope of the minimum pressures was taken to define the post-buckling pressures under large deflections.

Von Kármán and Tsien, applying Donnell's basic theory of 1934 to cylinders, found that results similar to those of Fig. 8 held for cylinders. There is, however, a significant difference in the spirit in which they applied the equations. Donnell assumed initial imperfections and attempted to find the upper buckling load where

$$\delta V = 0 \quad ,$$

and

$$\delta^2 V = 0 \quad ;$$

although, as previously noted, Donnell did not demonstrate that the second equation was obeyed. Von Kármán and Tsien, however, applied the

theory (with $K = 1$, i.e., no initial imperfections) to find the post-buckling configuration where

$$\delta V = 0 \quad ,$$

and

$$\delta^2 V > 0 \quad .$$

Experiments reveal, as previously discussed, that the post-buckling configuration is composed of large-deflection, diamond-shaped buckles. This was approximated by von Kármán and Tsien as

$$\frac{w}{R} = \left(f_0 + \frac{f_1}{4} \right) + \frac{f_1}{2} \left(\cos \frac{mx}{R} \cos \frac{ny}{R} + \frac{1}{4} \cos \frac{2mx}{R} + \frac{1}{4} \cos \frac{2ny}{R} \right) + \frac{f_2}{4} \left(\cos \frac{2mx}{R} + \cos \frac{2ny}{R} \right) \quad ,$$

where

$$m = \mu n \quad .$$

[For purposes of interpretation it is more convenient to follow Michielsen (18, 1948) and let

$$f_0 + \frac{f_1}{4} = g_0 \qquad f_0 = g_0 - \frac{g_1}{2}$$

$$\frac{f_1}{2} = g_1 \qquad f_1 = 2g_1$$

$$\frac{f_2}{4} + \frac{f_1}{8} = g_2 \qquad f_2 = 4g_2 - g_1$$

which gives

$$\frac{w}{R} = g_0 + g_1 \cos \frac{mx}{R} \cos \frac{ny}{R} + g_2 \left(\cos \frac{2mx}{R} + \cos \frac{2ny}{R} \right) \quad .$$

This is a superposition of

$w_0 = g_0$, a uniform expansion,

$w_1 = g_1 \cos \frac{mx}{R} \cos \frac{ny}{R}$, the classical solution,

and

$$w_2 = g_2 \cos\left(\frac{mx}{R} - \frac{ny}{R}\right)\cos\left(\frac{mx}{R} + \frac{ny}{R}\right) \quad ,$$

which has nodal lines in a helical pattern.]

Substitution of $m = \mu n$ into von Kármán and Tsien's format yields

$$\frac{w}{R} = \left(f_0 + \frac{f_1}{4}\right) + \frac{f_1}{2}\left(\cos\frac{\mu nx}{R}\cos\frac{ny}{R} + \frac{1}{4}\cos\frac{2\mu nx}{R} + \frac{1}{4}\cos\frac{2ny}{R}\right)$$
$$+ \frac{f_2}{4}\left(\cos\frac{2\mu nx}{R} + \cos\frac{2ny}{R}\right) \quad .$$

The quantities n and μ were prescribed by von Kármán and Tsien and the equilibrium equations used were

$$\frac{\partial V}{\partial f_0} = \frac{\partial V}{\partial f_1} = \frac{\partial V}{\partial f_2} = 0 \quad .$$

The equation

$$\frac{\partial V}{\partial f_0} = 0$$

was used with the constraint that v must be periodic, in order to show that the average value of T_y was zero.

The nature of von Kármán's and Tsien's results are given in Figs. 9a, and 9b, where

$$\eta = n^2\frac{t}{R} \quad \text{and} \quad e = \frac{1}{L}\left|\int_0^L \frac{\partial U}{\partial x}\,dx\right| \quad .$$

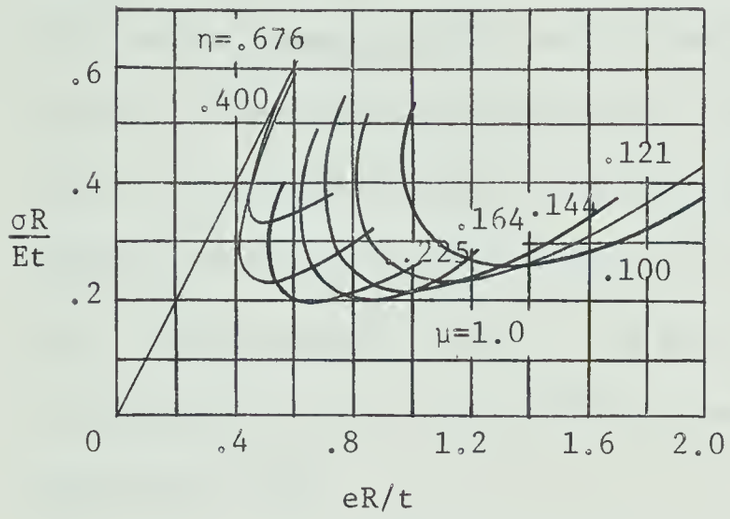

Fig. 9a Post-buckling Curve

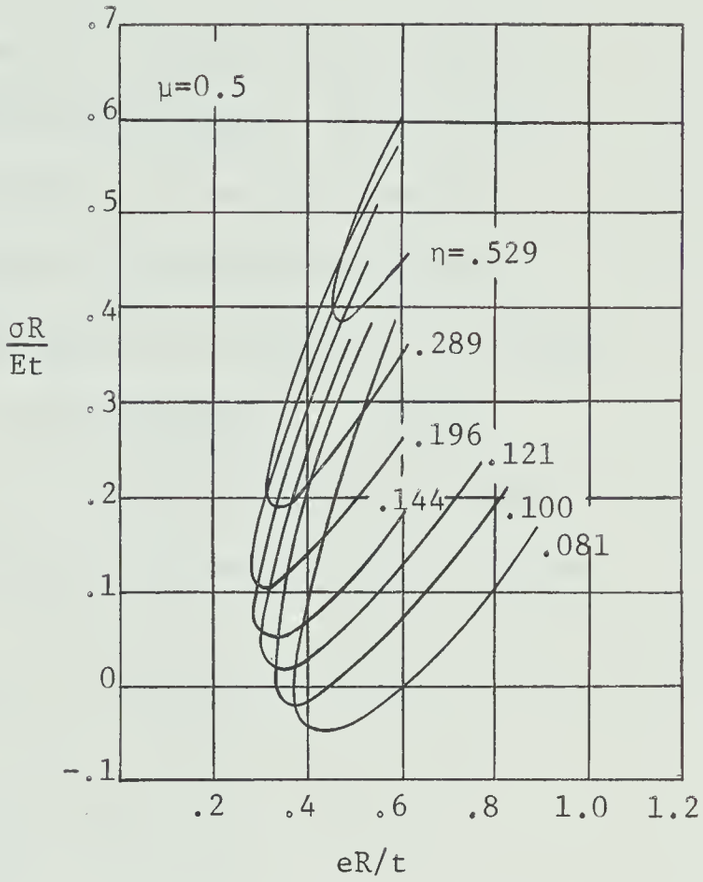

Fig. 9b Post-buckling Curve

It is evident that no minimum is realized for $\mu = 0.5$; however, the results do indicate the possibility of post-buckling states at loads much less than the classical buckling load.

Von Kármán and Tsien stated that the jump from the small-deflection state involves the release of elastic energy and thus explains the rapidity of the buckling process. The results of this thesis, although highly qualitative, indicate that the elastic energy of the large-deflection state is larger than that of the small-deflection state. This statement is based on the assumption that the "Ideal" shape of Fig. 1 is attained.

Figures 9a and 9b, when applied to a specific R/t, indicate that as n and μ vary, the post-buckling load varies. The question then arises concerning the best representation of the post-buckling curve. One method of representation might be to take the envelope to the η = constant curves, derived according to von Kármán's and Tsien's method, but there is still the problem of determining μ. Legget (19, 1946) suggested that for a given μ, the curve could be obtained by equating the areas under two successive n curves [see Fig. 10 from Michielsen (18)],

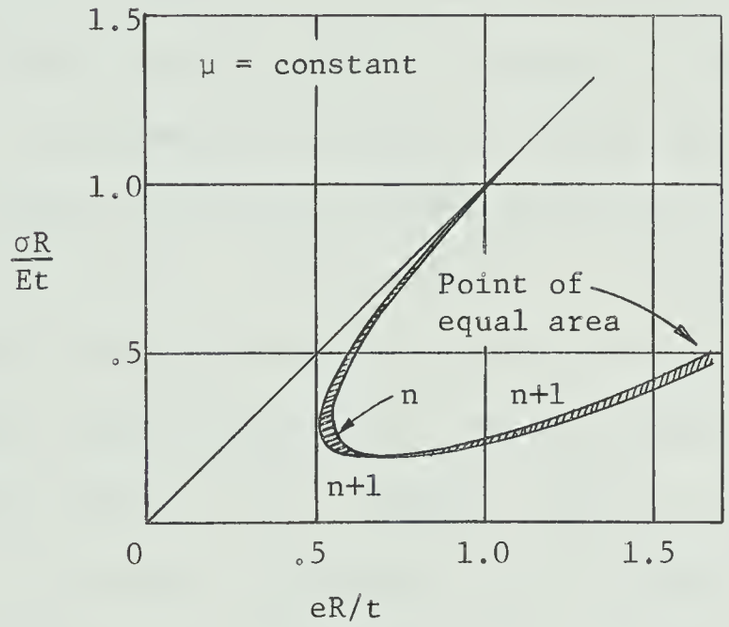

Fig. 10 Calculation of Areas

which, since

$$U = \int \sigma(e)de,$$

corresponds to conservation of elastic energy between the two states.

Michielsen (18, 1948) suggested that n and μ be allowed to change freely and so introduced the equations

$$\frac{\partial V}{\partial n} = \frac{\partial V}{\partial \mu} = 0 \quad .$$

Michielsen stated that his computations agreed with those of Legget and Jones (20, 1942).

Thielemann (21, 1963) has noted that the variation with respect to n is inadmissable since non-integral values of n will violate the constraint that the displacements must be continuous. The same objection logically holds for μ, if the length of the cylinder and the boundary conditions are prescribed. This objection is usually overcome by assuming the cylinder to be infinitely long. It is not at all clear to this author that Thielemann's objection is valid in the light of the fact that the methods of analysis are themselves highly approximate. Experiments would seem to confirm that n achieves preferred values, and one would therefore search for a criterion to determine these values. The variation of n about an integer could be a criterion, and since the discontinuity induced is infinitesimal, it is probably a less serious error than the inherent inaccuracy of the approximate method, and it probably results in a structure less stiff than the real one. Michielsen's (18) findings would tend to confirm this idea. Jones (16, 1966) carried through Thielemann's suggestion (i.e., to prescribe n) in detail. As the criterion to determine n, he used the integral value of n which, for prescribed σ, gave the minimum value of potential. Madson and Hoff (27, 1965) also performed computations which involved prescribing n.

Despite the above objections, the variation of n has been used in many papers. This thesis shall employ the variation of n about an integral value. Indeed, in the one example given by Jones (16),

it appears that his final equilibrium value of $n = 7$ could have been more rapidly computed by simply adding to his equations the equation

$$\frac{\partial V}{\partial n} = 0 \quad ,$$

and taking the nearest integer to the solution.

The above points are carefully and clearly considered by Mushtari and Galimov(39). They point out that the variation of n is permissible if the finite deflection extends over only part of the shell (as is usual in shell experiments); it is then necessary to assume that the part not covered by the assumed finite deflection pattern (termed by Mushtari and Galimov as the zone of edge effect) is small, and that its energy contribution is negligibly small.

1.2.3. Donnell and Wan (9, 1950)

Von Kármán and Tsien (8) studied the post-buckling state of initially perfect cylinders. Donnell and Wan extended these ideas to cylinders with initial imperfections and found that the peak load (not the post-buckling load which occurs at much higher deflections) was reduced from the classical value. Donnell and Wan varied u and n.

Their method is similar to that of Donnell (7), except for the following major changes:

i. The w format is altered to that of von Kármán and Tsien (8).

ii. In line with von Kármán's and Tsien's (17) criticisms of Donnell's 1934 paper, the process was assumed to be elastic, but the computations were checked to determine whether or not the maximum stress had reached the yield stress prior to the attainment of the peak load.

Thus the form of w assumed was

$$w = at \left(\cos \frac{\mu n x}{R} \cos \frac{ny}{R} + b \cos \frac{2\mu n x}{R} + c \cos \frac{2ny}{R} + d \right)$$

with

$$w_1 = \frac{a_1}{a} w \quad .$$

To determine the value of a_1, Donnell and Wan assumed that a reasonable initial shape for a column could be

$$a_1 t = \frac{cl^2}{t} \quad ,$$

which, extended to the two dimensional surface of a plate, would become

$$a_1 = \frac{U}{\pi^2} \frac{l_x l_y}{t^2} \quad ;$$

where $l_x = L_x/2$ and $l_y = L_y/2$. U is termed an "unevenness factor" and π^2 is included to improve the format. The form of a_1 was further altered to account for the fact that the process of rolling a plate into a cylinder should tend to decrease the imperfection amplitude in the y direction; hence a more correct formulation was assumed to be

$$a_1 = \frac{U}{\pi^2} \frac{{l_x}^{1+q} {l_y}^{1-q}}{t^2} \quad ,$$

with

$$0 \leq q \leq 1 \quad .$$

Donnell and Wan assumed $q = 0.5$ and, noting that

$$l_y = 2\pi R/2n$$

and

$$l_x = l_y/\mu \quad ,$$

they reduced a_1 to

$$a_1 = \frac{UR^2}{\mu^{1.5} n^2 t^2} \quad .$$

The equilibrium equations used by Donnell and Wan were

$$\frac{\partial V}{\partial a} = \frac{\partial V}{\partial b} = \frac{\partial V}{\partial c} = \frac{\partial V}{\partial n} = \frac{\partial V}{\partial \mu} = 0 \quad .$$

The parameter d was determined from the periodicity constraint on v. Donnell and Wan were able to solve the equilibrium equations for the range

$$0.75 \leq \sigma/\sigma_{cl} \leq 1 \quad ,$$

and beyond this they kept b, c, and μ constant. The subscript cl denotes the classical value. The major results of Donnell's and Wan's analysis are shown in Fig. 11.

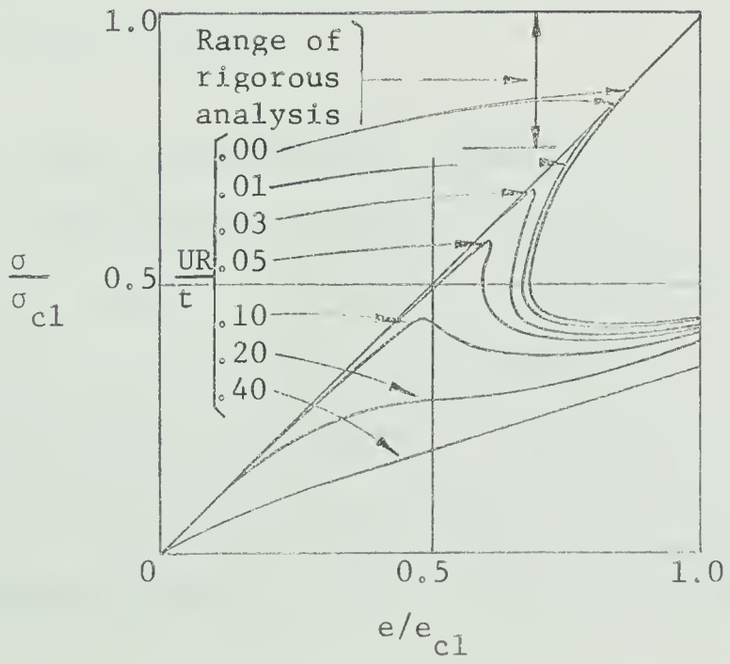

Fig. 11 The Effect of U on Peak Load

As previously mentioned, Donnell and Wan checked their computations to see if the maximum stress had exceeded the yield stress before the applied load reached its peak value. Their conclusions were that the load-carrying capacity could be reduced, due to elastic failure at the peak or by plastic yielding before the peak load is reached. This more complete method of calculation (as opposed to the 1934 paper) gave better values of a_1, as needed to explain the experimental results. Using $U = 0.00015$, it was found, for instance, that at $R/t = 1500$, the value of a_1 was approximately one. Thus these results explain in a reasonable way why σ_{c1} is not usually reached. They do not explain the low value of the experimental post-buckling load. The remaining papers to be discussed have as their main interest the post-buckling load.

1.2.4. Kempner (10, 1954)

It was noted, in the previous discussions, that von Kármán's and Tsien's 1941 work did not produce acceptable minimums in the post-buckling range. They varied only the three parameters d, a, and b = c, while n and μ were assigned.

As previously discussed, Michielsen (18, 1948) extended von Kármán's and Tsien's method to include minimization with respect to n and μ. This procedure resulted in a nondimensional load of 0.195 which occurred at a μ value of approximately 0.4. Legget and Jones (20) performed similar computations. Although Michielsen's result is much less than the classical value, it is still considerably above the experimental minimum of 0.06 as given by von Kármán and Tsien (8).

Kempner's extension consisted of minimizing the potential energy with respect to all five parameters a, b, c, n, and μ; he also determined the stability of the equilibrium states so found. The procedure used to obtain the basic equations differs from that of Donnell and von Kármán; therefore, it will be discussed briefly. Kempner's geometric equations, stress-strain law, and energy expressions were those of Donnell, except that w was taken positive radially inwards. The equilibrium equations were derived by variation of the potential energy and yielded

$$D\nabla^4 w = T_x \frac{\partial^2 w}{\partial x^2} + 2T_{xy} \frac{\partial^2 w}{\partial x \partial y} + T_y \left(\frac{\partial^2 w}{\partial y^2} + \frac{1}{R} \right) , \qquad (1.2.4.1)$$

$$\frac{\partial T_x}{\partial x} + \frac{\partial T_{xy}}{\partial y} = 0 , \qquad (1.2.4.2)$$

and

$$\frac{\partial T_{xy}}{\partial x} + \frac{\partial T_y}{\partial y} = 0 . \qquad (1.2.4.3)$$

Equation 1.2.4.1 is recognized as the plate equation, with a correction of 1/R for the initial curvature. Kempner enforced Eqs. 1.2.4.2 and 1.2.4.3 by defining

$$T_x = \frac{\partial^2 F}{\partial y^2} , \quad T_y = \frac{\partial^2 F}{\partial x^2} , \quad T_{xy} = - \frac{\partial^2 F}{\partial x \partial y} ,$$

and determined F from the compatability equation

$$\nabla^4 F = Et \left[\left(\frac{\partial^2 w}{\partial x \partial y} \right)^2 - \frac{\partial^2 w}{\partial x^2} \left(\frac{\partial^2 w}{\partial y^2} + \frac{1}{R} \right) \right] . \qquad (1.2.4.4)$$

Equations 1.2.4.1 and 1.2.4.4 are the governing partial differential equations for the von Kármán and Tsien mathematical model. As mentioned in the Introduction their analytical solution has not yet been obtained. Indeed because of the neglect of nonlinearity in the geometric equations, it is probable that these equations are not valid for deflections larger

than t and are therefore not applicable to the post-buckling problem. Von Kármán and Tsien (8, 1941) and Donnell and Wan (9, 1950) have made similar comments but this most important fact seems to have been completely overlooked by many investigators and they continue to apply the equations to the post buckling state which involves deflections of $50t$ or more.

The procedure is not sufficiently general to yield the correct equilibrium equations of

$$T^{\alpha\beta}{}_{;\alpha} = 0 \quad , \tag{1.2.4.5}$$

where the lateral shear contribution has been omitted. The semi-colon indicates covariant differentiation with respect to the Lagrangian co-ordinates on the middle surface of the deformed shell. Equation 1.2.4.5 is not so easily forced to be an identity by a stress function. Suppose one generalizes Kempner's solution of

$$T^{\alpha\beta} = e^{\alpha\delta} e^{\beta\gamma} F_{,\delta\gamma}$$

to

$$T^{\alpha\beta} = \varepsilon^{\alpha\delta} \varepsilon^{\beta\gamma} F_{;\delta\gamma} \quad ,$$

where the comma indicates partial differentiation and $e^{\alpha\delta}$ is the permutation symbol, while $\varepsilon^{\alpha\delta}$ is the permutation tensor. Substitution into Eq. 1.2.4.5 yields, for example,

$$F_{;2;2;1} - F_{;2;1;2} =$$
$$(F_{;2})_{;2;1} - (F_{;2})_{;1;2} = (R^{\delta}{}_{221} F_{;\delta}) g \tag{1.2.4.6}$$

where g is the determinant of the middle surface metric tensor coefficients. The right-hand side of Eq. 1.2.4.6 is not, in general, zero. Novozhilov (22) gives an extended discussion detailing when this equation

may be assumed to be sufficiently close to zero in small-deflection theory. Langhaar (23) appears to have found that Eq. 1.2.4.5 becomes an identity for

$$T^{\alpha\beta} = \varepsilon^{\alpha\delta}\,\varepsilon^{\beta\gamma}\,F;_{\delta\gamma} + g^{\alpha\beta}\,G \quad ;$$

where

$$G = \kappa F - \int F d\kappa \quad .$$

The symbol κ represents the Gaussian curvature of the deformed middle surface. This formulation represents considerable complication over Kempner's assumed form. However, Langhaar and Boresi (24) argue that Eq. 1.2.4.5 may readily be replaced by

$$T^{ij}{}_{,i} = 0 \quad ,$$

since the part neglected involves the Christoffel symbols. The Christoffel symbols, being functions of $g_{\alpha\beta}$, must approximate their original zero values if the deformation is largely inextensional.

Kempner obtained his w format by iterating the classical solution in the following manner. Substitute

$$w_1 = a_1 t \left(\cos \frac{\pi x}{1_x} \cos \frac{\pi y}{1_y} + d_1 \right)$$

in Eq. 1.2.4.4 to obtain F_1, then use F_1 and w_1 on the right-hand side (i.e., the nonlinear side) of Eq. 1.2.4.1 to obtain

$$w_2 = at \left(\cos \frac{\pi x}{1_x} \cos \frac{\pi y}{1_y} + b \cos \frac{2\pi x}{1_x} + c \cos \frac{2\pi y}{1_y} + d \right.$$
$$\left. + e \cos \frac{\pi x}{1_x} \cos \frac{3\pi y}{1_y} + g \cos \frac{3\pi x}{1_x} \cos \frac{\pi y}{1_y} \right) \quad . \qquad (1.2.4.7)$$

Kempner did not retain the last two terms; he obtained the final form of F from Eq. 1.2.4.4 and varied the potential energy with respect to

b, c, μ, $\eta = n^2(t/R)$, and $\omega = a\eta$.

While studying the literature, the author compared Kempner's format with the Fourier series expansion of an ideal buckle given by Cox (25) to be

$$w = \frac{4\Psi h}{\pi^2}\left[\sum_m \frac{1}{m^2}\left(\cos m\theta \cos m\phi + \frac{1}{4}(1 - \cos 2m\theta - \cos 2m\phi)\right)\right] ,$$

where

Ψ = inclination of facet to axis of cylinder,

h = axial facet length,

b = half width of facet,

x = axial co-ordinate,

y = circumferential co-ordinate,

$$\theta = \frac{\pi x}{h} = \frac{2\pi R}{2b}\frac{\mu x}{R} = \frac{\mu n x}{R} \quad \text{where} \quad \mu = \frac{b}{h} ,$$

and

n = number of buckles.

Then

$$\sin\Psi \doteq \frac{R(1 - \cos \pi/n)}{h} \doteq \frac{\mu}{2}\frac{\pi}{n} ,$$

so that the coefficient in w becomes

$$\frac{4\Psi h}{\pi^2} \doteq \frac{4}{\pi^2}\frac{\mu\pi}{2n}\frac{b}{\mu} = \frac{2R}{n^2} .$$

This indicates that it would probably be better to normalize Eq. 1.2.4.7 with respect to R/n^2 instead of t. This normalization was first introduced by Yoshimura (15) and more recently by Hoff, Madsen, and Mayers (12, 1966).

Von Kármán and Tsien (8) discussed the two loading methods of prescribed σ and prescribed e (see Fig. 12). Kempner noted that

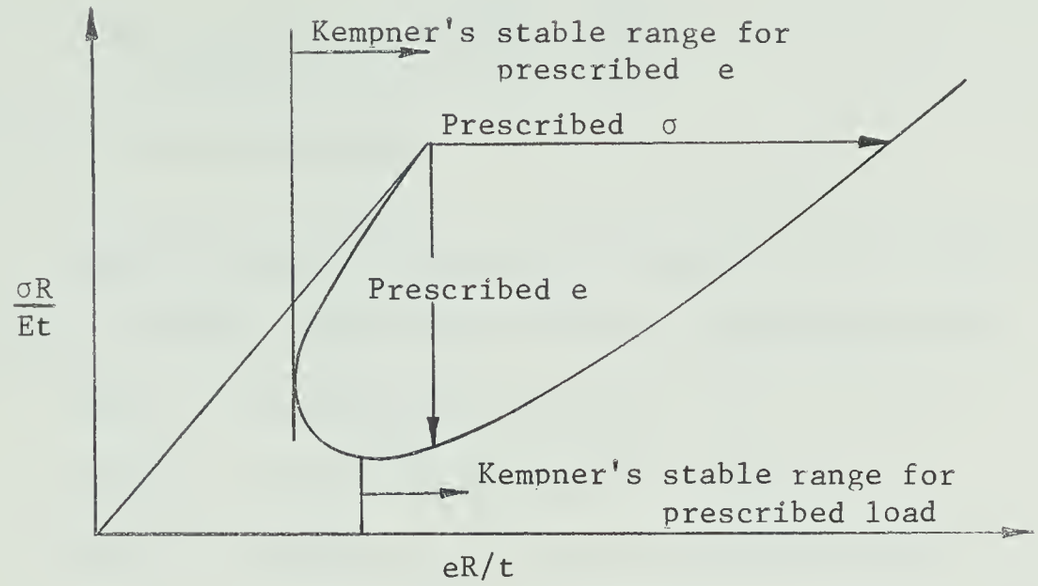

Fig. 12 Loading Methods

the parameters (b, c, μ, η, ω) were the same for the two loading conditions in the post-buckling range, but that the stability of the state depended on the method of loading (see Fig. 12). He obtained a minimum post-buckling load of 0.182 which occurred at $\mu = 0.362$. This minimum is independent of R/t, as have been the previous results. The value of (ad)t was found to be

$$t(ad) = \left(\frac{\omega^2}{8\eta} (1 + 8c^2) - \frac{\nu\sigma R}{Et} \right) t \quad ,$$

a positive quantity which was approximately t at the minimum load. The maximum radial deflection at the mimimum load was 8t.

1.2.5. Almroth (11, 1963)

It can be shown [see Hoff, Madsen, and Mayers (12)] that the "Ideal" shape of Fig. 1 is described in part by the following radial deflection from the middle surface of a circular cylinder:

$$w = \sum_{j=0} \sum_{i=0} A_{ij} \cos \frac{i\pi x}{l_x} \cos \frac{j\pi y}{l_y} \quad ;$$

where $i + j$ is an even number.

Almroth made the advance of considering more terms of the series and of noting their effect. He made computations for:

CASE 1: A_{00}, A_{20}, A_{11}, A_{40}, A_{22}

CASE 2: A_{00}, A_{20}, A_{11}, A_{40}, A_{60}, A_{33}

CASE 3: A_{00}, A_{20}, A_{11}, A_{40}, A_{31}, A_{22}, A_{13}, A_{60}, A_{33} .

By use of the Newton-Raphson method he was able to eliminate the cross-plots, etc., which had been used in previous solutions and thus considered a large number of terms with comparative ease. By letting q_i be the generalized co-ordinates, then for prescribed σ it is required to solve the equilibrium equations

$$\frac{\partial V}{\partial q_i} = 0 \quad .$$

Almroth included the variable n among his generalized co-ordinates. These equations have the approximate solution

$$\left(q_i\right)^{(k+1)} = \left(q_i\right)^{(k)} - \left[\left(\frac{\partial^2 V}{\partial q_i \partial q_j}\right)^{(k)}\right]^{-1} \left(\frac{\partial V}{\partial q_j}\right)^{(k)} \quad ,$$

where k and $k + 1$ denote successive approximations. Almroth's basic results are given in Fig. 13.

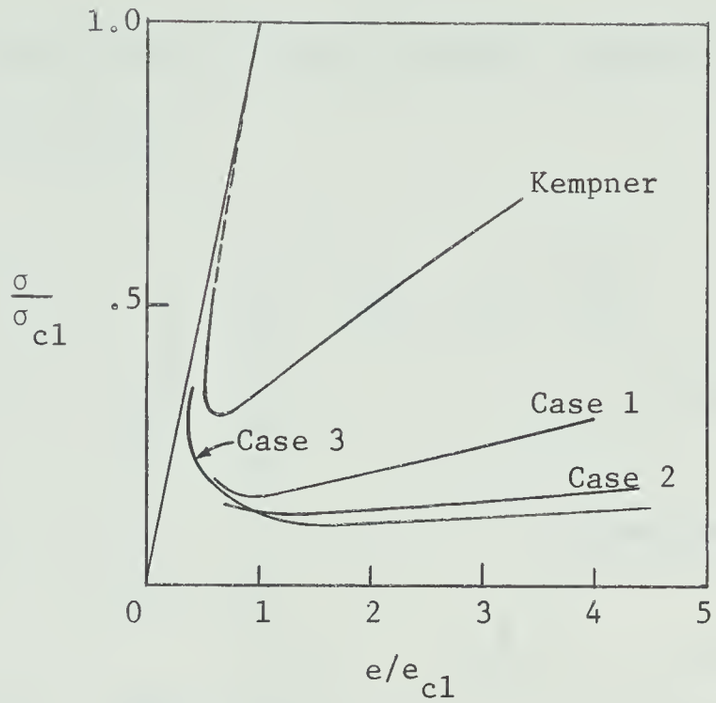

Fig. 13 Almroth's Results

It is interesting to note that Almroth feels that the variation with respect to n may be termed as "definitely reasonable". Almroth obtained the approximate experimental value of 0.06 (for $\sigma R/Et$) and he stated that additional terms did not seem important, but this conclusion was not supported by the results of Hoff, Madsen, and Mayers (12). One notes that the addition of four terms, previously considered unimportant and also neglected because of the intractable computations, has decreased the post-buckling load to one-third of Kempner's value. A comparison of both Kempner's and Almroth's results with Thielemann's (21) experimental results yields excellent correspondence for axial shortening (see Fig. 14).

Again, because of the fact that Almroth varied n and because of the neglect of nonlinear u and v terms [Tsao (26) has shown that retention of these terms in the strain energy introduces an R/t effect]

a single load-deflection curve was obtained. The radial deflection at the minimum load was 50t.

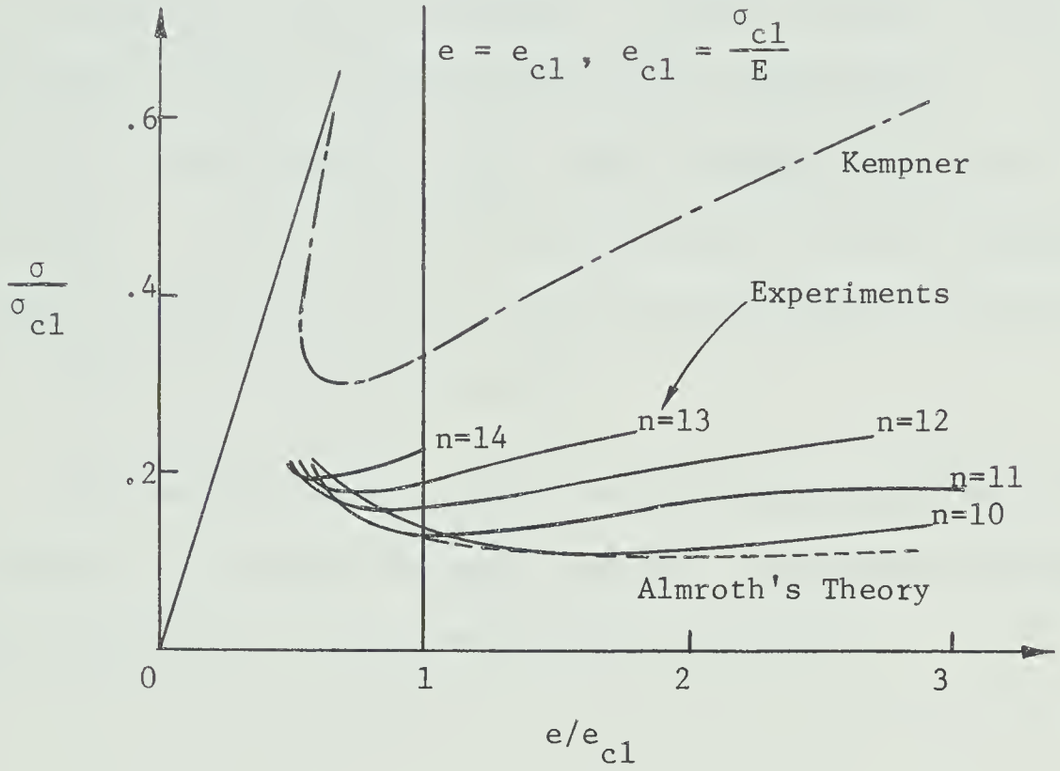

Fig. 14 Thielemann's Experiments versus Theory

1.2.6. Hoff, Madsen, and Mayers (12, 1966)

It was the interest of these authors to test the previously discussed procedures for a larger number of terms. The terms they found most important were A_{00}, A_{11}, A_{02}, A_{20}, A_{22}, A_{13}, A_{31}, A_{33}, A_{40}, A_{44}, A_{55}, A_{60}, A_{66}, A_{80}, A_{100}, A_{120}, μ, and n.

A major change from the previous papers was their use of the format

$$w = \frac{R}{n^2} \sum_i \sum_j A_{ij} \cos \frac{i\pi x}{l_x} \cos \frac{j\pi y}{l_y} \quad ,$$

which agrees with comments made previously concerning Kempner's paper. The significance of this form is that the exact diamond pattern has A_{ij} as a function of i and j alone, and not of l_x and n; so that if the derived shape approximates a diamond pattern, then the A_{ij} values should approach the theoretical values independent of n and l_x. Hoff, et. al., found that the A_{ij} values appeared to converge to the ideal values. It is to be noted that Yoshimura (15) first suggested this form of normalization, and he also commented upon the constancy of the coefficient values so obtained.

The maximum lateral deflection was found to be 236t. Figures 15a, 15b, and 15c contain the major results. The numbers in brackets indicate the number of A_{ij} coefficients considered.

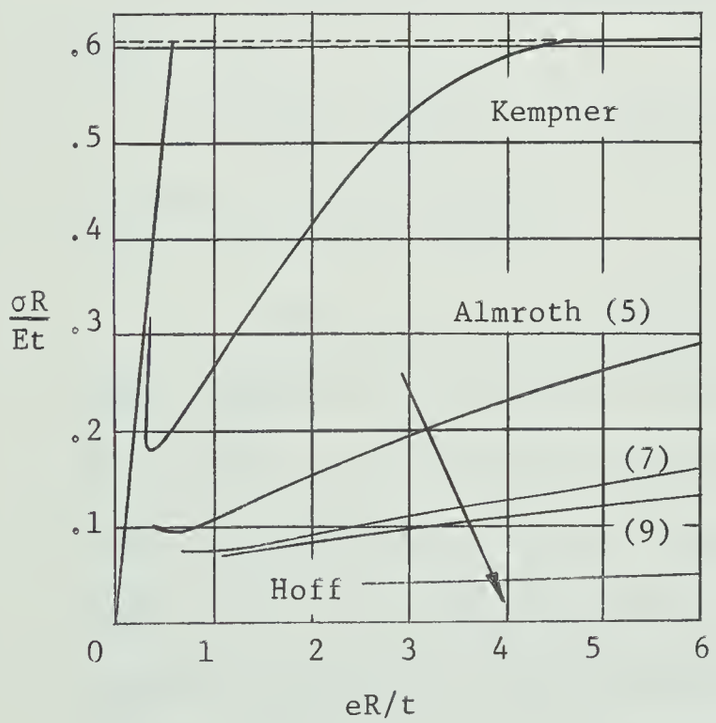

Fig. 15a σR/Et versus eR/t

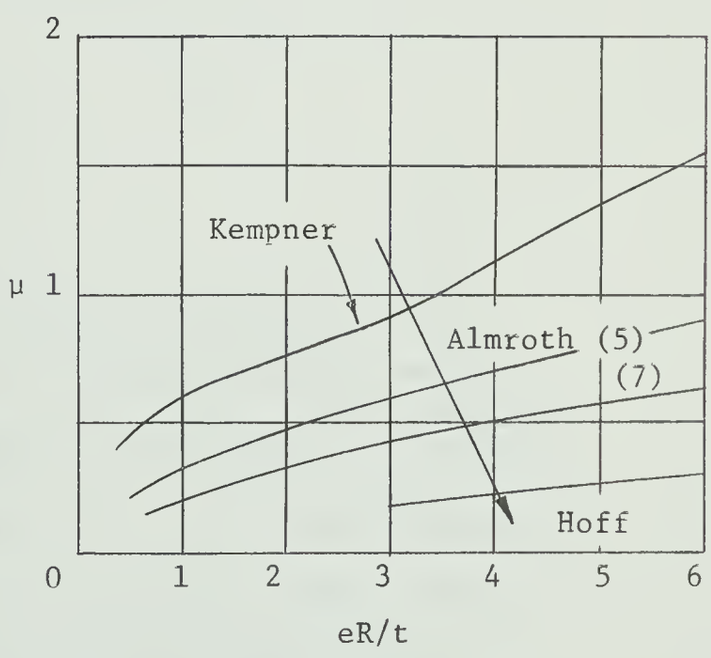

Fig. 15b μ versus eR/t

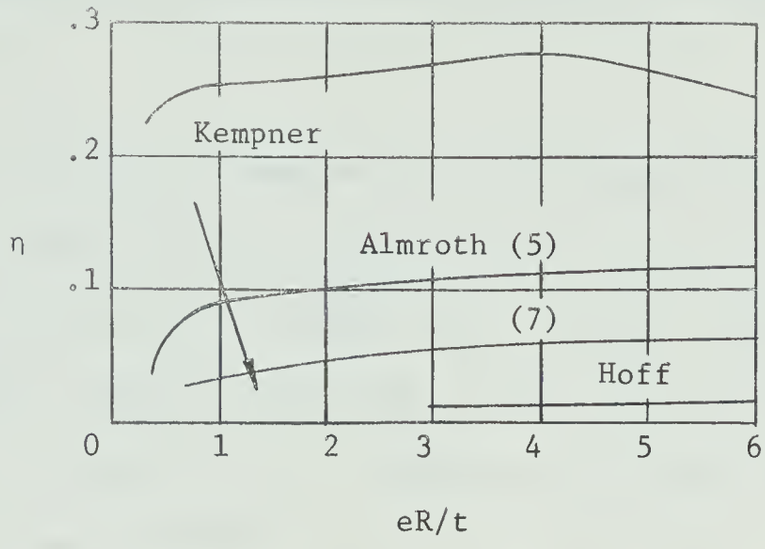

Fig. 15c η versus eR/t

It is clear that as the number of terms retained increases, $\sigma R/Et$, η, and μ all shift downward, as indicated by the arrows. Hoff, et. al., concluded that the use of an infinite number of terms of the series would yield the result of an exact diamond shape for which:

i. $\eta = 0$ and since $n \geq 2$ this implies $t/R = 0$

ii. $\mu = 0$ which implies $n = \infty$

and

iii. $\sigma R/Et = 0$ which implies $\sigma = 0$;

in short, a trivial result.

Since there is no logical objection to using all of the terms (there is, as noted, an objection to minimizing with respect to n and μ), and since the experiments of Thielemann (21) implied that there exists a non-trivial minimum load in the large-deflection state, then the conclusion would seem to be that the method fails. Further discussion on this point shall be reserved until Chapter 4 when the results of work done by Jones (16) and Hoff and Madsen (27)

will be considered and compared with the results of the present work.

Hoff, et. al., commented upon the relative inaccuracy of the present strain tensor for large deflections. Let us consider the example given by them for n equals six. In such a case, Donnell's strain relations, applied to the ideal diamond shape (assuming steel), gives a stress of 300,000 p.s.i. Yoshimura (15) gave a plot of the middle plane stress distribution for $\mu = 0.7$ and $n = 9.4$, which revealed axial tension stresses which were two thirds the magnitude of the axial compressive stresses. Legget and Jones (20, 1942) and Madsen and Hoff (27, 1965) have reported similar stress distributions. One does not expect the axial middle plane stresses to become tensile. It is felt that these results show that the von Kármán-Tsien model is not applicable to the post-buckling problem. That Hoff, et. al., probably did not have axial tension stresses must be attributed to their value of μ, which gives an axial wave length approximately six times that indicated by experiment.

1.2.7. Uemura (13, 1963)

It was previously noted that buckles usually occur over only a portion of the cylinder. Uemura considered a large-deflection approximation to the "Tier" configuration of Fig. 2a, and he made use of an asymptotic unperiodic w displacement function. His procedure, which is involved algebraically and not sufficiently explained with respect to method and approximations, will not be discussed, save to

mention that he eventually minimized with respect to four variables, one of which was n. Uemura found that nearly square, damped buckles could occur at a post-buckling load of approximately $0.5\sigma_{cl}$. The results were dependent upon $\sqrt{Rt}/L$ and so exhibited an L/R effect. The solution did not maintain complete geometric continuity. Yoshimura (15), who presented a qualitative analysis of local buckling, was also unable to maintain geometric continuity in his solution.

1.2.8. Pogorelov (14, 1962)

In a series of papers, Pogorelov considered thin-shell buckling based upon a neglecting of the membrane energy. The buckled form considered was approximately isometric to a cylinder and was constructed by way of a mapping procedure through a $2n$ regular prism. The term "approximate" is used because, like Yoshimura (15) and Uemura (13), Pogorelov was unable to maintain complete geometric continuity. Pogorelov's arguments are largely geometric in nature and are strictly qualitative.

Pogorelov assumed that the post-buckling wave was square (i.e., $\mu = 1$) and that n was determined from the solution for the minimum classical neutral load under the boundary conditions:

i. $w = 0$,

ii. $M_{xx} = 0$,

iii. $v = 0$,

and

iv. buckling occurs under constant load.

Under the assumption of a square wave, the classical relation between μ and n gives

$$n(t/R)^{\frac{1}{2}} \doteq 0.9 \quad .$$

Thus n and μ were assumed by Pogorelov to be established before the post-buckling era. By way of contrast, this study will use n and μ as the fundamental unknowns and the results indicate that, if one wishes to determine a stable post-buckling configuration, there is good reason to assume n to be initially established.

Pogorelov's analysis was based on the assumption that the undeformed cylinder was the virgin state of the material, and covered three distinct stages:

1. Classical analysis: The classical analysis determined n under the assumption of a square buckle pattern.

2. Unstable post-buckling era: Using $\mu = 1$, Pogorelov found

$$\sigma R/Et = 0.138 \quad ,$$

but the solution was unstable.

3. Stable post-buckling era: Using $\mu > 0.91$ (the exact value of μ was not determined), Pogorelov obtained

$$\sigma R/Et = 0.15 \quad .$$

Since the classical n exceeds the experimental, a better value of n might possibly be found from alternate solutions to the neutral equilibrium equations [see Ohira (28), Hoff (29), Hoff and Rehfield (30)]. However, the highspeed photographic experiments of Almroth, Holmes, and Brush (31) have shown that the number of initial buckles decreases

by half when the stable state is reached, therefore indicating that the classical n does not apply to the post-buckling problem.

It is clear that Pogorelov's procedure differs radically from that of the previously discussed works; indeed, this author has not read a major American work which even referenced his contributions. Pogorelov's work is of interest to this author because Pogorelov's methods are comparable to his own and are, from the outset, designed as qualitative approaches.

1.2.9. Closure to the Literature Discussion

Thielemann (32, 1960), in a survey of thin-cylinder buckling, suggested that further advances could possibly consist of the following:

a more accurate analysis of initial imperfections with a view to reducing the upper critical load;

the use of a w function involving more terms and a determination of the most important terms;

and the use of asymptotic unperiodic displacement functions to cover local buckling.

Hoff, et. al., (12, 1966) considered the use of a more complete w function in detail and Uemura has initiated a study of the use of asymptotic unperiodic displacement functions. The results of Hoff, et. al., are most surprising and indicate that the current procedures lead to a trivial result. The author is not aware of an initial imperfection analysis, using large-deflection theory, which differs significantly from that of Donnell and Wan (9). The upper

critical load has received much consideration by means of the neutral equilibrium approach. If these equations are solved subject to the boundary conditions

$$u = 0, \quad v = 0, \quad M_{xx} = 0,$$

and if the buckling is assumed to occur under constant load, then σ_{cl} is obtained. Hoff (29), Hoff and Rehfield (30), and Ohira (28), have shown that enforcing other reasonable boundary conditions leads to approximately a fifty percent reduction in the neutral load. If one notes that the neutral partial differential equations are linear, and that the post-buckling total deflection equations are highly nonlinear, then it would seem that the more accurate solution of the linear system is the easier task. From a structural point of view the non-linear analysis would seem to be the most desirable. Mathematically and physically both problems are of interest.

In conclusion, the preceding discussion of the literature has made evident the following:

1. A comparison of the theoretical results with experimental evidence has shown that the theoretical solutions must be judged as qualitative and not quantitative as some authors imply.

2. Despite the passage of nearly thirty years since the problem was first defined by von Kármán and Tsien, there is still no generally accepted method by which to define the values of μ and n.

3. The ability of the von Kármán-Tsien model to represent the large-deflection post-buckling state is to be questioned. Von Kármán and Tsien (8, 1941) and Donnell and Wan (9, 1950) have pointed

this out, yet many authors continue to apply the model without, it seems, sufficient justification.

4. The works of Legget and Jones (20, 1942), Yoshimura (15, 1951), and of Madsen and Hoff (27, 1965) have shown that the von Kármán-Tsien model may yield tensile values of T_{xx}. One does not expect tensile values of T_{xx}. This indicates the need to include the T_{xx} distribution in published reports (as well as the value of $\sigma R/Et$) in order that the solution may be properly assessed.

5. The use of modern computation techniques has allowed the consideration of many variables; however, the conclusions reached cannot be regarded as final.

1.2.10. Purpose of the Thesis

It is the purpose of this study to further consider the post-buckling behavior of an axially compressed thin circular cylindrical shell. For reasons to be explained, the analysis will largely neglect the middle plane deformation and will consist of "patching" the deformed surface together as suggested by Kennedy (33). In his treatment of the middle plane deformation, the author of this thesis recognized the difficulty of obtaining a large deflection mapping which would map the middle surface almost inextensionally; thus it was the aim of his procedure to take note of whether or not the μ value so obtained would be closer to the experimental results than is the μ value of Hoff, et. al., (12).

The w deflection function of Hoff, et. al., (12) will not be assumed; rather, the large deflection form will be approximated by zones of bending (described in closed form as spiral curves), plus a flat portion. The undeformed cylinder will be assumed to be developed from a flat plate. It seemed desirable to express the bending zone in closed form with the hope that the number of parameters could be reduced and the analysis simplified. Unfortunately, it was not possible to maintain complete geometric continuity and this probably resulted in a less stiff structure. As mentioned in the Introduction, the model presented employed three parameters and yielded results comparable to present theory.

CHAPTER 2

GEOMETRY OF THE LARGE DEFLECTION MODEL

It is the purpose of this chapter to establish an approximate large deflection geometry for the post-buckling configuration of a thin circular cylindrical shell under axial load.

The entire cylinder is assumed to have buckled into a periodic diamond pattern and no end effect is considered. The unbuckled shell will be assumed to be developed from a flat plate. Bending will be considered to be the primary mode of deformation; the zones of bending are indicated below in the diagram of the ideal buckle pattern (see Fig. 16). A typical cross section is shown in Fig. 17.

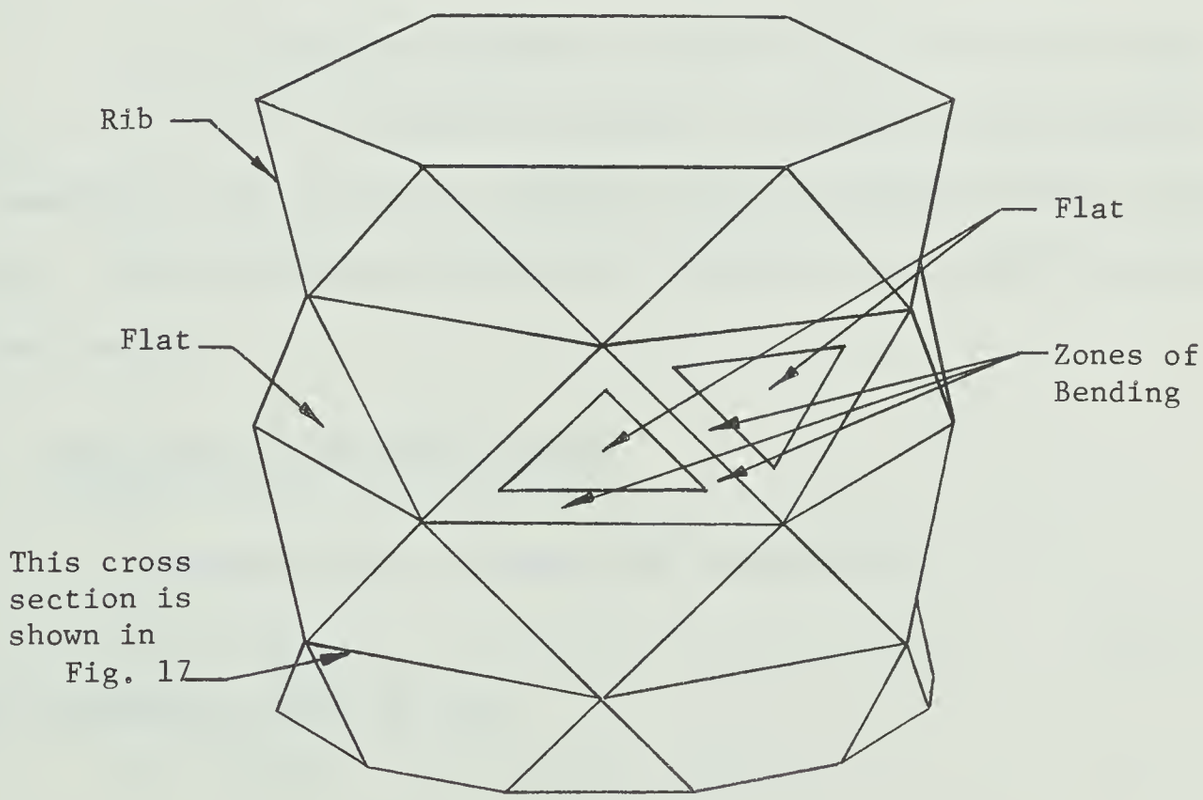

Fig. 16 Idealized Shape

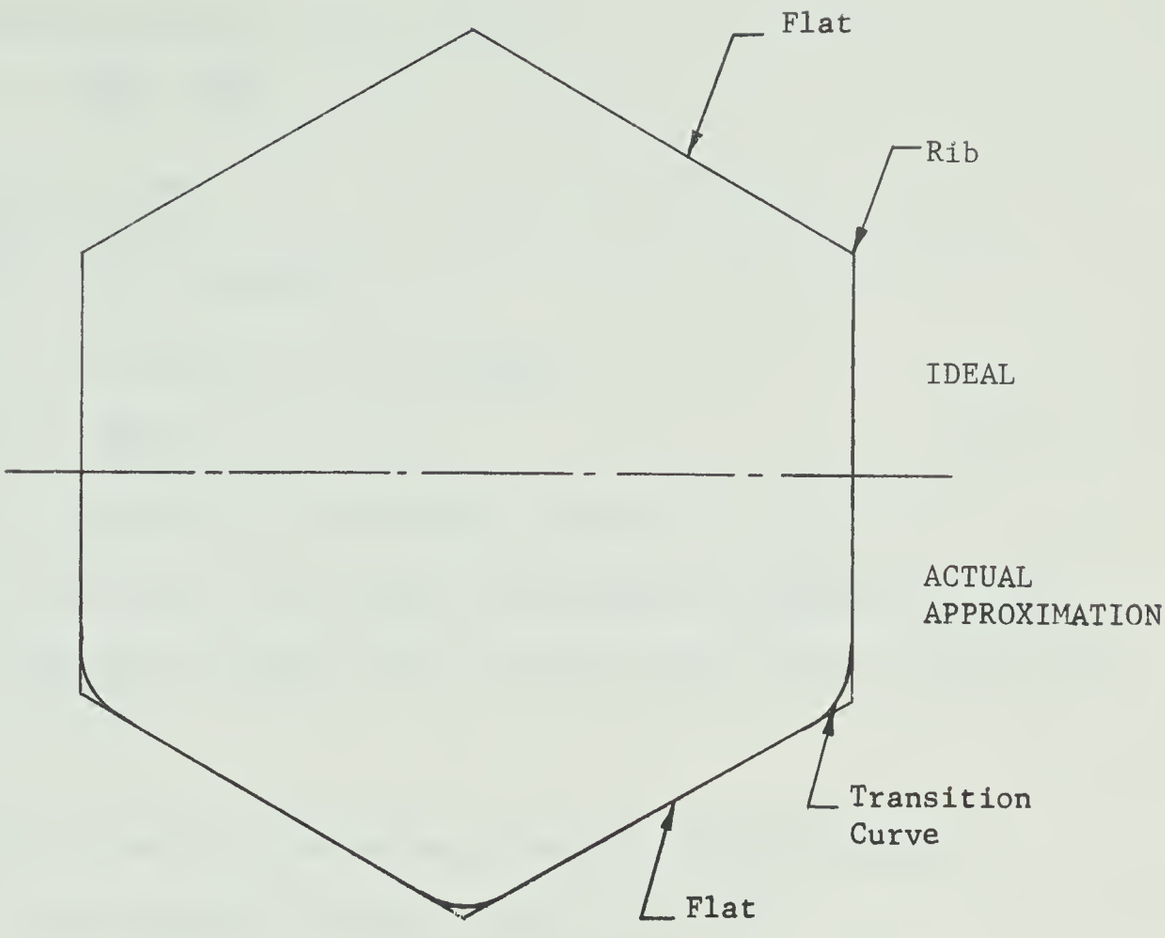

Fig. 17 Cross Section of Fig. 16

It is clear that the ideal portion of Fig. 17 is valid only if $t = 0$ (i.e., no bending stiffness); in the actual approximation a transition curve of finite curvature must be provided between adjacent flats. In the following analysis, the transition curve will be assumed to be a spiral.

2.1. Discussion of the Spiral Curve

The spiral curve possesses the property that

$$r1 = RL \quad . \tag{2.1.1}$$

With reference to Fig. 18, let

$$l = f(\phi) \quad .$$

The differential equation of the curve is

$$r = \frac{dl}{d\phi} = \frac{RL}{l} \quad ,$$

and integration yields

$$\frac{l^2}{2} = RL\phi + \text{constant} \quad ,$$

which, if $l = 0$ when $\phi = 0$, becomes

$$l^2 = 2RL\phi \quad . \tag{2.1.2}$$

From Eqs. 2.1.2 and 2.1.1 it is evident that at $\phi = 0$, $r = \infty$ and that at $\phi = \Delta$, $r = R$; hence, the spiral is useful as a transition curve between a straight line (the flat) and a curve of prescribed radius (at the rib).

The cartesian co-ordinates, expressed parametrically in terms of ϕ, are obtained as follows. From Eq. 2.1.2

$$dl = \frac{A\phi^{-\frac{1}{2}}}{2} d\phi \quad , \tag{2.1.3}$$

where

$$A = (2RL)^{\frac{1}{2}} = 2R\Delta^{\frac{1}{2}} \quad . \tag{2.1.4}$$

Since

$$\frac{dx}{dl} = \cos\phi \quad , \quad \text{and} \quad \frac{dy}{dl} = \sin\phi \quad ,$$

then

$$dx = \frac{A\phi^{-\frac{1}{2}}}{2} \cos\phi d\phi \quad , \quad \text{and} \quad dy = \frac{A\phi^{-\frac{1}{2}}}{2} \sin\phi d\phi \quad .$$

When the sine and cosine functions are replaced by their Taylor's series expansion about $\phi = 0$ and the resulting expressions are integrated, the x and y co-ordinates are found to be

$$x = A\phi^{\frac{1}{2}} \left(1 - \frac{\phi^2}{5.2!} + \frac{\phi^4}{9.4!} - \frac{\phi^6}{13.6!} + \ldots \right) \quad , \tag{2.1.5a}$$

and

$$y = A\phi^{\frac{1}{2}}\left(\frac{\phi}{3} - \frac{\phi^3}{7.3!} + \frac{\phi^5}{11.5!} - \frac{\phi^7}{15.7!} + \ldots \right) \quad . \qquad (2.1.5b)$$

The distance to any point on the curve from the origin is given by

$$l = A\phi^{\frac{1}{2}} \quad , \qquad (2.1.6)$$

and the total length of the spiral is

$$L = 2R\Delta \quad .$$

The angle Δ, as shown in Fig. 18, represents the total angle of turning of the curve.

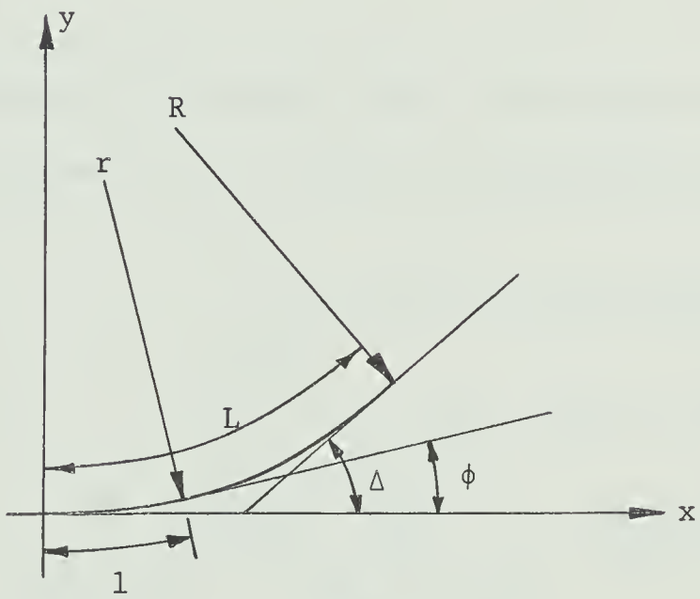

Fig. 18 Notation for the Spiral Curve

2.2. General Procedure to be Followed in Developing the Mapping Functions

Figure 19 explains some necessary geometry. The diamond pattern is to be mapped onto the space frame as shown in Fig. 19,

where R equals the initial cylinder radius and MR equals the rib radius.

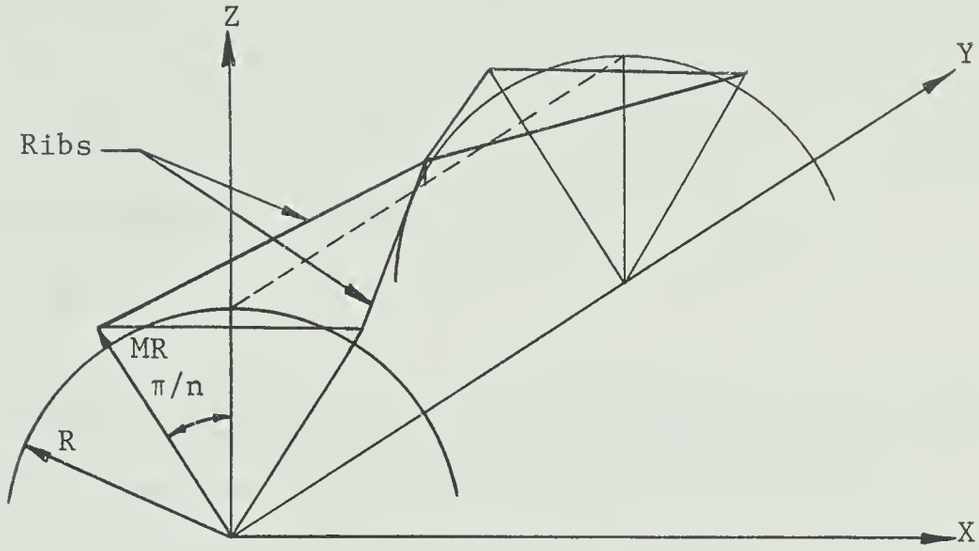

Fig. 19 Space Frame

A typical diamond of the buckled shell will appear as shown in Fig. 20. Figure 20 serves to define some of the necessary notation.

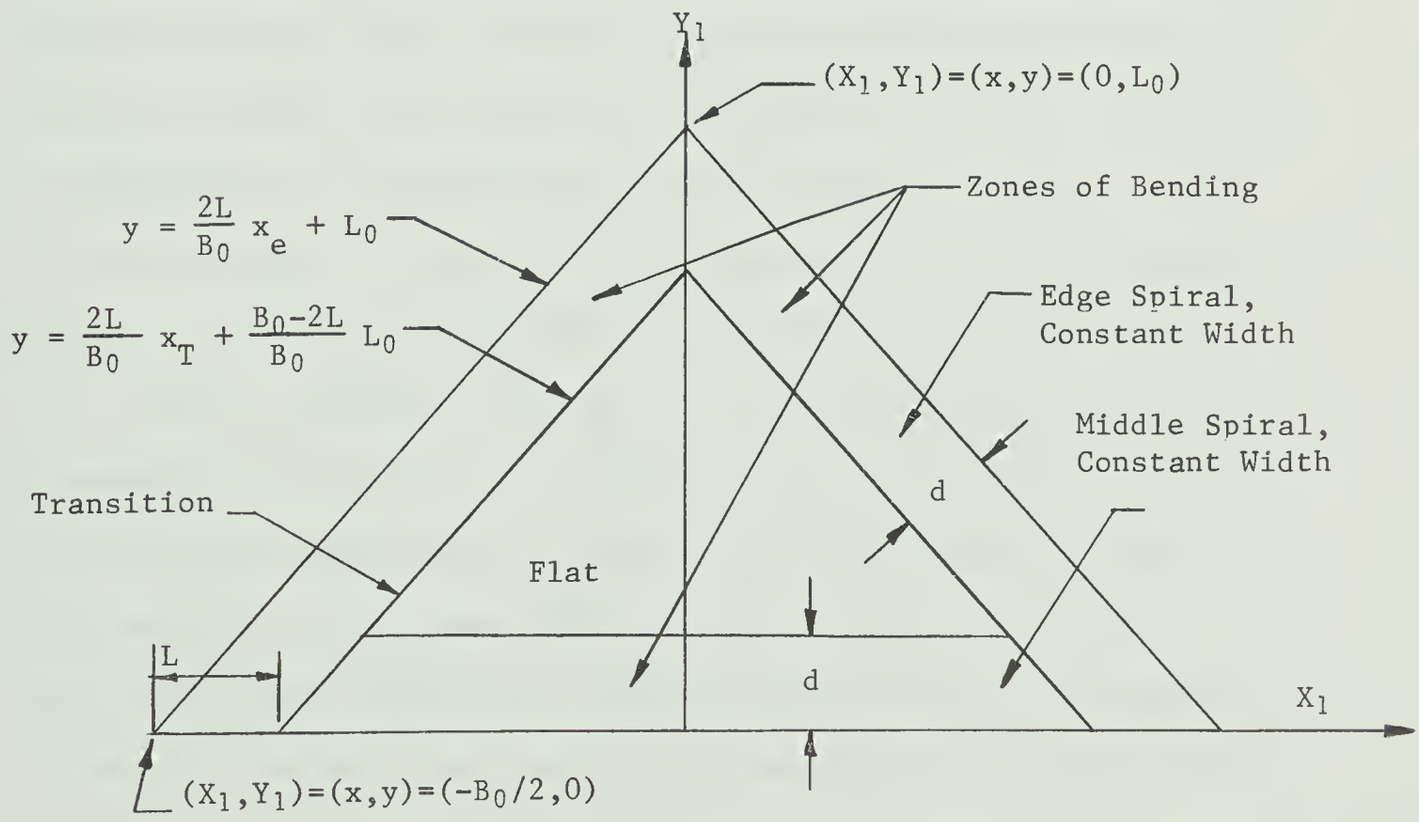

Fig. 20 Diagram of State 1

If n is the number of buckles, then

$$B_0 = \frac{2\pi R}{n} \quad , \tag{2.2.1}$$

and

$$L_0 = BB_0 \quad , \tag{2.2.2}$$

where the relation between μ and B is

$$B = \frac{1}{2\mu} \quad .$$

As indicated in Fig. 20, the zones of bending in the edge and middle spirals have been arbitrarily taken of equal width d; this simplified the computations and forced the geometric constraint discussed below.

A series of mappings using Lagrangian co-ordinates (x,y), initially the orthogonal cartesian co-ordinates of the middle plane of the flat plate, state 1, will now be developed which will map the flat plate (shown in Fig. 20) onto the space frame (shown in Fig. 19). The middle surface will be mapped inextensionally in the x direction; the Lagrangian x co-ordinates of the edge spiral at the rib and at the transition are x_e and x_T. The mapping functions will not be periodic; to this end, the geometric constraints of $c \neq 0$ and $c \neq \infty$ must be imposed. (See Eq. 2.5.1 for the definition of c.) The geometric constraint on c accounts for the requirement that the plate was to be mapped into a closed cylinder which should buckle into a periodic closed shape with continuous tangents. The net result should then approximate a diamond-shaped buckle. This mapping is normally effected by the use of a displacement $\overline{U}$ from the initial

cylinder; however, this procedure was abandoned since the easiest way to get $\bar{U}$ seemed to be the method used. One could, for instance, specify a kinematically admissable w displacement function with respect to a local reference frame based on the middle surface of the undeformed cylinder, and then obtain v by the constraint that

$$e_{11} = 0 \quad ,$$

where e_{11} is defined by Eq. 2.9.6. Assuming that u has a small effect in this equation, then the equation may be considered as a nonlinear partial differential equation defining v. An unsuccessful attempt was made to use this method. The differential equation was integrated by a method of successive approximations; the procedure was involved, difficult, and made the consideration of many terms necessary. However, it was found that the procedure used in section 2.3, etc., converted this complicated problem to a problem which was readily and easily solved. The mapping technique of section 2.3 obviated the need to solve a nonlinear differential equation in order to enforce the inextensional constraint in the x direction.

The basic co-ordinate frame is orthogonal cartesian (X, Y, Z) and is oriented as shown in Fig. 19. The various mappings will be called "states" and the corresponding basic co-ordinates will be suitably subscripted [say, (X_1, Y_1, Z_1)]. The additional subscripts of R and T will denote rib and transition values respectively; for example, (X_{1R}, Y_{1R}, Z_{1R}), or (X_{1T}, Y_{1T}, Z_{1T}).

2.3. Mapping of the Edge Spiral

The transition equations for state 1 are:

$$X_1 = x \quad , \tag{2.3.1a}$$

$$Y_1 = y \quad , \tag{2.3.1b}$$

and

$$Z_1 = 0 \quad . \tag{2.3.1c}$$

The transformation equations for state 2 are:

$$X_2 = x \quad , \tag{2.3.2a}$$

$$Y_2 = Ny \quad , \tag{2.3.2b}$$

and

$$Z_2 = 0 \quad . \tag{2.3.2c}$$

State 3 is shown in Fig. 21. Assign to x_e the co-ordinates (X_{3R}, Y_{3R}, Z_{3R}). The equations of the spiral in terms of (X^1, Z^1), see Fig. 21, are known by Eqs. 2.1.5.

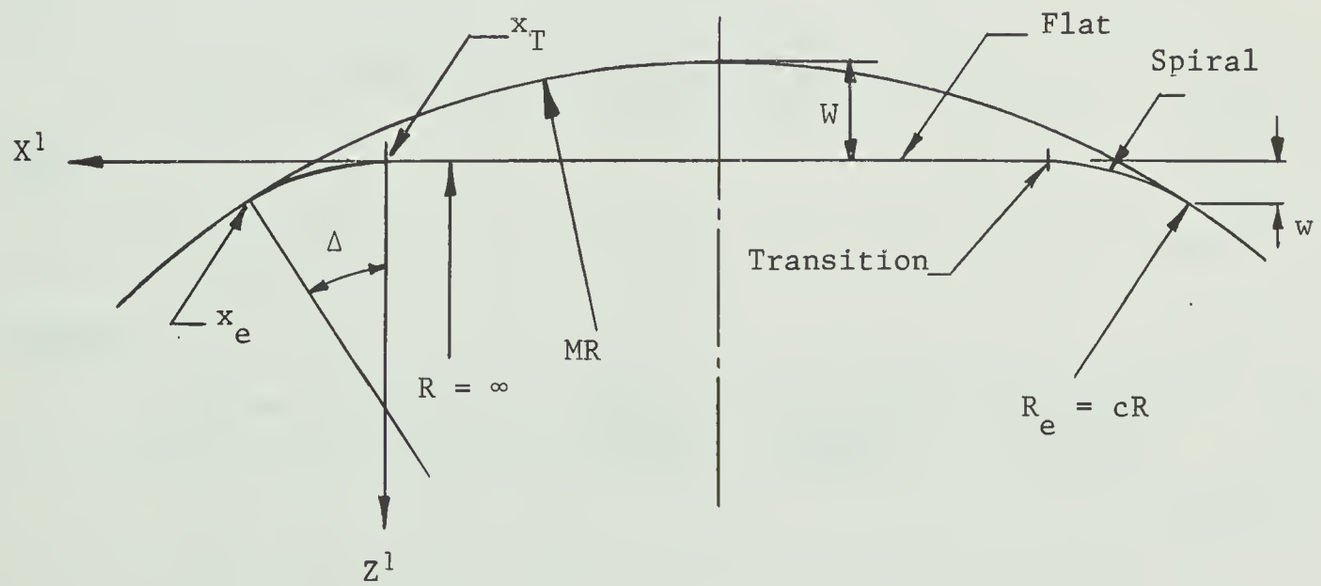

Fig. 21 State 3 at y = 0

If the middle line is mapped inextensionally, then

$$l = |x - x_T|$$

$$= x_T - x \quad ,$$

so that

$$\phi = \frac{(x_T - x)^2}{A^2} \quad . \tag{2.3.3}$$

Letting

$$X'' = -X^1 \quad ,$$

and

$$Z'' = -Z^1 \quad ,$$

then

$$X_3 = X_{3R} + (X'' - X''_R) \quad , \tag{2.3.4a}$$

$$Y_3 = Y_2 \quad ,$$

and

$$Z_3 = Z_{3R} + (Z'' - Z''_R); \tag{2.3.4c}$$

where

$$X''_R = -A\Delta^{\frac{1}{2}}\left(1 - \frac{\Delta^2}{5.2!} + \frac{\Delta^4}{9.4!} - \frac{\Delta^6}{13.6!} + \ldots\right) \quad , \tag{2.3.5a}$$

and

$$Z''_R = -A\Delta^{\frac{1}{2}}\left(\frac{\Delta}{3} - \frac{\Delta^3}{7.3!} + \frac{\Delta^5}{11.5!} - \frac{\Delta^7}{15.7!} + \ldots\right) \quad , \tag{2.3.5b}$$

where

$$\Delta = \frac{\pi}{n} \quad . \tag{2.3.6}$$

Further,

$$X'' = -(x_T - x)\left(1 - \frac{(x_T - x)^4}{5.2!A^4} + \frac{(x_T - x)^8}{9.4!A^8} - \frac{(x_T - x)^{12}}{13.6!A^{12}} + \ldots\right), \tag{2.3.7a}$$

and

$$Z'' = -(x_T - x)\left(\frac{(x_T - x)^2}{3A^2} - \frac{(x_T - x)^6}{7.3!A^6} + \frac{(x_T - x)^{10}}{11.5!A^{10}} - \frac{(x_T - x)^{14}}{15.7!A^{14}} + \ldots\right) . \tag{2.3.7b}$$

The co-ordinates of x_e are given by

$$X_{3R} = - MR \frac{L_0 - y}{L_0} \sin \Delta \quad , \tag{2.3.8a}$$

$$Y_{3R} = Ny \quad , \tag{2.3.8b}$$

and

$$Z_{3R} = MR - MR \frac{L_0 - y}{L_0} (1 - \cos \Delta) \quad . \tag{2.3.8c}$$

2.4. Mapping of the Flat

The co-ordinates of the transition are obtained by evaluating Eqs. 2.3.4 at $X'' = Z'' = 0$. Hence

$$X_{3T} = x_T \quad , \tag{2.4.1a}$$

$$Y_{3T} = Ny \quad , \tag{2.4.1b}$$

and

$$Z_{3T} = Z_{3R} - Z''_R \quad . \tag{2.4.1c}$$

The co-ordinates of a general point on the flat become,

$$X_3 = x \quad , \tag{2.4.2a}$$

$$Y_3 = Ny \quad , \tag{2.4.2b}$$

and

$$Z_3 = Z_{3T} \quad . \tag{2.4.2c}$$

2.5. Determination of the Independent Parameters

The radius of the edge spiral at the rib is defined by

$$R_e = cR \quad . \tag{2.5.1}$$

The parameters introduced so far are n, N, M, B, and c. However, they are not all independent, as will now be shown. The mapping of the edge spiral and flat has been under the constraint that the middle line was neutral; hence, at $y = 0$, there must hold the relation

$$L - x_T = \frac{\pi R}{n} \quad . \tag{2.5.2}$$

From continuity in the X direction it is also required that

$$X_{3R} = x_T + X''_R \quad . \tag{2.5.3}$$

Substituting for x_T from Eq. 2.5.3 into Eq. 2.5.2 results in

$$L - (X_{3R} - X''_R) = \frac{\pi R}{n} \quad . \tag{2.5.4}$$

Replacing X_{3R} by Eq. 2.3.8a and X''_R by Eq. 2.3.5a and, noting that $L = 2cR\Delta$, reduces Eq. 2.5.4 to

$$\frac{\pi R}{n} = c2R\Delta - \left[-MR \sin\Delta + A\Delta^{\frac{1}{2}} \left(1 - \frac{\Delta^2}{5.2!} + \frac{\Delta^4}{9.4!} - \frac{\Delta^6}{13.6!} + \ldots \right) \right]$$

which, upon replacing A by

$$A = 2cR\Delta^{\frac{1}{2}} \quad , \tag{2.5.5}$$

becomes

$$c = \frac{\Delta - M \sin\Delta}{2\Delta - 2\Delta \left(1 - \frac{\Delta^2}{5.2!} + \frac{\Delta^4}{9.4!} - \frac{\Delta^6}{13.6!} + \ldots \right)} \quad . \tag{2.5.6}$$

Therefore, c, M, and n are not independent. As indicated in section 2.2 the parameter c is subject to a geometric constraint; hence, Eq. 2.5.6 serves to define $M = M(c,n)$.

2.6. Calculation of the Base Vectors for the Edge Spiral and for the Flat

The position vector of a typical point on the middle surface of the spiral is

$$\bar{R} = X_3 \underline{i} + Y_3 \underline{j} + Z_3 \underline{K} \quad , \tag{2.6.1}$$

where the components are given by Eqs. 2.3.4.

The equation of the x_T line is

$$y = \frac{2L_0}{B_0} x_T + \left(\frac{B_0 - 2L}{B_0} \right) L_0 \quad , \tag{2.6.2}$$

which, solving for x_T, becomes

$$x_T = [y - (1 - 2c)\ 2\Delta BR] \frac{1}{2B} \quad .$$

Defining

$$\bar{y} = (1 - 2c)\ 2\Delta BR \quad , \tag{2.6.3}$$

then x_T is given by

$$x_T = \frac{(y - \bar{y})}{2B} \quad . \tag{2.6.4}$$

This is the value of x_T to be substituted into Eq. 2.6.1.

By definition, the base vector on the middle surface and in the x direction is

$$\bar{G}_{01} = \frac{\partial \bar{R}}{\partial x} \quad . \tag{2.6.5}$$

Performing the computations indicated by Eq. 2.6.5 results in

$$\bar{G}_{01} = \left(1 - \frac{(x_T - x)^4}{2!A^4} + \frac{(x_T - x)^8}{4!A^8} - \frac{(x_T - x)^{12}}{6!A^{12}} + \ldots \right) \underline{i} + 0\underline{j}$$

$$+ \left(\frac{(x_T - x)^2}{A^2} - \frac{(x_T - x)^6}{3!A^6} + \frac{(x_T - x)^{10}}{5!A^{10}} - \frac{(x_T - x)^{14}}{7!A^{14}} + \ldots \right) \underline{K} \quad .$$

By use of Eq. 2.3.3 (i.e., $\phi = (x_T - x)^2/A^2$), this equation simplifies to

$$\bar{G}_{01} = \cos\phi\ \underline{i} + 0\underline{j} + \sin\phi\ \underline{K} \quad . \tag{2.6.6a}$$

Thus, while the (X, Y, Z) co-ordinates of the spiral are not expressible in closed form, the constraint that the middle line is mapped inextensionally allows the base vector to go into closed form. This is a

noteworthy simplification, for otherwise, the computation of the metric tensor components would involve the multiplication of infinite sums.

Proceeding in a similar manner, one may derive that

$$\bar{G}_{02} = \frac{\partial \bar{R}}{\partial y}$$

$$= \left(\frac{MR}{L_0} \sin\Delta - \frac{\cos\phi}{2B} \right) \underline{i} + N\underline{j} + \left(\frac{MR}{L_0} (1 - \cos\Delta) - \frac{\sin\phi}{2B} \right) \underline{K} \quad . \tag{2.6.6b}$$

Analagous computations for the flat yield

$$\bar{G}_{01} = 1\underline{i} + 0\underline{j} + 0\underline{K} \quad , \tag{2.6.7a}$$

and

$$\bar{G}_{02} = 0\underline{i} + N\underline{j} + \frac{MR}{L_0} (1 - \cos\Delta) \underline{K} \quad . \tag{2.6.7b}$$

The continuity of the base vectors may be checked by comparing Eqs. 2.6.6, evaluated at $\phi = 0$, with Eqs. 2.6.7. The former yield

$$\bar{G}_{01} = 1\underline{i} + 0\underline{j} + 0\underline{K} \quad ,$$

and

$$\bar{G}_{02} = \left(\frac{MR}{L_0} \sin\Delta - \frac{1}{2B} \right) \underline{i} + N\underline{j} + \frac{MR}{L_0} (1 - \cos\Delta) \underline{K} \quad .$$

Continuity clearly requires that

$$\frac{MR}{L_0} \sin\Delta - \frac{1}{2B} = 0 \quad ,$$

or

$$M \sin\Delta - \Delta = 0 \quad . \tag{2.6.8}$$

If Eq. 2.6.8 is obeyed, then Eq. 2.5.6 yields $c = 0$, i.e., the perfect diamond shape. Therefore, while the surface has been mapped in a continuous fashion, the material in the spiral has been sheared. The shearing is exactly similar to that which would be required to cause

a piece of wax paper (Fig. 22) to roll onto the cylinder without advancing down the axis of the cylinder. This deficiency was not easily corrected, without introducing other discontinuities, and resulted in the need to neglect the middle plane shear energy. Equation 2.6.8 indicates that a better definition of M would be

$$M = kM_0 \quad , \tag{2.6.9}$$

where

$$M_0 = \frac{\Delta}{\sin\Delta} \quad .$$

The magnitude of k is a measure of how close the exact diamond configuration is approached; $k = 1$ is required for the perfect diamond and $k < 1$ is required for an approximation to the exact diamond pattern.

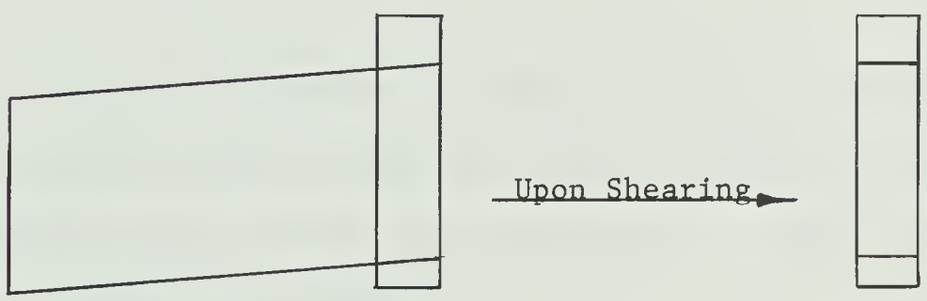

Fig. 22 Explanation of Shear Discontinuity

2.7. Transformation Equations for the Middle Spiral

Figure 23 shows the geometry of the middle spiral. It was previously decided to let the middle spiral length be d (see Fig. 20); hence,

$$d = 2R_M\Psi \quad . \tag{2.7.1}$$

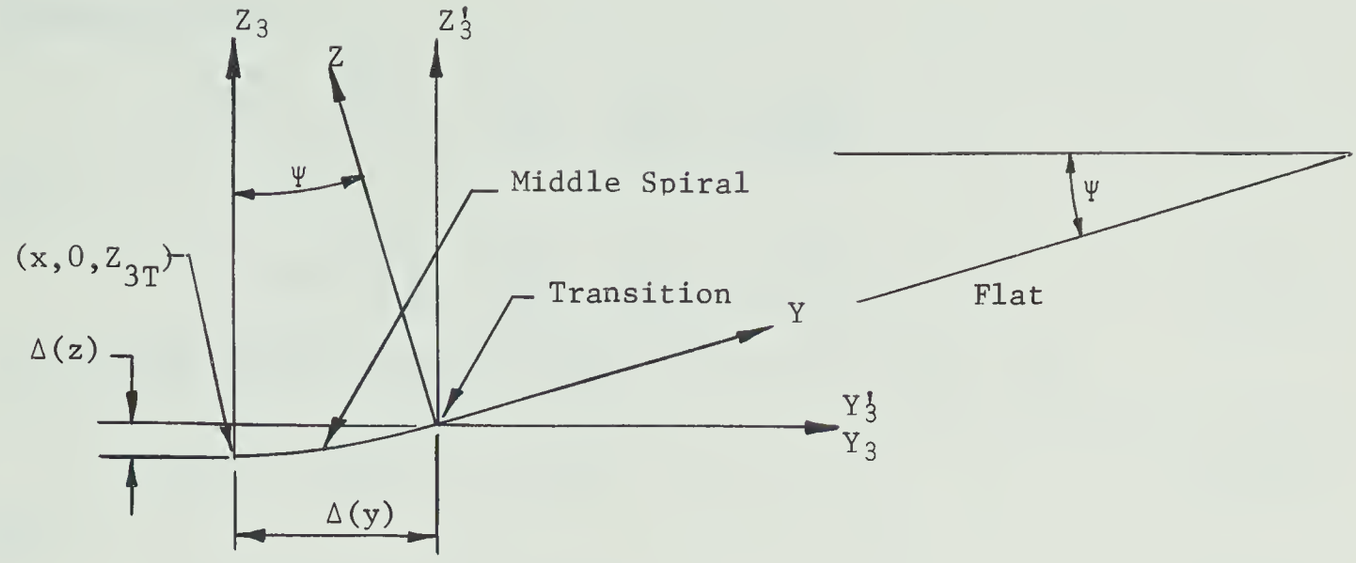

Fig. 23 Geometry for Middle Spiral

R_M is the radius of the middle spiral. States 1 and 2 are as previously given and the final mapping is obtained as follows. Introduce local intrinsic co-ordinates (x, z), where

$$z = -(d - y) \quad . \tag{2.7.2}$$

State 2 will be mapped maintaining its length. This is in error, since the curvature introduced must change the length, but must be accepted as an approximation which will be valid for small Ψ . Thus, the co-ordinate z corresponds to a length of

$$l = -Nz \tag{2.7.3}$$

which, using Eq. 2.1.6, is also expressible as

$$l = a\phi^{\frac{1}{2}} \quad , \tag{2.7.4}$$

where

$$a = 2R_M\Psi^{\frac{1}{2}} \quad . \tag{2.7.5}$$

The angle ϕ is therefore given by

$$\phi = \frac{N^2 (-z)^2}{a^2} \quad . \tag{2.7.6}$$

From Eq. 2.1.5,

$$Y = -a\phi^{\frac{1}{2}} \left(1 - \frac{\phi^2}{5.2!} + \frac{\phi^4}{9.4!} - \frac{\phi^6}{13.6!} + \ldots \right) \quad , \qquad (2.7.7a)$$

and

$$Z = a\phi^{\frac{1}{2}} \left(\frac{\phi}{3} - \frac{\phi^3}{7.3!} + \frac{\phi^5}{11.5!} - \frac{\phi^7}{15.7!} + \ldots \right) \quad . \qquad (2.7.7b)$$

The transformation equations from (Y, Z) to (Y_3', Z_3') are

$$Y_3' = Y \cos \Psi - Z \sin \Psi \quad , \qquad (2.7.8a)$$

and

$$Z_3' = Y \sin \Psi + Z \cos \Psi \quad . \qquad (2.7.8b)$$

Thus

$$X_3 = x \quad , \qquad (2.7.9a)$$

$$Y_3 = Y_3' + \Delta(y) \quad , \qquad (2.7.9b)$$

and

$$Z_3 = Z_{3_T} + \Delta(z) + Z_3' \quad . \qquad (2.7.9c)$$

The position vector of a point (x, z) on the spiral is

$$\bar{R} = x\underline{i} + (Y_3' + \Delta(y))\ \underline{j} + (Z_{3_T} + \Delta(z) + Z_3')\ \underline{K} \quad , \qquad (2.7.10)$$

from which

$$\bar{G}_{01} = \frac{\partial \bar{R}}{\partial x} = 1\underline{i} + 0\underline{j} + 0\underline{K} \quad , \qquad (2.7.11a)$$

and

$$\bar{G}_{02} = \frac{\partial \bar{R}}{\partial y} = \frac{\partial \bar{R}}{\partial z} \frac{\partial z}{\partial y}$$

$$= 0\underline{i} + N (\cos \Psi \cos \phi + \sin \Psi \sin \phi)\ \underline{j}$$

$$+ N (\sin \Psi \cos \phi - \cos \Psi \sin \phi)\ \underline{K} \quad . \qquad (2.7.11b)$$

2.8. Position Vector and Base Vectors of a General Point

Let z be a co-ordinate perpendicular to the middle surface of the initial flat plate. Its range is $-t/2 \leq z \leq + t/2$, where t is

the thickness. As is usual in shell theory, z will be assumed normal to the deformed surface [hence, (x, y, z) are Gaussian co-ordinates based on the middle surface] and unstrained.

The position vector of a typical point (x, y, z) is

$$\bar{R} = \bar{R}_0 (x, y) + z \bar{G}_{03} (x, y) \quad , \tag{2.8.1}$$

where $\bar{R}_0$ is the position vector of (x, y, 0). $\bar{G}_{03}$ is the unit normal to the deformed middle surface and is defined by

$$\bar{G}_{03} \doteq \bar{G}_{01} \times \bar{G}_{02} \quad . \tag{2.8.2}$$

Evaluating Eq. 2.8.2 for the edge spiral one obtains,

$$\bar{G}_{03} = -N \sin \phi \, \underline{i} + \left(\frac{MR}{L_0} \sin \Delta \sin \phi - \frac{MR}{L_0} (1 - \cos \Delta) \cos \phi \right) \underline{j}$$

$$+ N \cos \phi \, \underline{K} \quad . \tag{2.8.3}$$

Similar computations for the flat yield

$$\bar{G}_{03} = 0\underline{i} + \left(- \frac{MR}{L_0} (1 - \cos \Delta) \right) \underline{j} + N\underline{K} \quad , \tag{2.8.4}$$

and for the middle spiral

$$\bar{G}_{03} = 0\underline{i} + N (\cos \Psi \sin \phi - \sin \Psi \cos \phi) \, \underline{j}$$

$$+ N (\cos \Psi \cos \phi + \sin \Psi \sin \phi) \, \underline{K} \quad . \tag{2.8.5}$$

Using Eq. 2.8.1 the base vectors at a general point, (x, y, z), are calculated to be

$$\bar{G}_1 = \frac{\partial \bar{R}}{\partial x} = \bar{G}_{01} + z \frac{\partial \bar{G}_{03}}{\partial x} \quad , \tag{2.8.6a}$$

$$\bar{G}_2 = \frac{\partial \bar{R}}{\partial y} = \bar{G}_{02} + z \frac{\partial \bar{G}_{03}}{\partial y} \quad , \tag{2.8.6b}$$

and

$$\bar{G}_3 = \frac{\partial \bar{R}}{\partial z} = \bar{G}_{03} \quad . \tag{2.8.6c}$$

The base vectors for the edge spiral become:

$$\bar{G}_1 = \left[\cos\phi + z \left(\frac{2N\phi^{\frac{1}{2}}}{A} \cos\phi \right) \right] \underline{i}$$
$$+ \left[z \left(- \frac{2MR}{L_0 A} \sin\Delta \, \phi^{\frac{1}{2}} \cos\phi - \frac{2MR}{L_0 A} (1 - \cos\Delta) \, \phi^{\frac{1}{2}} \sin\phi \right) \right] \underline{j}$$
$$+ \left[\sin\phi + z \left(\frac{2N\phi^{\frac{1}{2}}}{A} \sin\phi \right) \right] \underline{K} \quad , \qquad (2.8.7a)$$

$$\bar{G}_2 = \left[\left(\frac{MR}{L_0} \sin\Delta - \frac{\cos\phi}{2B} \right) + z \left(- \frac{N\phi^{\frac{1}{2}}}{BA} \cos\phi \right) \right] \underline{i}$$
$$+ \left[N + z \left(\frac{MR}{BL_0 A} \sin\Delta \, \phi^{\frac{1}{2}} \cos\phi + \frac{MR}{BL_0 A} (1 - \cos\Delta) \, \phi^{\frac{1}{2}} \sin\phi \right) \right] \underline{j}$$
$$+ \left[\left(\frac{MR}{L_0} (1 - \cos\Delta) - \frac{\sin\phi}{2B} \right) + z \left(- \frac{N\phi^{\frac{1}{2}}}{BA} \sin\phi \right) \right] \underline{K} \quad , \qquad (2.8.7b)$$

and

$$\bar{G}_3 = - N \sin\phi \, \underline{i} + \left(\frac{MR}{L_0} \sin\Delta \sin\phi - \frac{MR}{L_0} (1 - \cos\Delta) \cos\phi \right) \underline{j}$$
$$+ N \cos\phi \, \underline{K} \quad . \qquad (2.8.7c)$$

The base vectors for the flat become:

$$\bar{G}_1 = 1\underline{i} + 0\underline{j} + 0\underline{K} \quad , \qquad (2.8.8a)$$

$$\bar{G}_2 = 0\underline{i} + N\underline{j} + \frac{MR}{L_0} (1 - \cos\Delta) \, \underline{K} \quad , \qquad (2.8.8b)$$

and

$$\bar{G}_3 = 0\underline{i} - \frac{MR}{L_0} (1 - \cos\Delta) \, \underline{j} + N\underline{K} \quad . \qquad (2.8.8c)$$

The base vectors for the middle spiral become:

$$\bar{G}_1 = 1\underline{i} + 0\underline{j} + 0\underline{K} \quad , \qquad (2.8.9a)$$

$$\bar{G}_2 = 0\underline{i} + (\cos\Psi \cos\phi + \sin\Psi \sin\phi) \, D\underline{j}$$
$$+ (-\cos\Psi \sin\phi + \sin\Psi \cos\phi) \, D\underline{K} \qquad (2.8.9b)$$

and

$$\bar{G}_3 = 0\underline{i} + N (\cos\Psi \sin\phi - \sin\Psi \cos\phi) \, \underline{j}$$
$$+ N (\cos\Psi \cos\phi + \sin\Psi \sin\phi) \, \underline{K} \quad ; \qquad (2.8.9c)$$

where

$$D = N + z \frac{N^2}{R_M} \left(\frac{\phi}{\Psi} \right)^{\frac{1}{2}} \quad . \tag{2.8.10}$$

2.9. Calculation of Strain Tensor Components

The metric tensor components are given by

$$G_{ij} = \overline{G}_i \cdot \overline{G}_j \quad . \tag{2.9.1}$$

By construction

$$G_{13} = G_{23} = 0 \quad , \tag{2.9.2a}$$

and

$$G_{33} = 1 \quad . \tag{2.9.2b}$$

Terms containing z^2 will be neglected in G_{ij}. The remaining metric tensor components for the edge spiral are:

$$G_{11} = 1 + \frac{2N}{c} \frac{z}{R} r^{\frac{1}{2}} \quad , \tag{2.9.3a}$$

$$G_{22} = 2 \left(\frac{M}{2\Delta B} \right)^2 - 2\left(\frac{M}{2\Delta B} \right)^2 \cos \Delta - \frac{M}{2\Delta B^2} \sin \Delta \cos \phi$$

$$+ \frac{1}{4B^2} - \frac{M}{2\Delta B^2} \sin \phi + \frac{M}{2\Delta B^2} \cos \Delta \sin \phi + N^2 + \frac{N}{2cB^2} \frac{z}{R} r^{\frac{1}{2}} \quad , \tag{2.9.3b}$$

and

$$G_{12} = \frac{M}{2\Delta B} \sin \Delta \cos \phi - \frac{1}{2B} - \frac{M}{2\Delta B} \cos \Delta \sin \phi + \frac{M}{2\Delta B} \sin \phi$$

$$- \frac{N}{cB} \frac{z}{R} r^{\frac{1}{2}} \quad ; \tag{2.9.3c}$$

where

$$r = \frac{\phi}{\Delta} \quad . \tag{2.9.3d}$$

The metric components for the flat are:

$$G_{11} = 1 \quad , \tag{2.9.4a}$$

$$G_{22} = N^2 + \frac{M^2}{4\Delta^2 B^2} (1 - \cos \Delta)^2 \quad , \tag{2.9.4b}$$

and

$$G_{12} = 0 \quad . \tag{2.9.4c}$$

The metric components for the middle spiral are:

$$G_{11} = 0 \quad , \tag{2.9.5a}$$

$$G_{22} = N^2 + 2z \frac{N^3}{R_M} \left(\frac{\phi}{\Psi} \right)^{\frac{1}{2}} \quad , \tag{2.9.5b}$$

and

$$G_{12} = 0 \quad . \tag{2.9.5c}$$

The Lagrangian strain tensor components are defined by

$$e_{ij} = (G_{ij} - g_{ij})/2 \quad , \tag{2.9.6}$$

where g_{ij} are the metric tensor components of the initial flat plate:

$$g_{ij} = \delta_{ij} \quad . \tag{2.9.7}$$

The strain tensor components for the edge spiral are:

$$e_{13} = e_{23} = e_{33} = 0 \quad , \tag{2.9.8a}$$

$$e_{11} = \frac{N}{c} \frac{z}{R} r^{\frac{1}{2}} \quad , \tag{2.9.8b}$$

$$e_{22} = \left(\frac{M}{2\Delta B} \right)^2 (1 - \cos \Delta) - \frac{M}{4\Delta B^2} \sin \Delta \cos \phi + \frac{1}{8B^2}$$
$$- \frac{M}{4\Delta B^2} (1 - \cos \Delta) \sin \phi + \frac{N^2}{2} - \frac{1}{2} + \frac{N}{4cB^2} \frac{z}{R} r^{\frac{1}{2}} \quad , \tag{2.9.8c}$$

and

$$e_{12} = \frac{M}{4\Delta B} \sin \Delta \cos \phi - \frac{1}{4B} + \frac{M}{4B} (1 - \cos \Delta) \sin \phi$$
$$- \frac{N}{2cB} \frac{z}{R} r^{\frac{1}{2}} \quad . \tag{2.9.8d}$$

Similarly, for the flat,

$$e_{11} = 0 \quad , \tag{2.9.9a}$$

$$e_{22} = \frac{N^2}{2} - \frac{1}{2} + \frac{1}{2} \left(\frac{M}{2\Delta B} \right)^2 (1 - \cos \Delta)^2 \quad , \tag{2.9.9b}$$

$$e_{12} = 0 \quad ; \tag{2.9.9c}$$

and for the middle spiral,

$$e_{11} = 0 \quad , \tag{2.9.10a}$$

$$e_{22} = \frac{N^2}{2} - \frac{1}{2} + z \frac{N^3}{R_M} \left(\frac{\phi}{\Psi} \right)^{\frac{1}{2}} \tag{2.9.10b}$$

and

$$e_{12} = 0 \quad . \tag{2.9.10c}$$

It is readily shown that due to deficiencies of the mapping (such as, for example, that discussed in section 2.6), B and n must be large, indeed, much larger than the experimental values in order that the middle surface strains be less than the yield point. The experiments of Ricardo (34) have shown that on buckling, the change of bending energy predominates. These experiments confirm Kennedy's (33) contention that the deformation is largely inextensional. The point of view is therefore taken that even though the middle plane strain of the mapping is excessive, the primary deformation of the shell is due to displacement via bending, and the mapping should approximate this. The middle plane strain energy will accordingly be computed by considering the edge and middle spirals to be members of a pinned space truss (The geometry of the space truss is fixed by its bending deflections.), subjected to the applied axial load. Cox (35) has noted this procedure as a possible approximation and has stated that the flat does not participate greatly in the carrying of the load. Based on these considerations, the membrane terms in the strain tensors will be dropped from further considerations. The parameter N, which appears in the bending terms of the strain tensor, will be set equal to one; this procedure is

justified if the axial shortening is small so that N approximates unity.

This problem with the middle plane strain was to be expected; one has but to note Rayleigh's comment that (35): "We can bend a piece of sheet metal easily with our fingers but we cannot stretch it noticeably". Clearly, the large deflection mapping would have to be extremely accurate to keep the strain (which must be compressive), less than, say 0.0005 in./in. in the flat. Indeed, this value of strain is still probably much larger than the usual post-buckling values. Pogorelov's (14) procedure approximated a surface isometric to a cylinder but, as in this thesis, he was unable to maintain geometric continuity. Difficulties with the middle plane strain have already been indicated in the discussion of Hoff, et. al., (12, 1966).

CHAPTER 3

ENERGY COMPUTATIONS AND THE MINIMIZATION PROCEDURE

The geometrical considerations of Chapter 2 introduced the parameters n, B, k and N. It was noted that c was subject to a geometric constraint, and an expression $c = c(k, n)$ was obtained. Thus, if c is prescribed, and n is chosen as an independent parameter, then k is determined. The actual procedure shall be modified so that k is prescribed, n is considered as independent, and hence c is determined. A consideration of the magnitudes and continuity of the middle plane strains indicated that while the mapping may be able to approximate the bending deformation, it could not produce acceptable middle plane deformations. The conclusion was reached that the middle plane deformation would have to be accounted for in an alternate, more reasonable, fashion. To this end, N was set equal to one. The axial shortening, which N represented, was to be calculated as a function of the remaining parameters, as is explained below.

The principle of virtual work will be employed to determine B and n. If V is the potential energy, then it is required that

$$\frac{\partial V}{\partial n} = 0 \quad , \tag{3.1a}$$

and

$$\frac{\partial V}{\partial B} = 0 \quad , \tag{3.1b}$$

for prescribed k and σ. V is computed from

$$V = (U - W) / \frac{EB_0 L_0 t}{2} \quad , \tag{3.2}$$

where

$$U = \frac{1}{2} \int_v \sigma_{ij} \, e_{ij} \, dV \quad ,$$

and

$$W = \int_{S_T} T_i \, U_i \, dS \quad .$$

S_T represents the area upon which the stress vector [i.e., $(0, 0, -\sigma)$] is prescribed. U shall be calculated as

$$U = U_M + U_B \quad ,$$

where the subscripts denote membrane and bending energy, respectively. The regions of integration are shown in Fig. 24. The volume of this region is:

$$\begin{aligned} \text{Volume} &= \frac{B_0 L_0 t}{2} \\ &= \left(\frac{2\Delta R}{2}\right) \left(B 2\Delta R\right) \; t \\ &= 2B\Delta^2 \, t^3 \, (R/t)^2 \quad . \end{aligned} \tag{3.3}$$

Further, from Fig. 24,

$$d = L \cos \phi \quad , \tag{3.4}$$

$$L_0' = (1 - c) \, L_0 \quad , \tag{3.5}$$

and

$$1 = B_0 \, (B^2 + 0.25)^{\frac{1}{2}} \quad . \tag{3.5a}$$

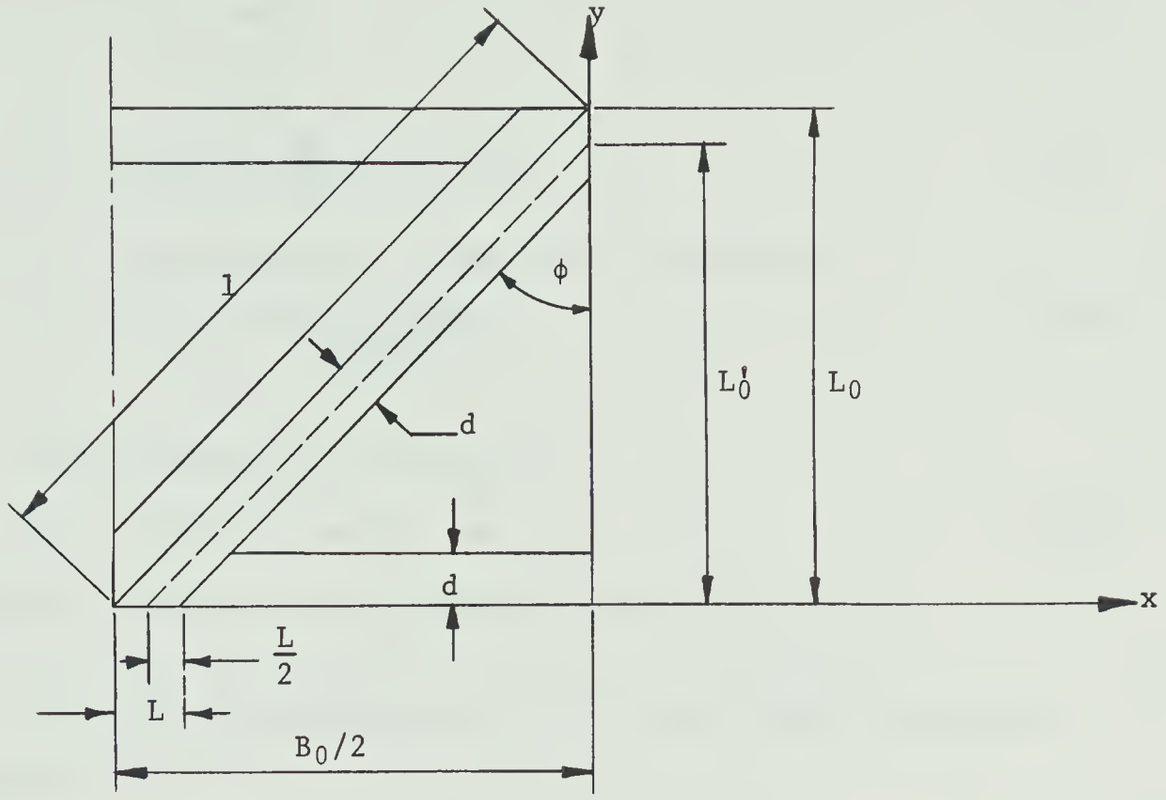

Fig. 24 Regions of Integration

The geometrical shortening e (which replaces N) is obtained by the following approximate procedure. Consider a section, x = 0, as shown in Fig. 25. The

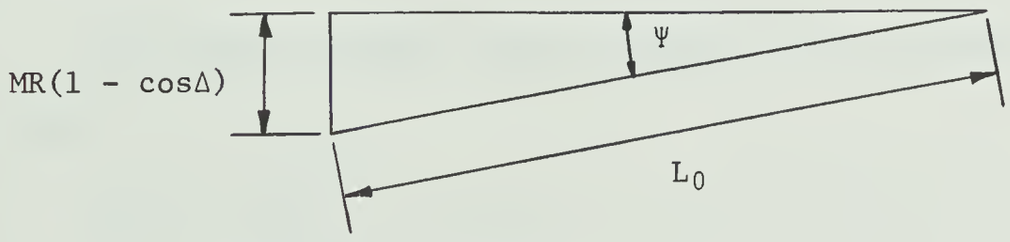

Fig. 25 Calculation of e

shortening, e, is given by

$$e = 1 - \cos \Psi \quad , \tag{3.6}$$

where

$$\Psi = \sin^{-1} \frac{MR}{L_0} (1 - \cos \Delta) \quad . \tag{3.7}$$

Using $M = k\Delta/\sin\Delta$ and $L_0 = BB_0$, Eq. 3.7 becomes

$$\Psi = \sin^{-1} \frac{k\ (1 - \cos \Delta)}{2B \sin \Delta} \quad . \tag{3.8}$$

The expression (see Fig. 21)

$$W = MR\ (1 - \cos \Delta) - w \quad , \tag{3.9}$$

was taken as a measure of the maximum lateral deflection.

The stresses are assumed to be in the elastic range and are given by:

$$\sigma_{xx} = \frac{E}{(1 - \nu^2)} (e_{xx} + \nu e_{yy}) \quad ,$$

$$\sigma_{yy} = \frac{E}{(1 - \nu^2)} (e_{yy} + \nu e_{xx}) \quad ,$$

and

$$\sigma_{xy} = \frac{E}{(1 + \nu)} e_{xy} \quad .$$

3.1. Calculation of the Elastic Energy of Bending and of the Potential of the Applied Load

The bending strain tensor components for the edge spiral are (with $N = 1$):

$$e_{11} = \frac{1}{c} \frac{z}{R} r^{\frac{1}{2}} \quad , \tag{3.1.1a}$$

$$e_{22} = \frac{1}{4cB^2} \frac{z}{R} r^{\frac{1}{2}} \quad , \tag{3.1.1b}$$

and

$$e_{12} = \frac{-1}{2cB} \frac{z}{R} r^{\frac{1}{2}} \quad . \tag{3.1.1c}$$

Similarly, for the middle spiral,

$$e_{22} = \left(\frac{z}{R_M}\right) \frac{\phi}{\Psi}^{\frac{1}{2}} \quad . \tag{3.1.1d}$$

U_B is calculated from

$$U_B = \frac{1}{2} \int_v \sigma_{ij} \; e_{ij} \; dV \quad . \tag{3.1.2}$$

Expanding Eq. 3.1.2 for the side spiral, there results

$$U_B = \frac{1}{2} \int_v (\sigma_{xx} \, e_{xx} + \sigma_{yy} \, e_{yy} + 2\sigma_{xy} \, e_{xy}) \, dV$$

which, after substitution from the stress-strain laws, becomes

$$U_B = \frac{1}{2} \int_v \left[\frac{E}{1+\nu} \left(\frac{e^2_{xx}}{1-\nu} + \frac{e^2_{yy}}{1-\nu} + 2e^2_{xy} \right) + \frac{2E\nu}{(1-\nu)^2} \, e_{xx} e_{yy}\right] dV. \tag{3.1.3}$$

An exact integration over the region shown in Fig. 24 was excessively complicated; since the method is approximate in nature, the regions of integration were simplified as shown in Fig. 26.

The evaluation of Eq. 3.1.3 proceeds as follows:

$$\int_v \left(\frac{e^2_{xx}}{1-\nu} + \frac{e^2_{yy}}{1-\nu} + 2 e^2_{xy} \right) dV =$$

$$\frac{1}{c^2R^2} \left[\frac{1}{1-\nu} \left(1 + \frac{1}{16B^4}\right) + \frac{1}{2B^2} \right] \frac{t^3}{12} \iint r \, dx \, dy \quad ,$$

where

$$\iint r \, dx \, dy = \int_{y=0}^{y=L_0'} \int_{x=x_e}^{x=x_T} \frac{(x_T - x)^2}{4c^2R^2\Delta^2} \, dx \, dy = \frac{4}{3} cB\Delta^2 (1-c) R^2 \, ,$$

and also

$$\int_v e_{xx}\, e_{yy}\, dV = \frac{1}{4c^2B^2}\,\frac{1}{R^2}\int_v r^2 z\, dV$$

$$= \frac{1}{36}\,\frac{1}{B^2}\,\frac{1-c_B}{c}\,\Delta^2 t^3 \quad .$$

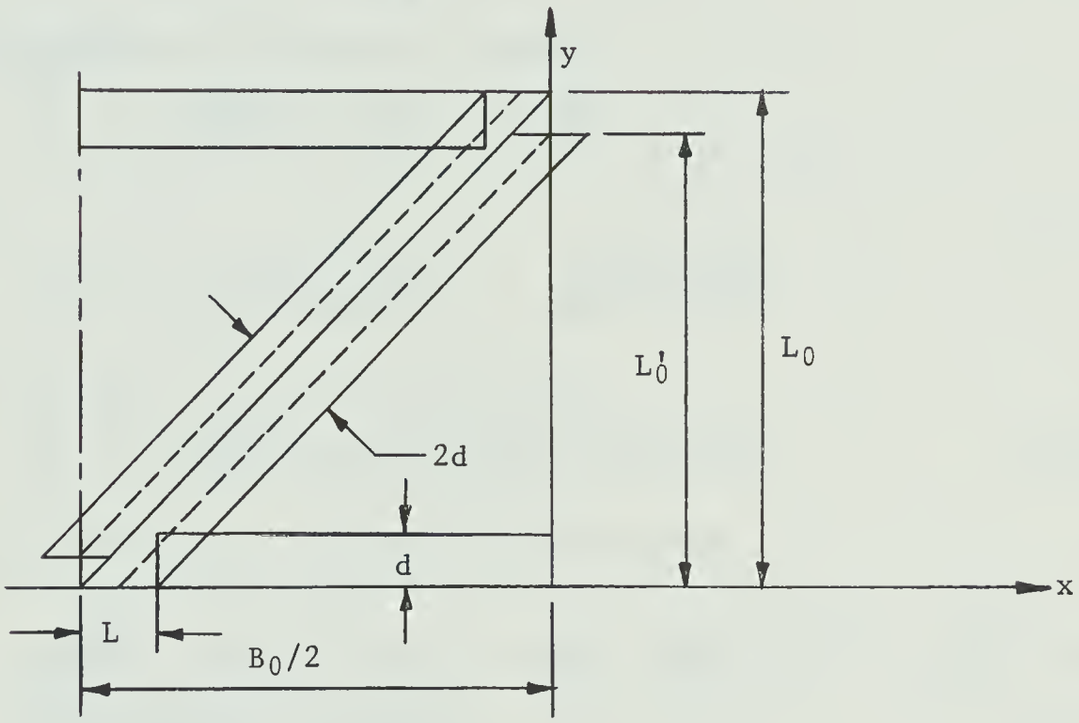

Fig. 26 Simplified Region of Integration

Combining the various results, the elastic bending energy of two edge spirals is given by:

$$U_B = \frac{E}{9(1-\nu^2)}\left(1 + \frac{1}{16B^4} + \frac{1}{2B^2}\right)\frac{1-c_B}{c}\Delta^2 t^3 \quad . \qquad (3.1.4)$$

The elastic bending energy for the middle spiral reduces to

$$U_B = \frac{E}{2(1-\nu^2)}\int_v e_{yy}^2\, dV \qquad (3.1.5)$$

$$U_B = \frac{Et^3}{24(1-\nu^2)\Psi R_M^2} \int_{y=0}^{y=d} \int_{x=-x_T}^{x=+x_T} \phi \, dx dy \quad ,$$

where

$$\phi = (-z)^2/A^2 \quad , \quad A = 2R_M\Psi^{\frac{1}{2}} \quad , \text{ and } \quad z = y - d \quad .$$

Upon integration, Eq. 3.1.5 reduces to

$$U_B = \frac{Et^3}{24(1-\nu^2)} \frac{d^3}{R_M^4\Psi^2} \frac{\Delta R}{6} (1 - 2c)$$

which, noting Eqs. 2.7.1 and 3.4, becomes

$$U_B = \frac{Et^3}{18(1-\nu^2)} \frac{\Psi^2}{\cos\phi} \frac{(1-2c)}{c} \quad .$$

However,

$$\cos\phi = \frac{L_0}{\sqrt{(L_0^2 + (B_0/2)^2)}} = \frac{B}{\sqrt{(B^2 + 0.25)}} \quad ,$$

so that the final form of Eq. 3.1.5 is

$$U_B = \frac{Et^3\Psi^2}{18(1-\nu^2)} \frac{(B^2 + 0.25)^{\frac{1}{2}}}{B} \frac{(1-2c)}{c} \quad . \qquad (3.1.6)$$

The sum of the bending energies therefore yields

$$\frac{U_B}{EB\Delta^2 t^3} = \frac{1}{9_1(1-\nu^2)} \left(1 + \frac{1}{16B^4} + \frac{1}{2B^2}\right) \frac{1-c}{c} + \frac{\Psi^2}{18(1-\nu^2)} \frac{(B^2 + 0.25)^{\frac{1}{2}}}{B^2\Delta^2} \frac{(1-2c)}{c} \quad . \qquad (3.1.7)$$

Equation 3.1.7 will now be linearized in the following fashion. From Eq. 3.8,

$$\Psi = \sin^{-1} \frac{k(1 - \cos\Delta)}{2B \sin\Delta}$$

$$\doteq \sin^{-1} \frac{k(\Delta^2/2)}{2B\Delta}$$

$$\doteq \frac{k\Delta}{4B} \, . \qquad (3.8a)$$

From Eq. 2.5.6,

$$c = \frac{\Delta - M \sin\Delta}{2\Delta - 2\Delta\left(1 - \frac{\Delta^2}{5.2!} + \frac{\Delta^4}{9.4!} - \frac{\Delta^6}{13.6!} + \ldots\right)}$$

which, using Eqs. 2.6.9 and 2.6.10, becomes

$$c \doteq \frac{\Delta - k(\Delta/\sin\Delta)\sin\Delta}{\frac{\Delta^3}{5} - \frac{2\Delta^5}{9.4!} + \frac{2\Delta^7}{13.6!}} \doteq \frac{5(1-k)}{\Delta^2} \quad .$$

The final linearized form of c is

$$c = \frac{(1-k)\,n^2}{2} \quad . \tag{3.1.8}$$

Equation 3.1.7 becomes

$$\frac{U_B}{EB\Delta^2 t^3} = U_B^*$$

$$= \frac{1}{9(1-\nu^2)}\left(1 + \frac{1}{16B^4} + \frac{1}{2B^2}\right)\left(\frac{2}{(1-k)n^2} - 1\right)$$

$$+ \frac{1}{18(1-\nu^2)}\,\frac{(B^2 + 0.25)^2}{16B^4}\,k^2\left(\frac{2}{(1-k)n^2} - 2\right) \quad . \tag{3.1.9}$$

The potential of the load is

$$-(B_0/2\,t\,\sigma)\,L_0(1-\cos\Psi) =$$

$$-2\left(\frac{\sigma R}{Et}\,\frac{R}{t}\right)(1-\cos\Psi)\,EB\Delta^2 t^3 \doteq$$

$$-2\left(\frac{\sigma R}{Et}\,\frac{R}{t}\right)\frac{\Psi^2}{2}\,EB\Delta^2 t^3$$

which, upon normalization, becomes

$$W^* = -2\left(\frac{\sigma R}{Et}\,\frac{R}{t}\right)\frac{k^2\,\pi^2}{32B^2n^2} \quad . \tag{3.1.10}$$

3.2. Approximation to the Membrane Energy

If the spirals are treated as members of a pinned space truss, then a typical diamond will carry an axial load of $2\Delta R\,t\sigma$ and a typical node will appear as in Fig. 27.

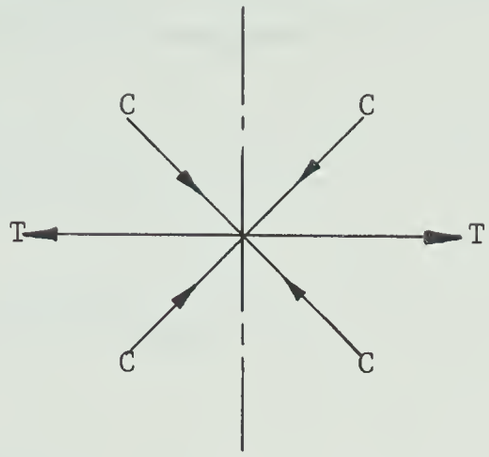

Fig. 27 Typical Node

Let,

C = compressive (positive) force in the rib,

and

T = tensile (positive) force in the middle transition.

The equilibrium equations to be obeyed are:

2 · (Y component of C) = applied load

$$= 2\Delta R\, t\sigma \quad , \tag{3.2.1a}$$

and

2 · (Radial component of C) = radial component of T. (3.2.1b)

Some necessary geometrical relations are obtained from Fig. 28:

$$\alpha = \mathrm{Tan}^{-1} \frac{MR\,(1 - \cos\Delta)}{MR \sin\Delta} \overset{\circ}{=} \sin^{-1} \frac{(1 - \cos\Delta)}{\sin\Delta} \quad , \tag{3.2.2a}$$

and

$$\beta = \sin^{-1} \frac{L_0 \cos\Psi}{l} \quad . \tag{3.2.2b}$$

The Y component of C is $C \sin\beta$, and the radial component is $(C \cos\beta) \sin\alpha$. The radial component of T is $T \sin\Delta$. Equations 3.2.1 therefore become:

$$2\ C \sin\beta = 2\ \Delta\ R\ t\ \sigma \quad ,$$

and

$$2\ C \cos\beta \sin\alpha = T \sin\Delta \quad ,$$

which yield

$$C = \sigma\Delta R\ t/\sin\beta \quad , \qquad (3.2.3a)$$

and

$$T = 2\ C \cos\beta \sin\alpha/\sin\Delta \quad . \qquad (3.2.3b)$$

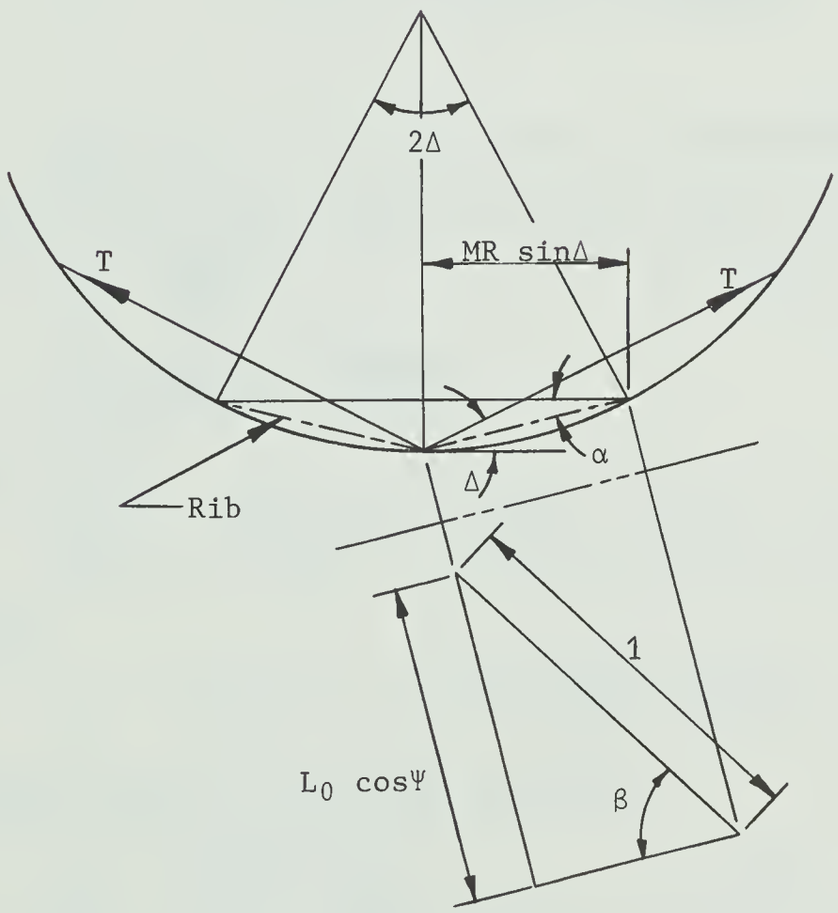

Fig. 28 Approximate Geometry at Node

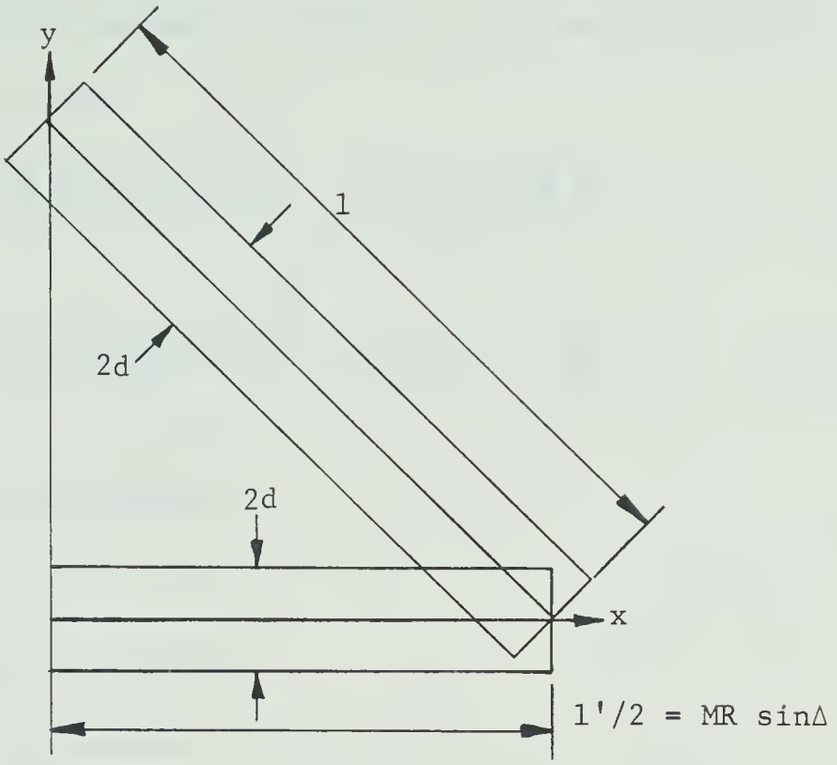

Fig. 29 Dimension of Members

The members of the space truss are approximated as shown in Fig. 29. The elastic energy of the side spiral is:

$$U_c = \frac{C^2 l}{2AE} \qquad A = 2dt$$

$$= \frac{1}{8} \frac{1}{c \cos \phi} \frac{1}{E} \frac{\sigma^2 \Delta R t}{\sin^2 \beta} \quad .$$

From Eq. 3.2.2b,

$$\sin \beta = \frac{BB_0 \cos \Psi}{l} \doteq \frac{BB_0}{l} = \cos \phi \quad .$$

Therefore,

$$U_c = \frac{1}{4} \frac{1}{cB^4} (0.25 + B^2)^2 \left(\frac{\sigma R}{Et} \right)^2 EB\Delta^2 t^3 \quad . \qquad (3.2.4)$$

The elastic energy of the middle spiral is:

$$U_T = \frac{1}{2} \left(\frac{T}{2} \right)^2 \frac{l'}{AE} \qquad A = dt$$

$$= \frac{1}{32} \frac{(0.25 + B^2)^{\frac{1}{2}}}{B^4} \frac{k}{c} \left(\frac{\sigma R}{Et} \right)^2 EB\Delta^2 t^3 \quad . \qquad (3.2.5)$$

Upon normalization with respect to $EB\Delta^2 t^3$ and linearization of c, Eqs. 3.2.4 and 3.2.5 become

$$\frac{U_c}{EB\Delta^2 t^3} = \frac{1}{2}\frac{(0.25 + B^2)^2}{B^4}\frac{1}{(1-k)n^2}\left(\frac{\sigma R}{Et}\right)^2 = U_c^* \quad , \quad (3.2.6a)$$

and

$$\frac{U_T}{EB\Delta^2 t^3} = \frac{1}{16}\frac{(0.25 + B^2)^{\frac{1}{2}}}{B^4}\frac{k}{(1-k)n^2}\left(\frac{\sigma R}{Et}\right)^2 = U_T^* \quad . \quad (3.2.6b)$$

3.3. The Minimization Procedure

Define:

$$V^* = U_B^* + U_c^* + U_T^* + W^* \quad .$$

The governing equations become

$$\frac{\partial V^*}{\partial B} = 0 \quad , \quad (3.2.7a)$$

and

$$\frac{\partial V^*}{\partial n} = 0 \quad , \quad (3.2.7b)$$

for prescribed k and σ. In expanded form, these equations are:

$$\frac{\partial V^*}{\partial B} = b\left(\frac{-1}{4B^5} - \frac{1}{B^3}\right)\left(\frac{2}{(1-k)n^2} - 1\right) + d\frac{(B^2 + 0.25)^{-\frac{1}{2}}}{B^3}\frac{k^2}{16}$$
$$\left(\frac{2}{(1-k)n^2} - 2\right) - d\frac{(B^2 + 0.25)^{\frac{1}{2}}}{B^5}\frac{k^2}{4}\left(\frac{2}{(1-k)n^2} - 2\right)$$
$$+ \left(\frac{\sigma R}{Et}\frac{R}{t}\right)\frac{\pi^2}{8}\frac{k^2}{B^3 n^2} + \left(\frac{(B^2 + 0.25)^{-\frac{1}{2}}}{16B^3} - \frac{(B^2 + 0.25)^{\frac{1}{2}}}{4B^5}\right)\frac{k}{(1-k)n^2}\left(\frac{\sigma R}{Et}\right)^2$$
$$+ 2\left(\frac{(B^2 + 0.25)}{B^3} - \frac{(B^2 + 0.25)^2}{B^5}\right)\frac{1}{(1-k)n^2}\left(\frac{\sigma R}{Et}\right)^2 = 0 \quad , \quad (3.2.8a)$$

and

$$\frac{\partial V^*}{\partial n} = b\left(1 + \frac{1}{16B^4} + \frac{1}{2B^2}\right)\left(\frac{-4}{(1-k)n^3}\right) + d\frac{(B^2 + 0.25)^{\frac{1}{2}}}{B^4}$$
$$\frac{k^2}{16}\left(\frac{-4}{(1-k)n^3}\right) + \left(\frac{\sigma R}{Et}\frac{R}{t}\right)\frac{\pi^2}{8}\frac{k^2}{B^2 n^2} - \frac{1}{8}\frac{(B^2 + 0.25)^{\frac{1}{2}}}{B^4}\frac{k}{(1-k)n^3}\left(\frac{\sigma R}{Et}\right)^2$$

$$- \frac{(B^2 + 0.25)^2}{B^4} \frac{1}{(1 - k)n^3} \left(\frac{\sigma R}{Et} \right)^2 = 0 \quad ; \qquad (3.2.8b)$$

where

$$b = \frac{1}{9(1 - \nu^2)} \qquad \text{and} \qquad d = \frac{1}{18(1 - \nu^2)} \quad .$$

The parameter k should be very close to one; hence, in Eqs. 3.2.8, all reference to k other than in the $(1 - k)$ form will be dropped. These equations can be further simplified in form by introducing the following symbols, which are compatible with Fortran coding:

$$A = b \left(- \frac{1}{4B^5} - \frac{1}{B^3} \right)_1 \qquad BB = d \frac{(B^2 + 0.25)^{-\frac{1}{2}}}{16B^3}$$

$$C = - d \frac{(B^2 + 0.25)^2}{4B^5} \qquad D = \left(\frac{\sigma R}{Et} \frac{R}{t} \right) \frac{\pi^2}{8B^3}$$

$$E = \frac{(0.25 + B^2)^{-\frac{1}{2}}}{16B^3} - \frac{(0.25 + B^2)^{\frac{1}{2}}}{4B^5} \qquad F = \left(\frac{\sigma R}{Et} \right)^2$$

$$G = 2 \left(\frac{(0.25 + B^2)}{B^3} - \frac{(0.25 + B^2)^2}{B^5} \right)$$

$$H = b \left(1 + \frac{1}{16B^4} + \frac{1}{2B^2} \right) \qquad J = d \frac{(B^2 + 0.25)^{\frac{1}{2}}}{16B^4}$$

$$K = \left(\frac{\sigma R}{Et} \frac{R}{t} \right) \frac{\pi^2}{8B^2} \qquad L = - \frac{(0.25 + B^2)^{\frac{1}{2}}}{8B^4}$$

$$M = - \frac{(0.25 + B^2)^2}{B^4}$$

Thus, Eqs. 3.2.8 become

$$\frac{\partial V^*}{\partial B} = A \left(\frac{2}{(1 - k)n^2} - 1 \right) + BB \left(\frac{2}{(1 - k)n^2} - 2 \right)$$

$$+ C \left(\frac{2}{(1 - k)n^2} - 2 \right) + \frac{D}{n^2} + \frac{F(E + G)}{n^2(1 - k)} = 0 \qquad (3.2.9a)$$

and

$$\frac{\partial V^*}{\partial n} = H \left(\frac{-4}{(1 - k)} \right) + J \left(\frac{-4}{(1 - k)} \right) + K + \frac{F(L + M)}{(1 - k)} = 0 \quad .$$

(3.2.9b)

It was previously stated that the equilibrium equations served to define n and B for prescribed k and σ. The parameter B appears

in Eqs. 3.2.9 in a very complicated fashion; hence, the following procedure was adopted. Solving each equation for $(1 - k)$ there results

$$(1 - k) = \frac{2(A + BB + C) + F(E + G)}{n^2(A + 2BB + 2C) - D} , \qquad (3.2.10a)$$

and

$$(1 - k) = \frac{4H + 4J - F(L + M)}{K} . \qquad (3.2.10b)$$

Upon equating these equations one obtains

$$n^2 = \left(\frac{[2(A + BB + C) + F(E + G)]K}{4H + 4J - F(L + M)} + D \right) \frac{1}{A + 2(BB + C)} . \qquad (3.2.11)$$

Thus, for prescribed B, the parameter n was obtained from Eq. 3.2.11, and k was determined from Eq. 3.2.10b. A program was written to evaluate these equations over the range $0.1 \leq B \leq 0.75$ using B increments of 0.01. The results showed that the neglect of k in Eqs. 3.2.8 was justified. For example, when $\sigma R/Et = 0.1$ and $R/t = 1000$, B values of 0.45, 0.40, and 0.35 gave values for $(1 - k)$ of 0.0045, 0.0048, and 0.0052 respectively.

CHAPTER 4

RESULTS AND CONCLUSIONS

4.1. Results

Because of the failure to enforce a periodicity constraint on the mapping functions, it was noted that the parameter k would have to be prescribed. Rather than prescribe k, the computations were simplified by assigning B and calculating the corresponding k and n. Figures 30 to 38 contain a summary of the results.

The parameter B appears as a constant in the various graphs. Equation 3.2.9 was not valid for $B \geq 0.53$ because the solution for n^2 became negative. The wave number n reached a maximum value at $B \doteq 0.31$. The significance of these points is not clearly understood. However, it is noted that experiments do not, in general, show $B > 0.5$ if the buckling occurs periodically over the entire surface; the model, hopefully, reflects this fact. The exact solution for the periodic buckle pattern would, by comparison to experiment, yield $B < 0.5$. It would seem that the procedure used by Hoff, et. al., (12) (They termed their method of solution the von Kármán-Tsien-Legget procedure) produces $B > 0.5$ in order to prevent the axial stress due to deep deflections from becoming tensile. It should be emphasized that the axial wave length of Hoff, et. al., is

approximately six times that indicated by experiment. Recently, Jones (16) has carried through the von Kármán-Tsien-Legget procedure for prescribed n; it would be of interest to prescribe, instead, $B \doteq 0.5$, vary n, and to then take note of whether this procedure would force a larger number of buckles in order to decrease the deep deflection stresses. Similarly, it might be of value to revert completely to the original procedure advanced by von Kármán and Tsien (8, 1941): prescribing both n and B. At present no conclusion can be drawn regarding the maximum value of n; however, mathematically, one expects a unique point, such as a maximum value of n, to occur on a $\sigma R/Et$ = constant line; but where it should occur is not clear.

It was observed that for all but the highest R/t considered, the c value computed using $B = 0.5$, was excessively small and did not correspond to experimental values; thus, it was decided that for the purposes of comparison with other theoretical and experimental results, the results for $B = 0.31$, 0.35, 0.40, and 0.45 would be considered.

In Eq. 3.2.8, n^2 and t/R were not related so that all reference to n^2 and t/R - other than in $\sigma R/Et$ - could be grouped into the dimensionless parameter n^2t/R; consequently the calculations were carried through for distinct values of R/t. This is in contrast to the common procedure as used by Hoff, et. al., (12). The R/t values considered were $500 \leq R/t \leq 5000$ in increments of 500.

Further consideration of Eq. 3.2.9b revealed that $\partial^2 V/\partial n^2 = 0$ (computation showed $\partial^2 V/\partial B^2 > 0$), so that the Hessian determinant is negative, which indicates, unfortunately, that the procedure yields unstable equilibrium configurations. It is possible that this is related to the essentially unstable results of Hoff, et. al., (12) where it was noted that $\sigma R/Et$ decreased continuously as the number of terms retained in the w function increased. The nature of the conclusions of Hoff, et. al., will be further discussed.

The comparison of computed results with experimental results is made difficult by the nature of the experimental results and the nature of the theoretical assumptions. By way of example, let us consider the experiments of Thielemann (21) (see Fig. 14). Thielemann's experiments yielded tier-type, approximately square, buckles and there would seem to be little doubt that the unbuckled material served to restrict the rotation of the diamond flats and so decreased the axial shortening from that which one would expect for periodic buckles over the entire surface as assumed in theory. Yet, it was noted when discussing Fig. 14, that Almroth's and Kempner's axial shortenings compared favorably with Thielemann's experimental results. It would seem that this comparison is fortuitous. Almroth (11) stated that his n was less than Thielemann's experimental value; indeed, from Hoff, et. al., (12), Case 3 at $e = e_{cl}$ yields $n \doteq 5$. This low value of n should serve to increase e. From Hoff, et. al., it is further seen that Almroth had a μ value of approximately 0.2, that is to say, his axial wave length is about five times larger than that indicated by experiment.

Thus, a wave length which is too large, has combined with a wave number which is too small, to yield results comparable to tier-type, approximately square, buckles, whose axial shortening has been restricted by the adjacent material. It is apparent from Yoshimura's (15) approximate formula for the ideal case

$$e = \frac{\pi^2}{8}\frac{\mu^2}{n^2} \quad ,$$

that, for $\mu = 1$, the axial shortening is severe. Using $n = 7$ (which corresponds to Jones' (16) value for $R/t = 788$ and $\sigma R/Et = 0.1$) and $\mu = 1$, there results $e = 0.0255$, which bears no comparison to the e_{cl} value (see Fig. 14, $e = e_{cl}$), which is 0.00078. However, replacing μ by 0.2 reduces e to 0.00102 which is comparable to the classical value. As previously discussed, this small value of μ is necessary in order to prevent the development of axial tension stresses.

Let us consider the series of graphs in Fig. 32a, b, c, d, and e. These graphs show that $\sigma R/Et$ decreases as n decreases and thus indicate the unstable nature of the equilibrium with respect to n. It is noted that the use of n as a continuous variable has allowed the prescription of $\sigma R/Et$ values which required $n < 2$ in order to obey the equilibrium equations. The value $n \geq 2$ is physically necessary in order that the solution may be associated with the problem of a closed cylinder; indeed, stable equilibrium would seem to demand $n \geq 3$, since $n = 2$ is a hinge and would appear to be naturally unstable. It is clear that n increases as R/t increases for a prescribed $\sigma R/Et$. Further, as noted above, n

increases with $\sigma R/Et$; this is confirmed by the experiments of Thielemann (21). Table 1 gives a comparison of the results of this thesis with the experiments of Thielemann (21). For a given n, the minimum value of the experimental load obtained by Thielemann is quoted. In Table 1 there are three computed values of n given: n_2 is the non-integer value associated with the load of Thielemann, while n_1 and n_3 are the closest integer values. For $\sigma R/Et = 0.1$

Table 1

Comparison to Thielemann's Experiments

$\frac{R}{t}$	Thielemann		$\frac{\sigma R}{Et}$	B					
	$\frac{\sigma R}{Et}$	n		0.45			0.40		
				n_1	n_2	n_3	n_1	n_2	n_3
788	.119	14	.109 .119 .14	7	7.18	8	8	8.8	9
	.109	13	.08 .109 .14	6	7	8	8	8.4	9
	.100	12	.08 .100 .109	6	6.55	7	7	7.8	8
	.0763	11	.06 .0763 .08	5	5.96	6	6	7	8
	.066	10	.056 .066 .08	5	5.35	6	5	6.5	7

Jones (16, 1966) obtained $n = 7$. No comparison can be made with the results of Hoff, et. al., (12) since their solution lies below the values of the loads quoted. It is observed that the experimental values of n exceed the calculated values. Further comparison is possible with the very refined experiments of Almroth, Holmes, and Brush (31). For an R/t value of 850, these investigators obtained post-buckling loads of 0.08 to 0.1, with the number of buckles varying from 8 to 12. For $\sigma R/Et = 0.08$, the method of calculation used in this thesis yields $n = 8.15$, 8.1, 7.5 and 6.3 corresponding to B values of 0.31, 0.35, 0.40 and 0.45. Similarly, for $\sigma R/Et = 0.1$ the values obtained were $n = 9.15$, 9.1, 8.4, and 7. Hoff, et. al., (12) obtained a minimum $\sigma R/Et$ of 0.0427. The value of μ was about 0.17 (this is to be compared to the experimental value of 1), and for $R/t = 1000$, the value of n was close to three. The calculations of this thesis, applied to the same case, yielded $n = 6.6$, 6.5, 5.9, and 4.9 for B values of 0.31, 0.35, 0.40, and 0.45.

The fact that n decreases to a value less than two would seem to correspond to the results of Hoff, et. al., (12). Suppose one applies the results of Hoff, et. al., to a specific R/t; then it is required that, in order for the solution to correspond to that for a closed cylinder, there exist the relation

$$\eta = n^2 t/R \geq 2^2 t/R .$$

Thus, if the calculated value of η is less than this bound, the equations are giving a value of n less than two and the solution can no longer be identified with the problem of a closed cylinder. In

the light of the fact that the computations of Hoff, et. al., give, in this authors opinion, decreasing values of n as the number of parameters is increased, let us return to the paper of Hoff, et. al. The synopsis states in part: "The results of the computations as well as theoretical considerations indicate that the solution for long shells of the von Kármán-Donnell equations with the aid of the von Kármán-Tsien-Legget procedure leads in the limit to the trivial solution in which the amplitudes of the displacements tends to zero, the number of waves around the circumference tends to infinity, and the average axial compressive stress capable of maintaining equilibrium in the post-buckling state tends to zero." This would not appear to agree with the ideas presented above, and in this authors opinion, cannot be deduced from the von Kármán-Tsien-Legget approach. It is the opinion of this author that Hoff, et. al., used the following line of reasoning. They first required that the values of the strains computed from the Donnell equations approach the exact; this required that n tend to infinity. That n tended to infinity then agreed with the result that

$$\mu = l_y/l_x = 2\pi R/2nl_x$$

decreases to zero. Next, since n has been allowed to tend to infinity and since the von Kármán-Tsien-Legget procedure yielded that

$$\eta = n^2 t/R$$

approach zero, then it was required that t/R go to zero. It is noted that here Hoff, et. al., used the argument $n \geq 2$; however, n tending to infinity is needed for the exactness of the geometric relations. Last, it was observed that the von Kármán-Tsien-Legget procedure gave

$\sigma R/Et$ decreasing to zero. Thus the von Kármán-Tsien-Legget approach does not yield the solution that n goes to infinity; rather, this would appear to be an arbitrarily introduced constraint to force exactness in Donnell's geometric relations. It should be observed that allowing l_x to increase and n to decrease can give the solutions of μ and η tending to zero; this argument is independent of t/R and uses only the results of the von Kármán-Tsien-Legget procedure. Certainly, Fig. 15a does not indicate that, as $\sigma R/Et$ decreases to zero, eR/t also decreases to zero, as would be required if n increased to infinity. Let us further consider the conclusion of Hoff, et. al., that: "In the limiting case n approaches infinity, the amplitude of the displacements tends to zero, the von Kármán-Donnell equations are rigorously valid, the t/R approaches zero, and the value of average axial stress capable of maintaining equilibrium in the post-buckling state is zero." Since, in their opinion, n tends to infinity, it would seem that the authors are unable to specify t/R; yet, the von Kármán-Donnell equations are written for a specific t/R. The conclusion would therefore seem to be that $t = 0$. With $t = 0$, the governing partial differential equations are no longer the von Kármán-Donnell equations subject to $w \in C^8$ but could be, say,

$$G_{\alpha\beta} - g_{\alpha\beta} = 0 \quad ,$$

the solution of which allows discontinuities of slope and curvature and whose solution does not demand that n go to infinity. The ideal diamond shape is a valid solution to the new system of equations with $n \geq 2$.

The simple model proposed in this thesis has aided in explaining the essentially unstable results of Hoff, et. al., (12). Previously, it was noted that $\partial^2 V/\partial B^2$ was positive; thus, if rather than employing the equation $\partial V/\partial n = 0$, one instead followed the method of Madsen and Hoff (27, 1965) and prescribed n (at the values found in this thesis), then stable configurations would be obtained.

Figures 33a and 33b give the variation of axial shortening for $B = 0.45$ and 0.40. The value of e is calculated from a linearized form of Eq. 3.6 which corresponds to Yoshimura's (15) approximation for the perfect diamond shape and therefore probably gives an e value which is too large. However, purely geometric considerations applied to the ideal experimental periodic buckle pattern, which is extremely flat, would reasonably indicate shortenings close to the values as calculated above. As previously mentioned, the ideal seldom happens and so it is difficult to compare theoretical and experimental values for axial shortening. Hoff, et. al., (12) obtained values comparable to the ideal diamond shape for a given μ and n; but, these results cannot, reasonably, be compared to experiment since their axial wave length was about six times the experimental value.

Figure 34 gives an indication of the maximum lateral deflection for the cases of $B = 0.45$ and 0.40. It is clear that the deflections and rotations are extremely large and as such, careful consideration must be given to including the non-linear effects of u and v in the

strain tensor components. With regard to the large rotations, Hoff, et. al., stated: "Indeed, use of the stress function insures equilibrium in the tangent plane only if the rotations are small." This does not agree with Langhaar (35) who states the stress function can be allowed for almost inextensional buckling. There would appear to be a matter of interpretation here. It is assumed that they mean the tangent plane to the original cylinder. If, indeed, this is so, then Hoff, et. al., have failed to recognize that x and y were used as Lagrangian co-ordinates (otherwise, the volume integrations would have been excessively difficult), and the equilibrium equations are therefore written with respect to a local reference frame based upon the deformed tangent plane, and not the original.

The dependence of c upon $\sigma R/Et$ is given in Fig. 35 for $B = 0.50$, 0.45, 0.40, 0.35, and 0.31; there is no R/t effect in c. As indicated at the beginning of this chapter, $B = 0.50$ yields a value for c which is too small and which would keep all but the highest R/t values plastic. This is undesirable, since a largely elastic configuration was assumed. Further, if one notes that the total spiral width of one buckle is

$$2L = 2(2cR\Delta) = 2c(2R\Delta) \quad ,$$

and that the maximum buckle width is $2R\Delta$, then it is necessary that

$$2c < 1 \quad ,$$

and a more reasonable limit would seem to be

$$2c < 0.50 \quad .$$

Based upon these considerations, $B = 0.35$ and 0.31 give c values which render the geometry extremely approximate in nature.

Pogorelov (14) gave the maximum bending strain as $3t/R$ (virgin state of the material was the undeformed cylinder); he obtained a minimum post-buckling load of $\sigma R/Et = 0.15$ with $B \leq 0.455$. For purposes of comparison with Pogorelov's results, Fig. 30 gives the maximum normal strain for $\sigma R/Et = 0.15$ and 0.10. It is clear that the maximum bending strain calculated in this thesis exceeds that of Pogorelov. The discrepancy may be partly explained by the fact that Pogorelov used the classical wave number. Let us consider the case of $\sigma R/Et = 0.15$ and $R/t = 1000$. Pogorelov computes n from

$$n(t/R)^{\frac{1}{2}} = 0.9 \quad ,$$

which yields

$$n = 28.5 \quad ;$$

while the results of the present thesis give for $B = 0.4$ the value

$$n = 11.3 \quad .$$

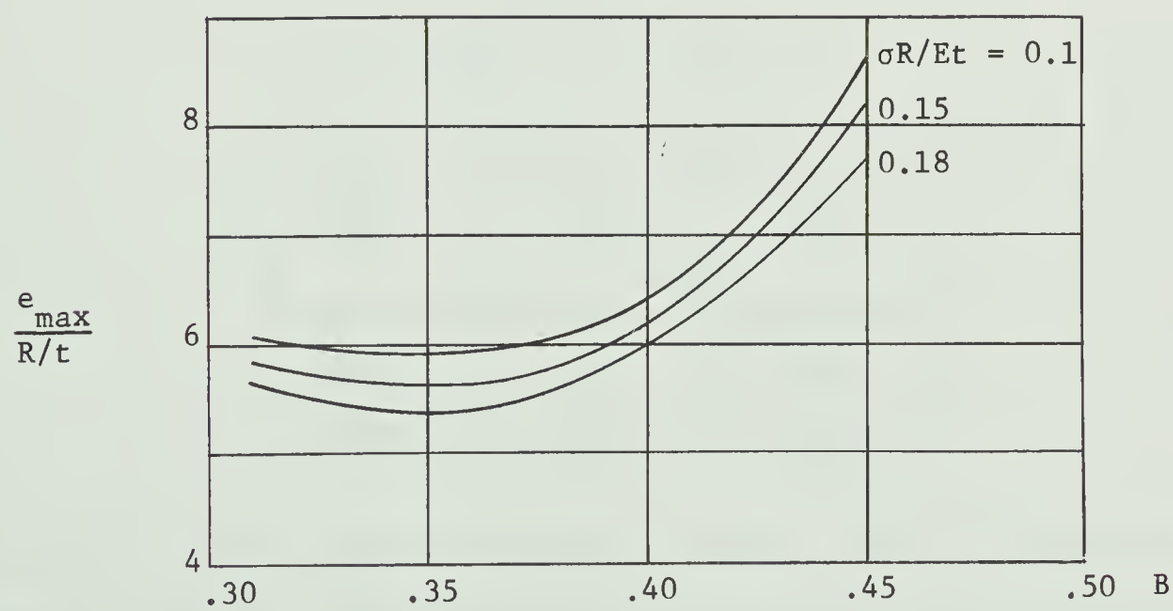

Fig. 30 Maximum Bending Strains

It is therefore clear that the lower n value of this thesis yields higher bending strains. Figure 30 indicates a minimum value of strain at $B \doteq 0.36$. Figure 30 further indicates that B is a very important parameter; a seemingly small change in B results in a considerable change of the maximum normal strain.

Tests were performed using cylinders of $R/t = 950$ (the proportional limit of the material was approximately 68000 p.s.i.), and plastic strain was noted on the ribs as well as, of course, at the singular points. While discussing the topic of plastic strains, it is useful to consider Figs. 36a and 36b which give the elastic energy density for $B = 0.45$ and 0.40 (E was taken as 30.10^6 p.s.i.). For yield point values of 30,000 p.s.i. and 60,000 p.s.i., the limiting values of elastic energy density are 15 p.s.i. and 60 p.s.i., respectively. Table 2 summarizes the minimum value of R/t as needed to maintain an average fully elastic energy density at $\sigma R/Et = 0.10$.

Table 2

Critical R/t values

Yield Point	B	
	0.45	0.40
	R/t	
30000	2150	1900
60000	1100	950

For high R/t, the strains are largely elastic. Figure 37, applied to a case of high R/t (this insures that the correct stress strain law has been used), indicates that at the approximate experimental value

of $\sigma R/Et = 0.1$, the elastic energy is 97% due to bending. This would imply that Yoshimura's (15) comment stating that the bending and membrane energies are comparable is not accurate. This would further justify Pogorelov's (14) procedure and would tend to verify Kennedy's (33) suggestion that the post-buckling configuration be treated as largely inextensional. Indeed, computations which neglected the membrane energy were performed for $R/t = 500$, and it was found that there was no significant change in the results. Figure 36b contains plots of the pre-buckling energy; these plots indicate that the elastic energy increases greatly on buckling. Von Kármán and Tsien (8) had indicated that a release of elastic energy on buckling served to explain the rapidity of the buckling; von Kármán's idea may, however, apply to local buckling. It must of course be remembered when commenting upon Yoshimura's, and von Kármán's statements, that the basis for the criticism is an acknowledged highly approximate model.

It was desired to test what part the flat played in carrying the axial load; it will be recalled that the load was assumed to be carried by a pinned space truss which had the edge and middle spirals as members. Figures 38a and 38b give plots of the rib compressive stress for $B = 0.45$ and 0.40. For low R/t values the compressive stress seems excessive and this would indicate that the flat does participate in carrying the load. If one could devise a loading system that could force an elastic periodic buckle pattern, it would be of interest to employ back-to-back strain rosettes to determine how the

load is carried through a typical buckle. An experimental study (using steel shells of $R/t = 950$ and proportional limit of 68000 p.s.i.) was initiated with this aim, but it was necessary to abandon the experiments since it was impossible to obtain an elastic configuration. The experiments used a buckle width of $n = 8$ as determined from random buckle patterns. It is therefore clear that if one uses steel shells in such experiments, then higher R/t ratios are needed.

A particularly interesting feature of the model presented in this thesis is the nature of the post-buckling V surface envelope, as determined by prescribing $\sigma R/Et$ and B and solving for n and k in the manner previously described. The envelope is a surface of translation and is generated by translating the line

$$V = \frac{-1}{9(1-\nu^2)} \left[\left(1 + \frac{1}{16B^4} + \frac{1}{2B^2} \right) + \frac{(B^2 + 0.25)^2}{16B^4} \right] \frac{E}{2(R/t)^2}$$

parallel to the n axis in $B - n - V$ space. Figure 31 gives a diagram of this surface. Also shown are the $\sigma R/Et$ = constant lines projected onto the $n - B$ plane. The neutral nature of the V envelope with respect to n is illustrated by Fig. 31; the diagram shows that there exist equilibrium states characterized by constant B and V values and in which n decreases as $\sigma R/Et$ decreases. This conservation of potential is not to be confused with Tsien's [(36, 1942) and (37, 1947)] proposed buckling criterion. Tsien considered V conserved between the pre-buckling and post-buckling configurations for the separate cases of $\sigma R/Et$ prescribed, or e prescribed. Figure 31 is strictly for the post-buckling configuration. Fung and Sechler (38) have stated that Tsien's criterion is not based on sound principles and

have given an example where it fails completely. However, in the present case, V in the post-buckling state is conserved for constant B as an analytical result, as opposed to an enforced constraint.

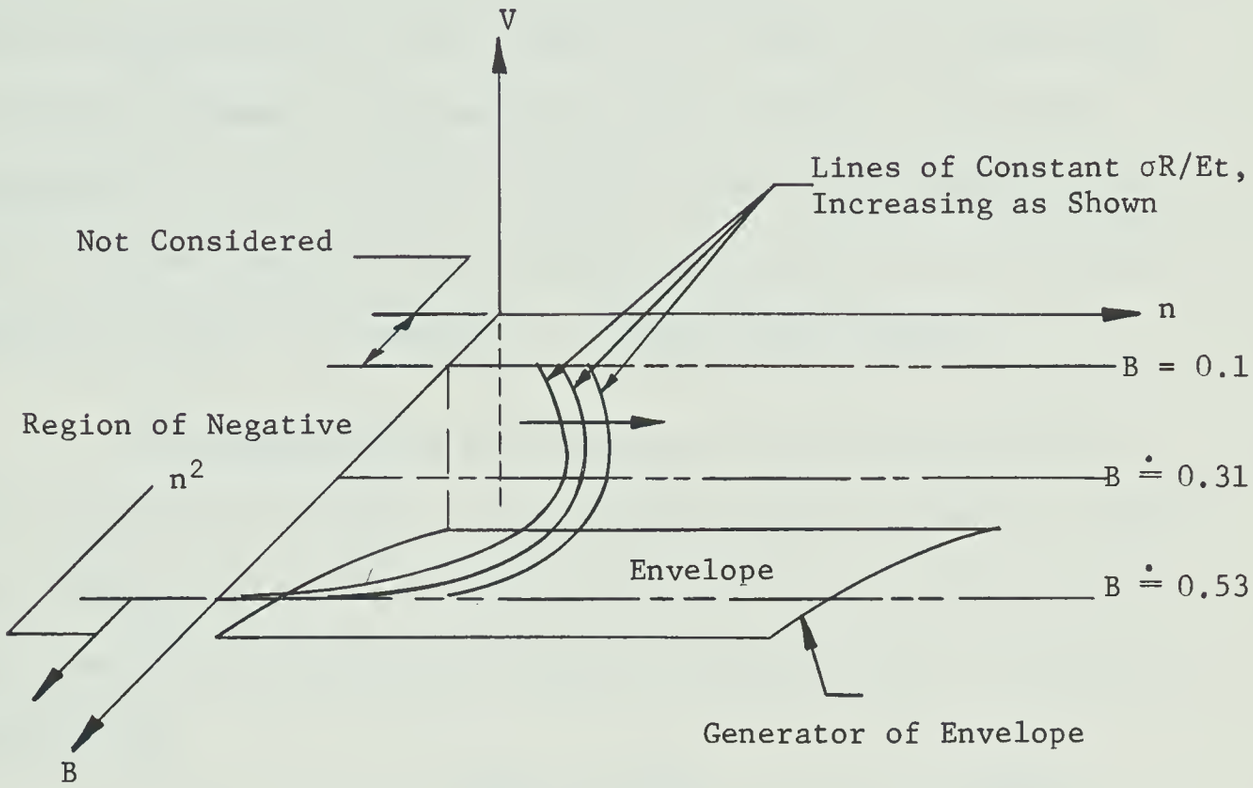

Fig. 31 B-n-V Space, R/t = constant

It is noted that in this thesis no distinction has been made between the equilibrium conditions for $\sigma R/Et$ prescribed and e prescribed. This is not necessary, since one expects a unique functional relationship between e and σ, say, $e = e(\sigma)$; and further one expects the functional relationship can be inverted as would be done by prescribing e and determining $\sigma = \sigma(e)$.

4.2. Conclusions

The author feels that the model used in this thesis has served to illustrate the following points:

1) The model has shown the inherent instability of the system if the only restriction on n is $\partial V/\partial n = 0$; thus, some additional criterion is necessary to determine the value of n. As previously mentioned the lower bound to n must be at least three. By physical argument, the prescription of a $\sigma R/Et$ value which necessitates $n = 2$ can be ruled out, since this load cannot be held in a stable equilibrium configuration, and if $n < 2$, then the solution no longer corresponds to a closed shell problem.

The determination of a criterion to fix the value of n is of the upmost importance. The procedure used by Jones (16, 1966) and by Madsen and Hoff (27, 1965) is considered to be unacceptable. They used the von Karman-Tsien model; the form of the w deflection function was

$$w = \sum_{i=0} A_{i,i} \cos \frac{i\pi x}{lx} \cos \frac{i\pi y}{ly} + \sum_{i=1} A_{2i,0} \cos \frac{2i\pi x}{lx} \quad .$$

The unknowns $A_{i,j}$, n, and μ were determined from the equations

$$\frac{\partial V}{\partial A_{i,i}} = 0 \qquad i > 1 \quad ,$$

$$\frac{\partial V}{\partial A_{2i,0}} = 0 \quad , \qquad \frac{\partial V}{\partial \mu} = 0$$

and

$$n = \text{prescribed} = n_0 \quad .$$

The value of A_{11} was determined from the periodicity constraint on v.

It is most unsatisfying to prescribe n without making it subject to some constraint; further, if one wishes to prescribe n then it also seems reasonable to prescribe μ since experiments indicate that μ is also largely constant in the post-buckling era. It is

therefore suggested that the procedure of Madsen and Hoff (27) be modified to include the prescription of both n and μ but that there be imposed the constraint conditions

$$\frac{\partial V}{\partial n}\Big|_{n=n_0} = 0 \qquad \text{and} \qquad \frac{\partial V}{\partial \mu}\Big|_{\mu=\mu_0} = 0 \quad .$$

The constraint conditions may be considered as equations for, say, A_{22} and A_{33}. The periodicity constraint on v may be used to determine A_{11}. The final set of equations to be solved would be

$$\frac{\partial V}{\partial A_{i,i}} = 0 \qquad\qquad i > 3$$

and

$$\frac{\partial V}{\partial A_{2i,0}} = 0 \quad .$$

The results of such computations, when compared to the results of Madsen and Hoff (27), will indicate the effect of the additional constraints on the solution.

2) The use of a smaller number of variables has eased the analysis and has yielded results comparable to other current methods. The parameter B has been shown to be most important. It is of interest to note that the approximation of middle plane strain energy used in this study indicates values of B much closer to experimental results than are the values of Hoff, et. al., (12). It has been noted that the large axial wave lengths of Hoff, et. al., are necessary to prevent the development of axial tension stresses due to deep deflections.

3) The results indicate that the middle surface deformation is largely inextensional. Further, it has been shown that under the assumption of periodic buckling, the post-buckling elastic energy exceeds

the pre-buckling values at the same $\sigma R/Et$. Indeed, the results indicate that for $\sigma R/Et = 0.1$, 97% of the elastic energy is due to bending.

4) The computations indicate that if periodic buckling is assumed to occur over the entire surface, then plasticity effects must be considered. For example, in Fig. 30, the case $\sigma R/Et = 0.1$ requires, if the yield point is 60,000 p.s.i., that the R/t ratio should exceed 3000 to ensure an essentially elastic configuration.

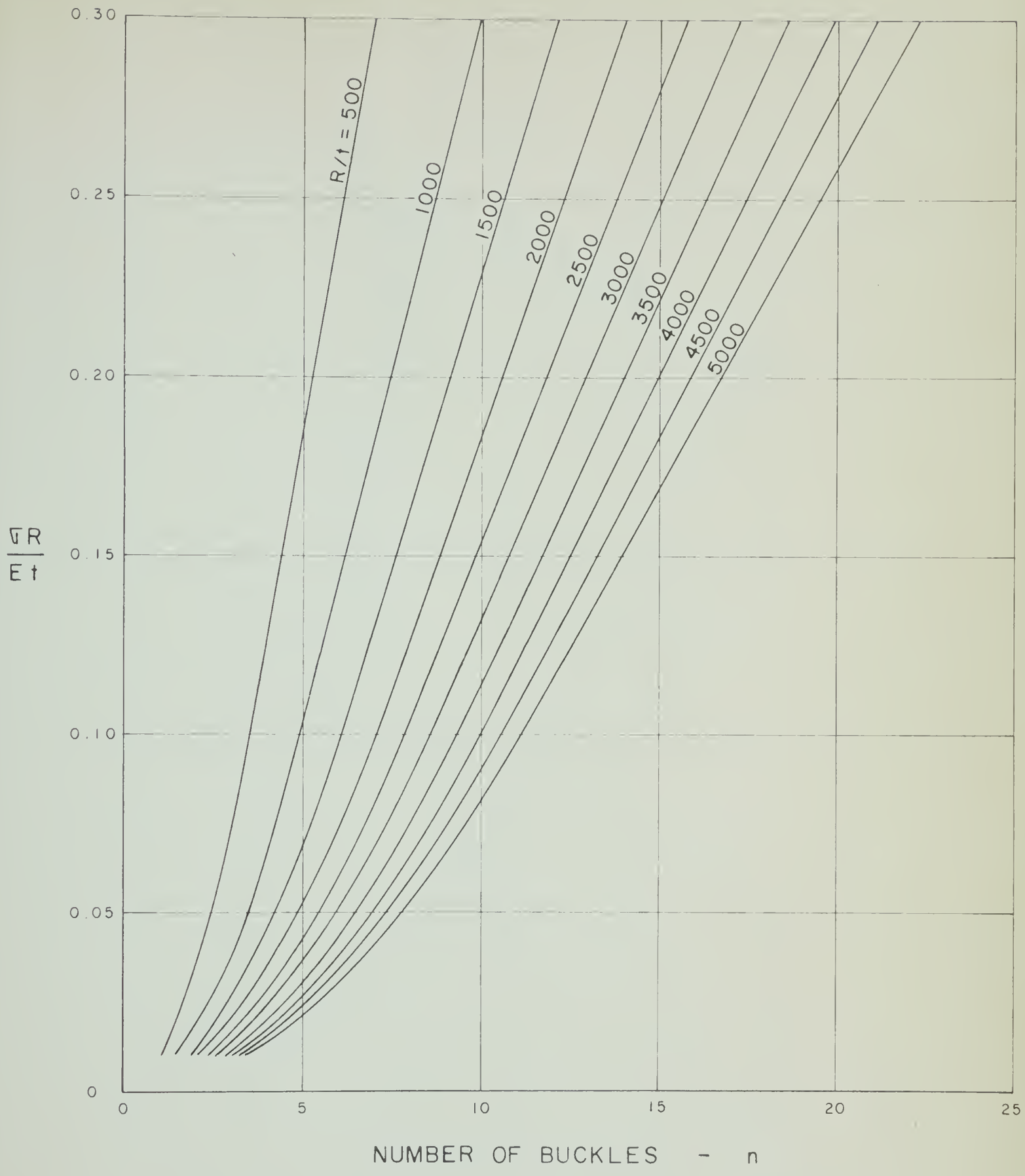

Fig. 32.a - $\sigma R/Et$ VERSUS n - B=0.50

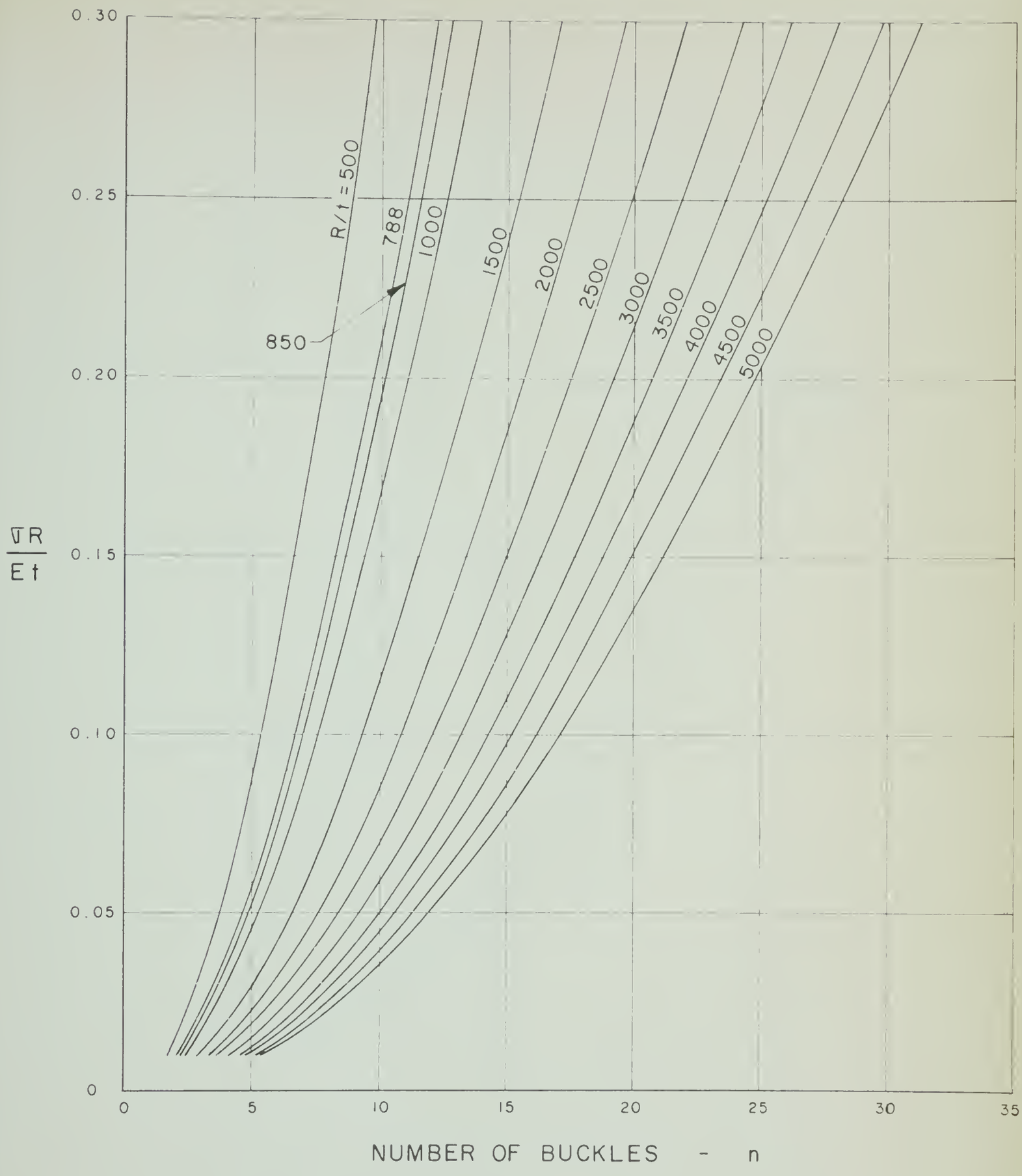

Fig. 32.b - $\sigma R/Et$ VERSUS n - B=0.45

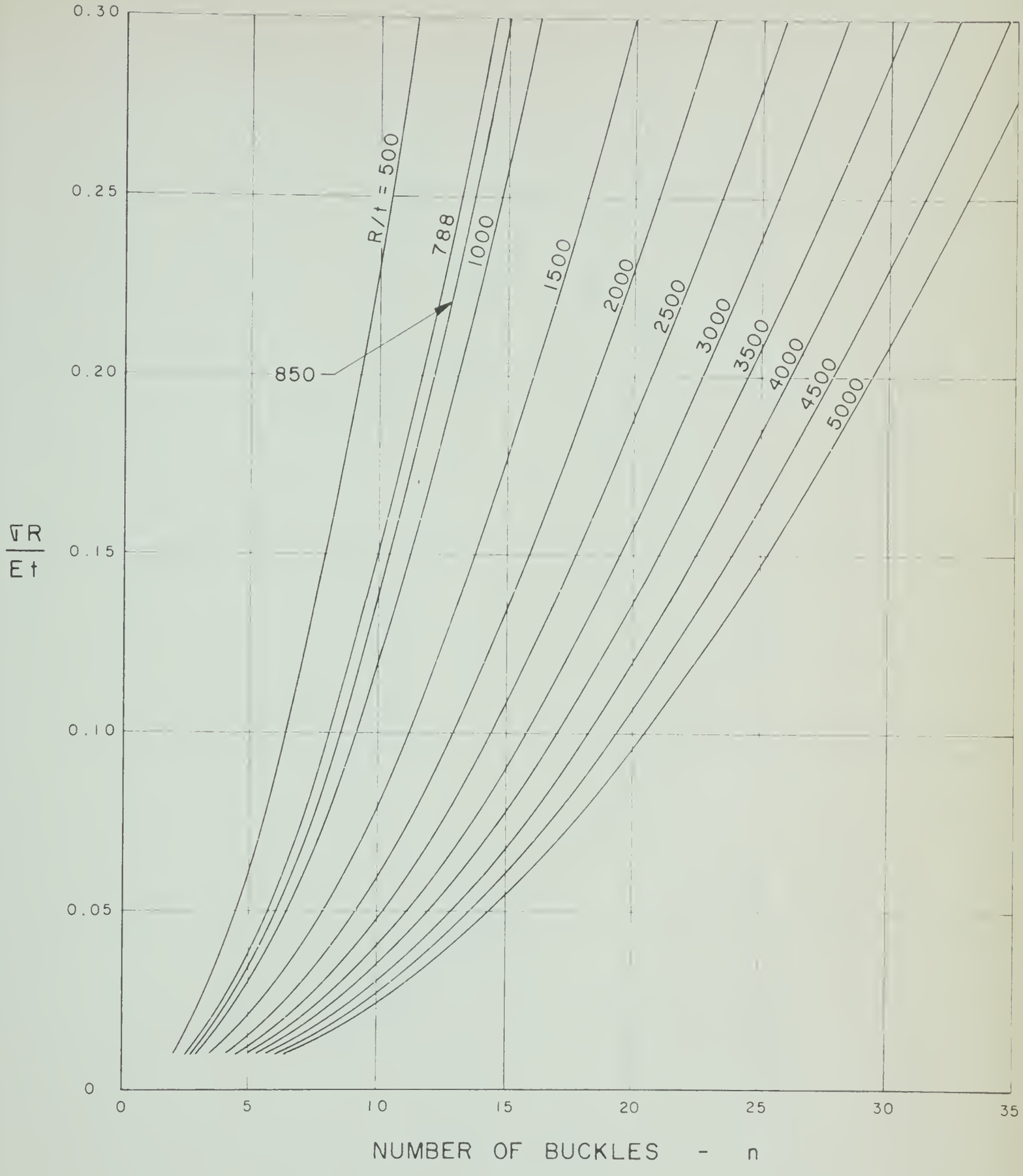

Fig. 32.c - $\sigma R/Et$ VERSUS n - B=0.40

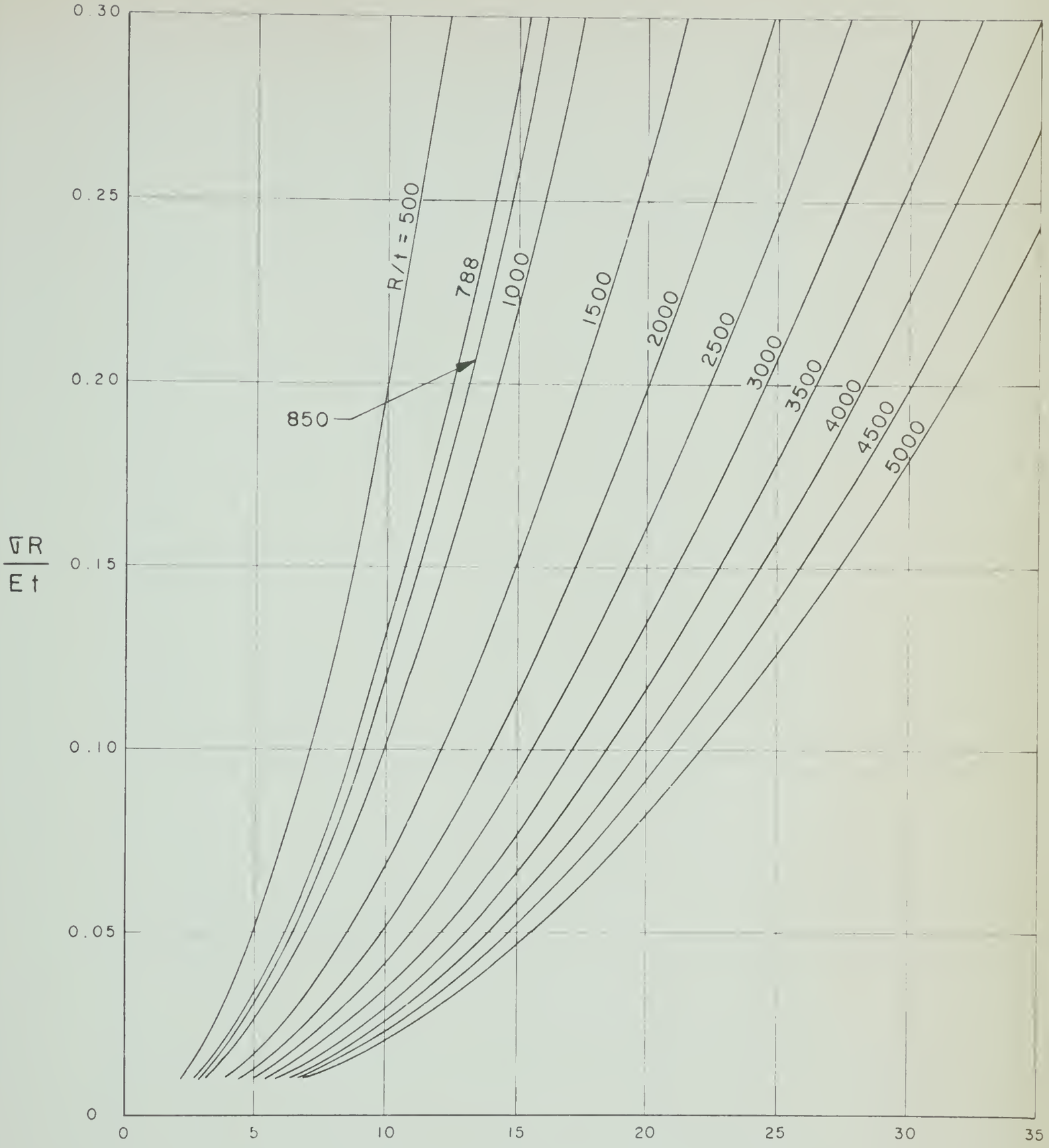

Fig. 32.d - σR/Et VERSUS n - B=0.35

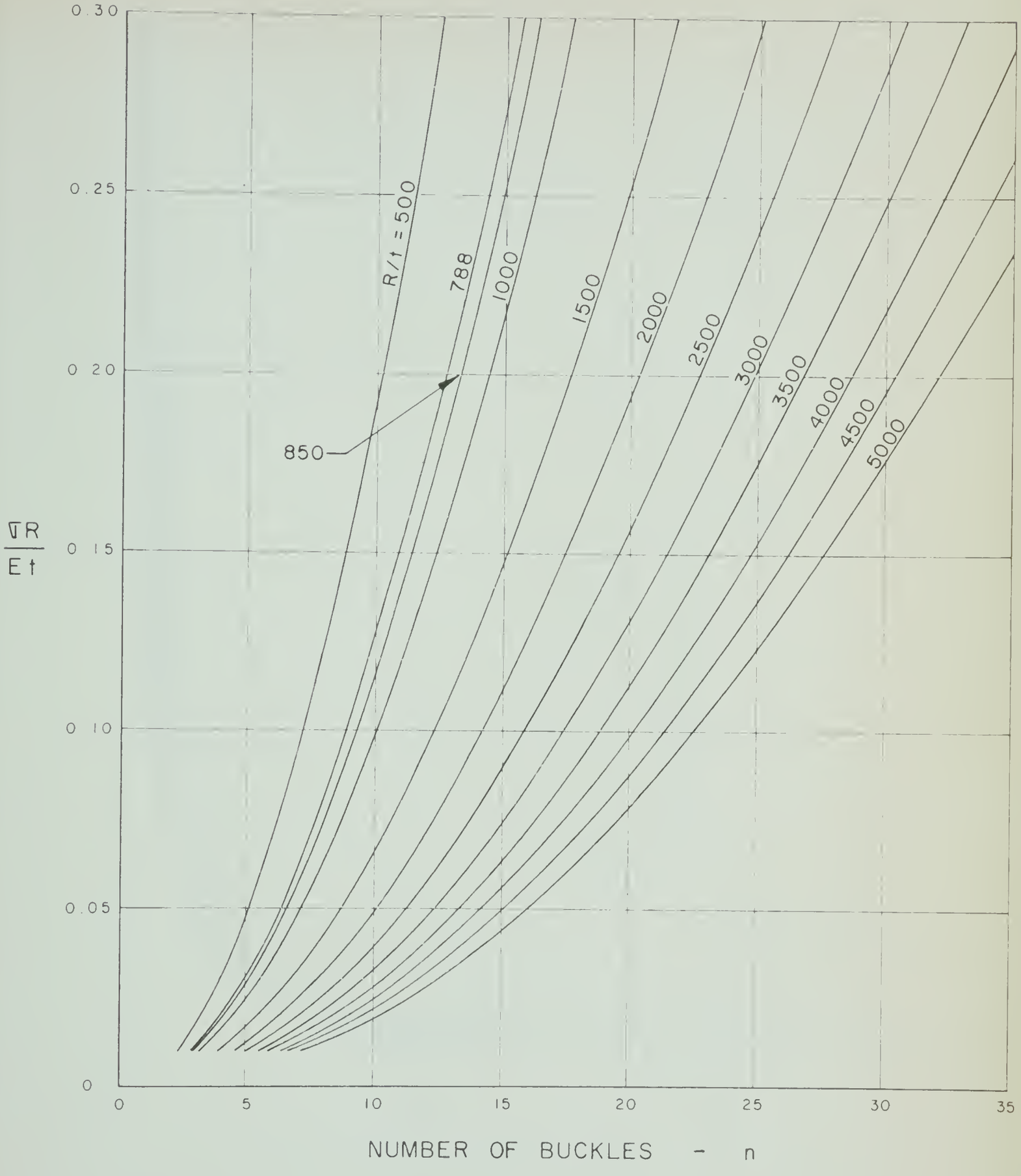

Fig. 32.e - $\sigma R/Et$ VERSUS n - B=0.31

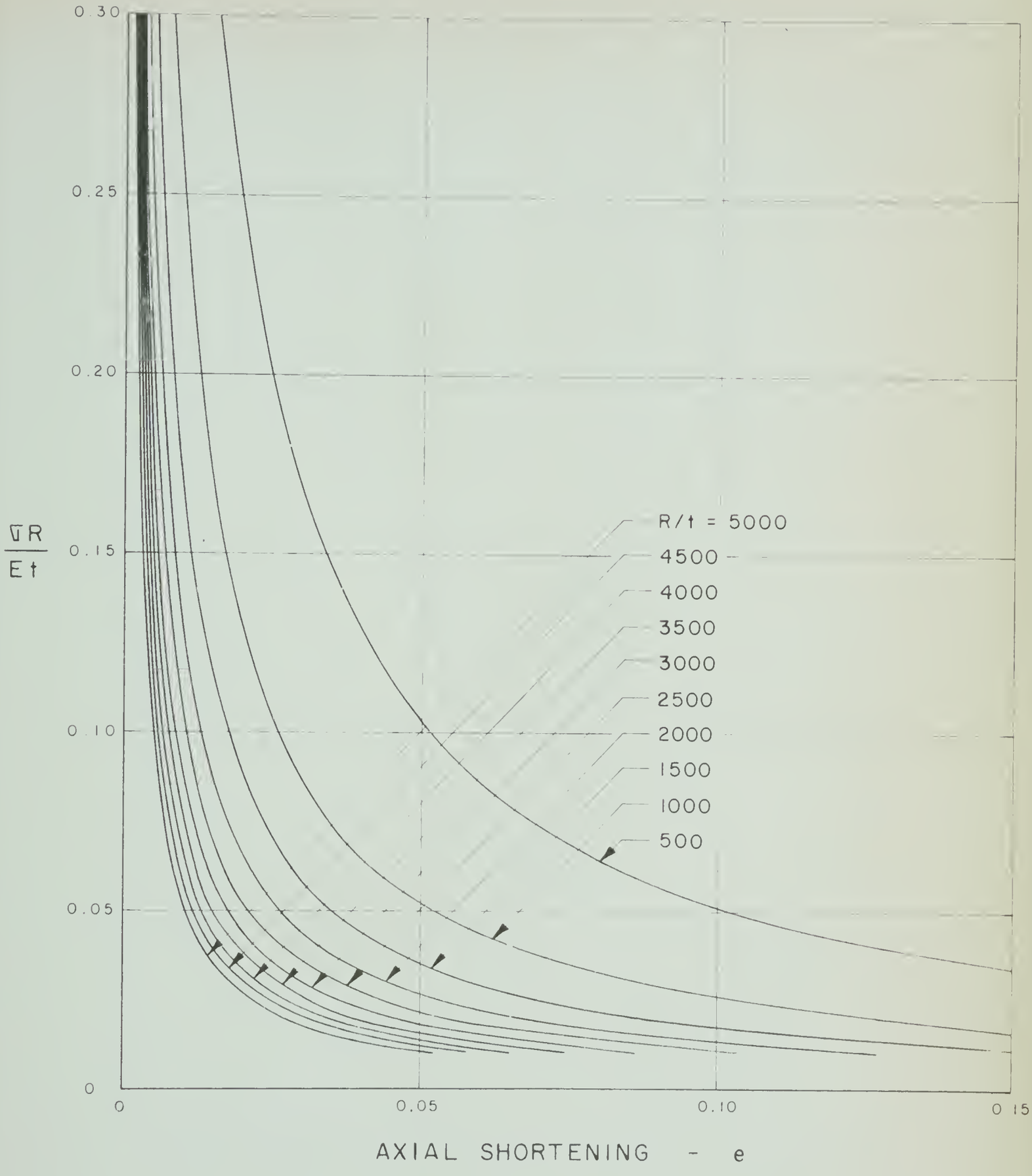

Fig. 33.a - $\sigma R/Et$ VERSUS e - B=0.45

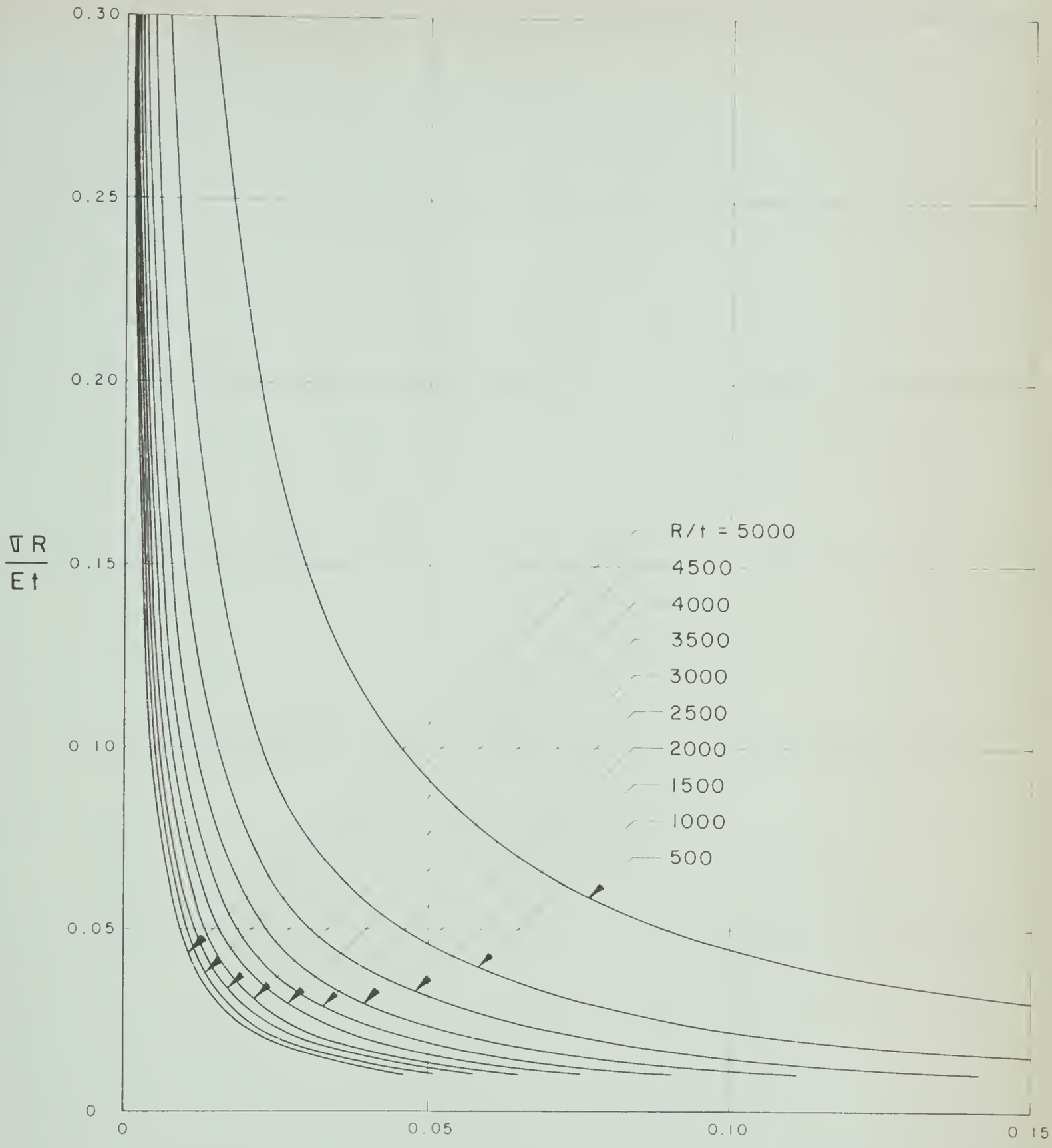

Fig. 33.b - $\sigma R/Et$ VERSUS e - B=0.40

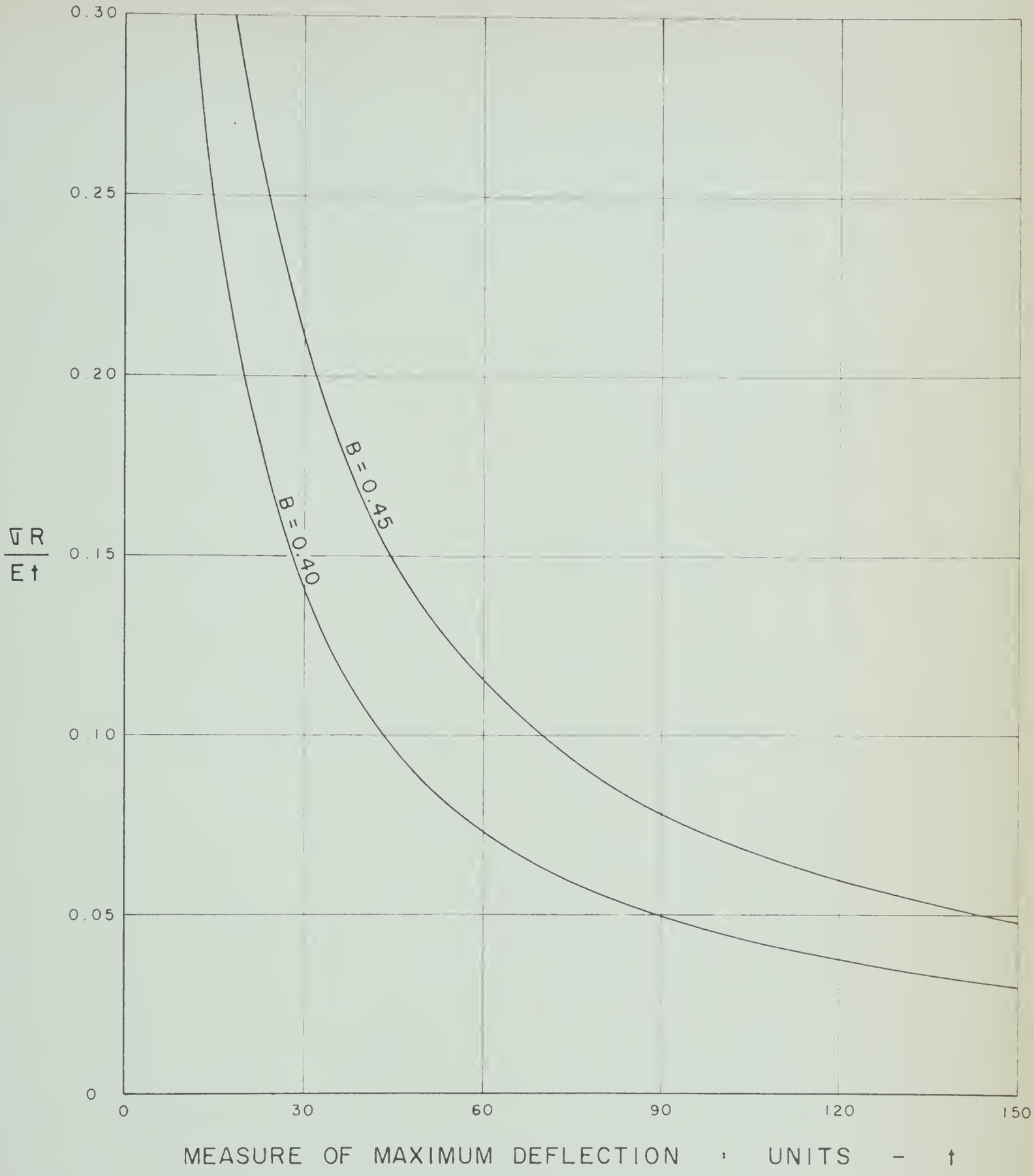

Fig. 34 - $\sqrt{3}R/Et$ VERSUS MAXIMUM LATERAL DEFLECTION

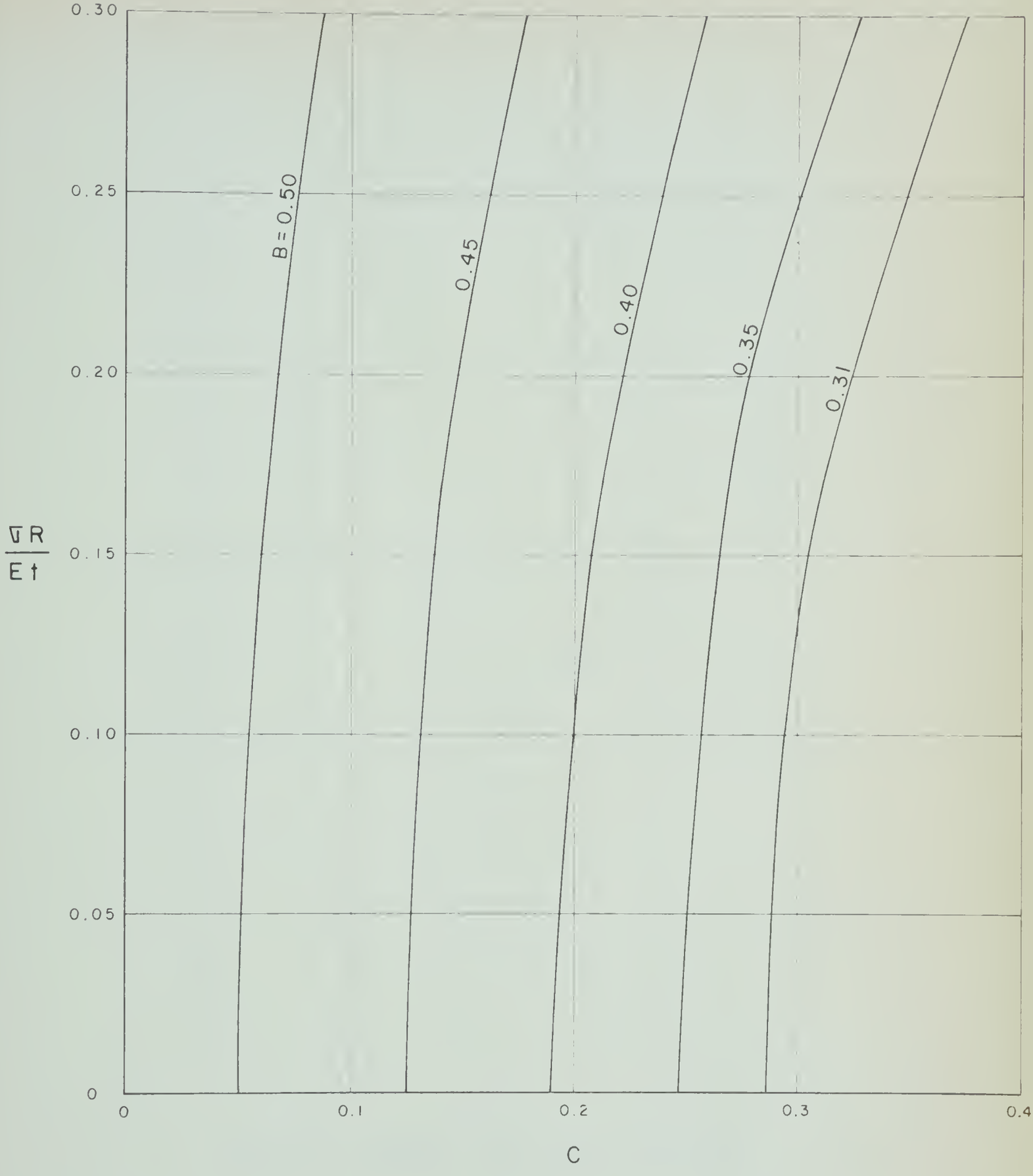

Fig. 35 - $\sigma R/Et$ VERSUS c

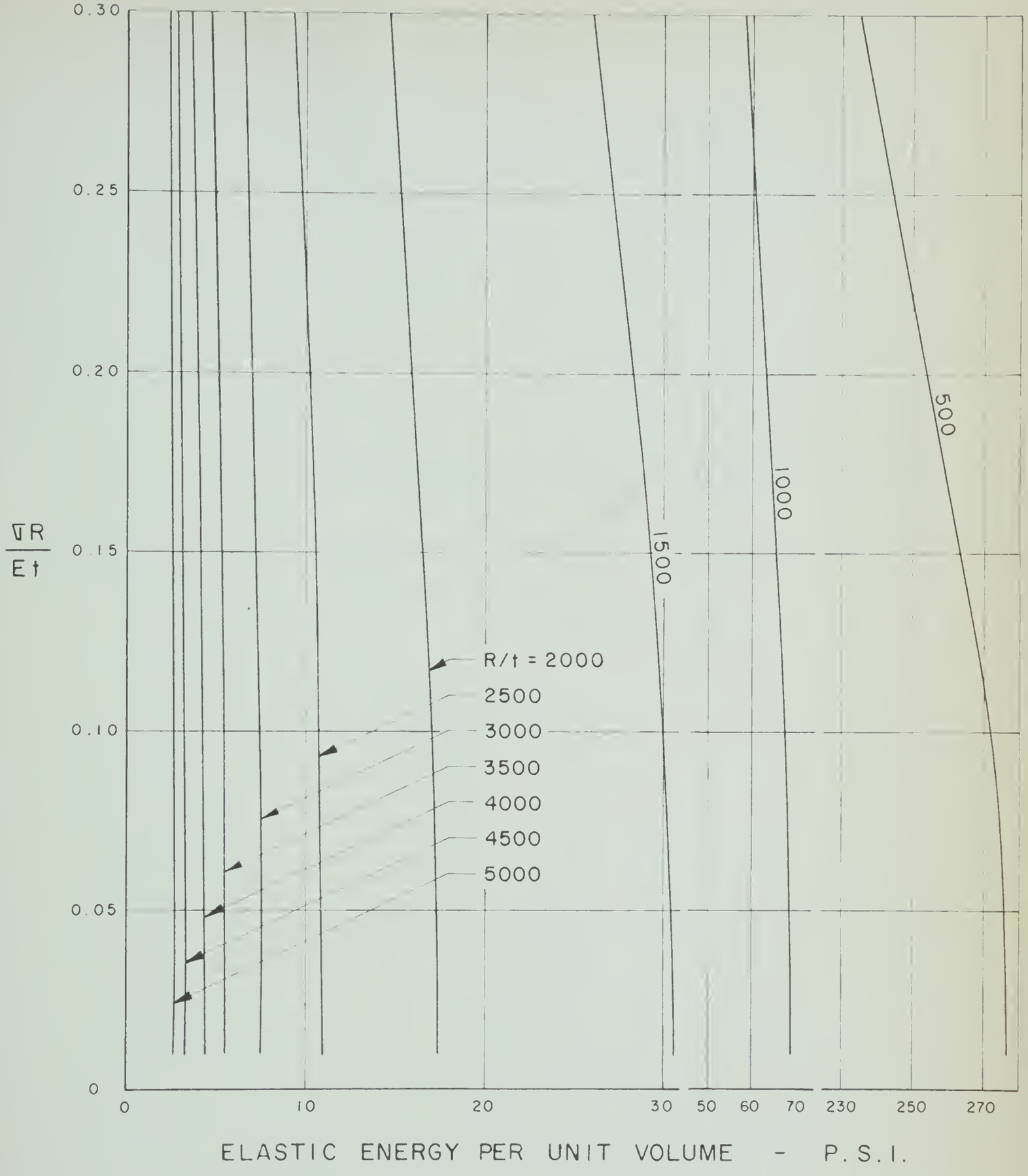

Fig. 36.a - $\sigma R/Et$ VERSUS ELASTIC ENERGY PER UNIT VOLUME - B=0.45

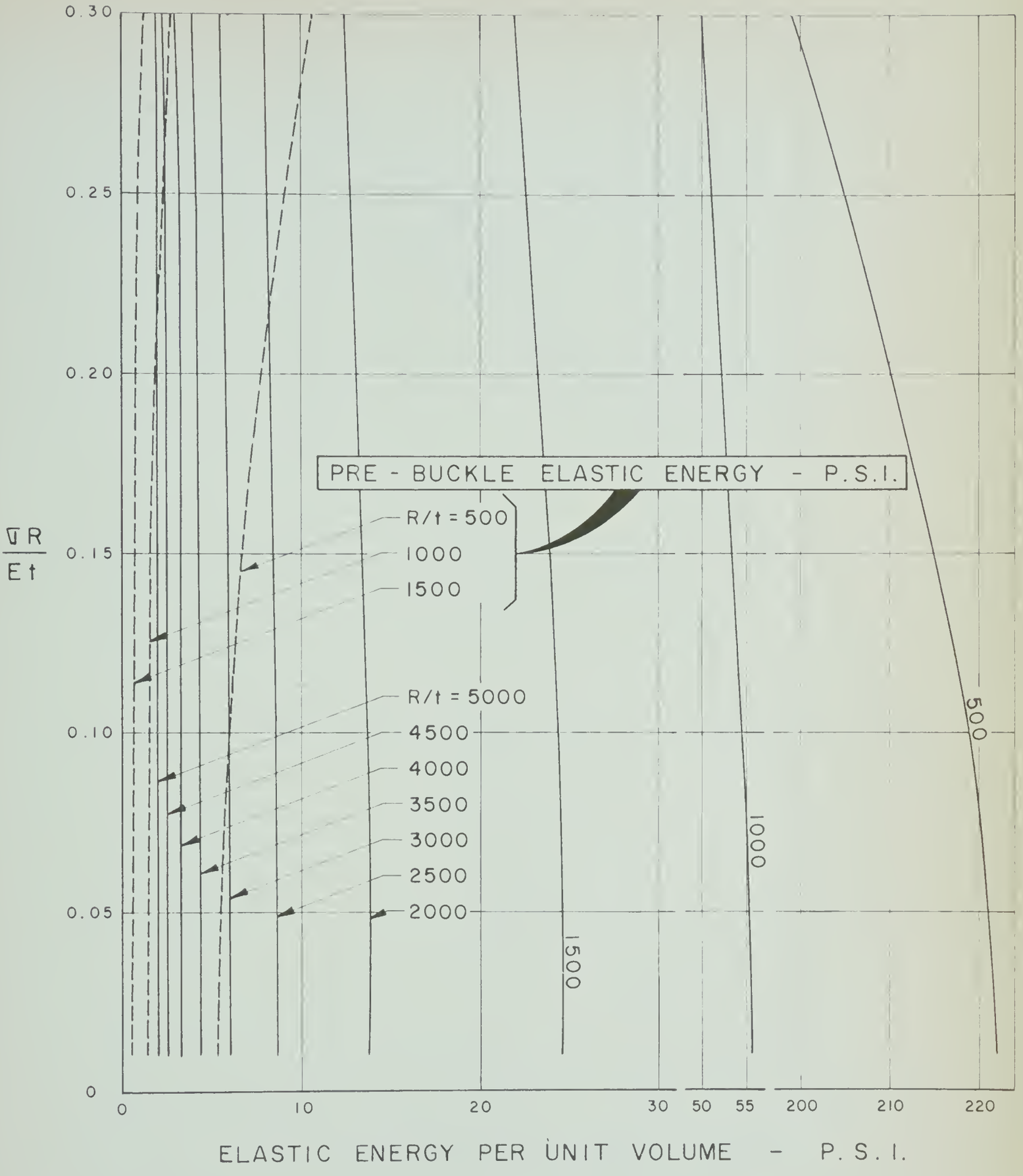

Fig. 36.b - $\sigma R/Et$ VERSUS ELASTIC ENERGY PER UNIT VOLUME - B=0.40

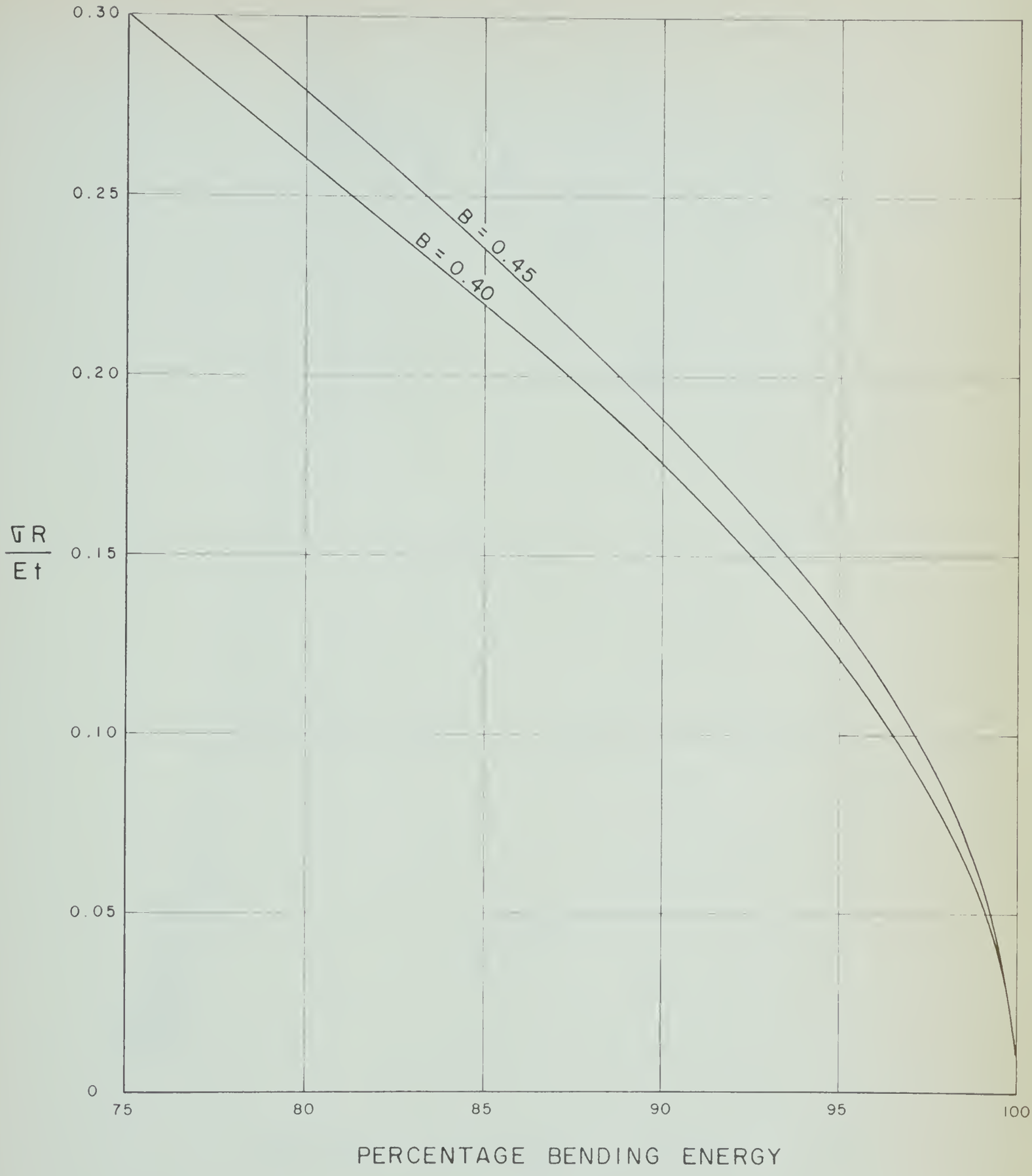

Fig. 37 - σR/Et VERSUS PERCENTAGE BENDING ENERGY

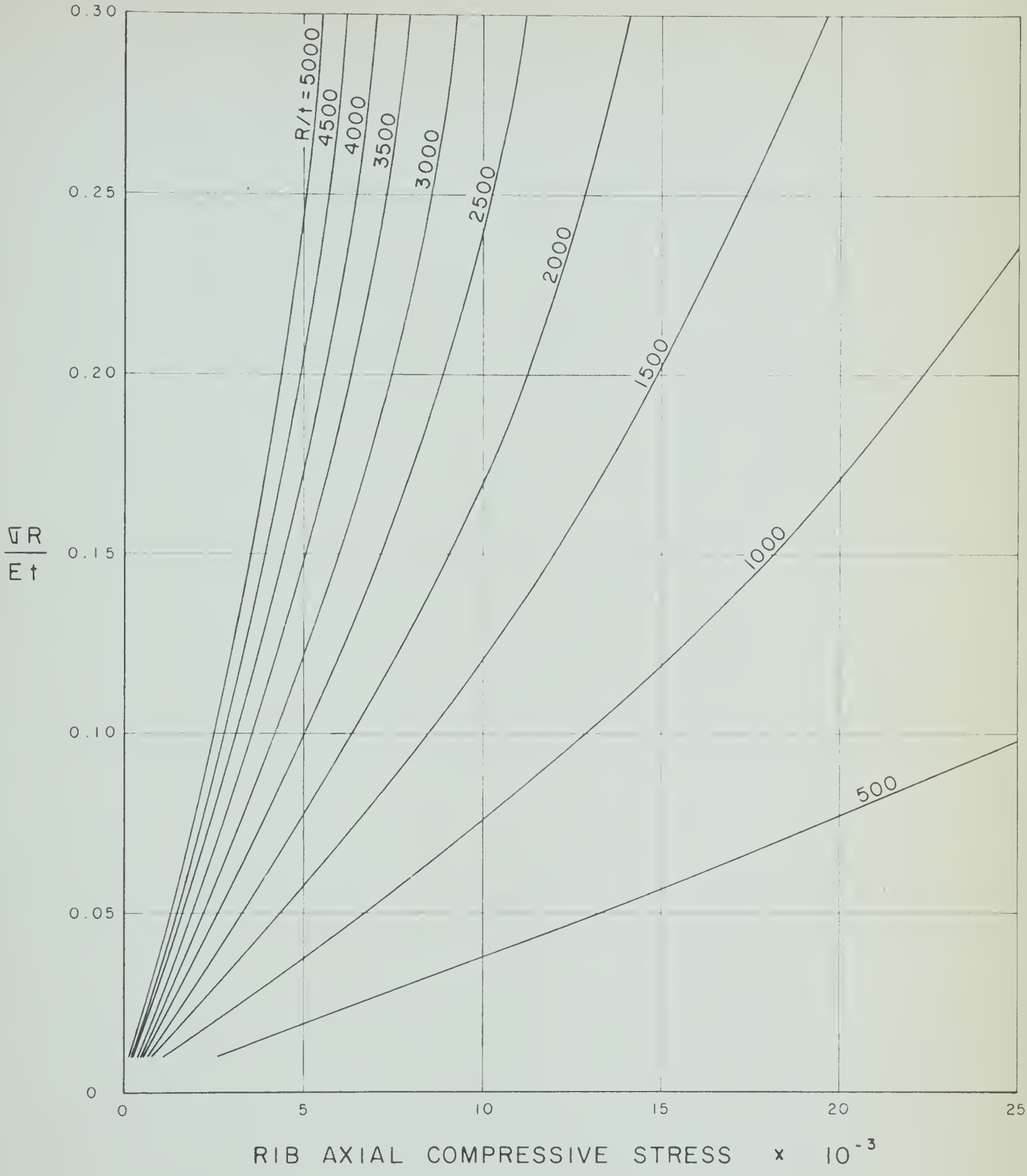

Fig. 38.a - σ_R/Et VERSUS RIB AXIAL COMPRESSIVE STRESS - B=0.45

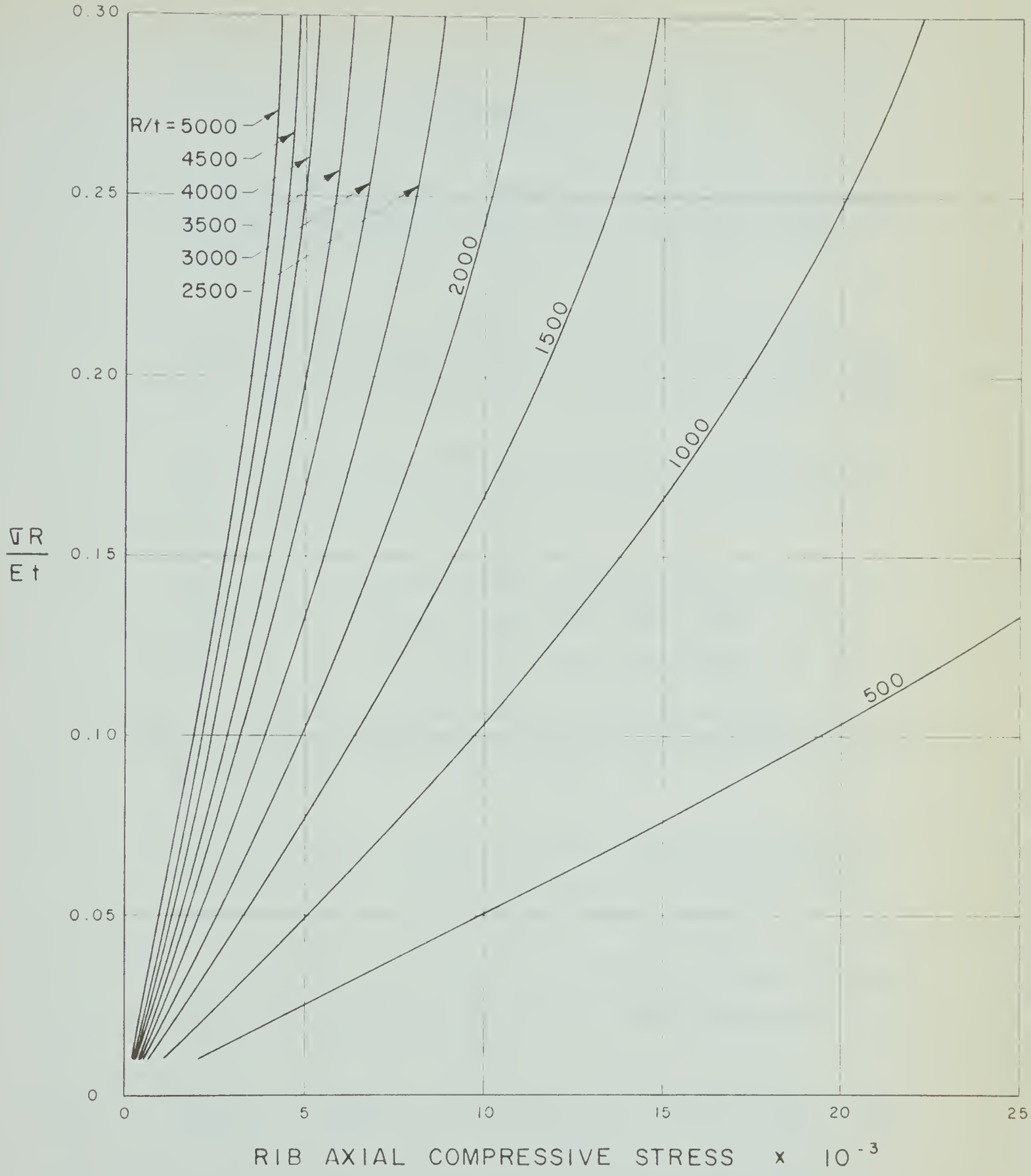

Fig. 38.b - $\sigma R/Et$ VERSUS RIB AXIAL COMPRESSIVE STRESS - B=0.40

BIBLIOGRAPHY

1. Richard L. de Neufville, "Influence of geometry on the number of geometry on the number of buckles in cylinders", AIAA Journal, Vol. 3, No. 2, 1965, pp. 364 - 365.

2. V. I. Weingarten, E. J. Morgan, and Paul Seide, "Elastic stability of thin-walled cylindrical and conical shells under axial load", AIAA Journal, Vol. 3, No. 3, 1965, pp. 500 - 505.

3. John C. Yao, "Dynamic stability of cylindrical shells under static and periodic axial radial loads", AIAA Journal, Vol. 1, No. 6, 1963, pp. 1391 - 1396.

4. John C. Yao, "Nonlinear elastic buckling and parametric excitation of a cylinder under axial load", Trans. of the ASME, Vol. 87, 1965, Journal of Applied Mechanics, pp. 109 - 115.

5. M. P. Bieniek, T. C. Fan, and L. M. Lackman, "Dynamic stability of cylindrical shells", AIAA Journal, Vol. 4, No. 3, 1966, pp. 495 - 500.

6. Robert S. Roth and Jerome M. Klosner, "Nonlinear response of cylindrical shells subjected to dynamic axial loads", AIAA Journal, Vol. 2, No. 10, 1964, pp. 1788 - 1794.

7. L. H. Donnell, "A new theory for the buckling of thin cylinders under axial compression and bending", ASME Transactions, Vol. 56, 1934, pp. 795 - 806.

8. Theodore von Kármán and Hsue-Shen Tsien, "The buckling of thin cylindrical shells under axial compression", Journal of the Aeronautical Science, Vol. 8, No. 8, 1941, pp. 303 - 312.

9. L. H. Donnell and C. C. Wan, "Effect of imperfections of the buckling of thin cylinders and columns under axial compression", ASME Transactions, Vol. 72, Journal of Applied Mechanics. 17, 1950, pp. 73 - 88.

10. Joseph Kempner, "Post-buckling behavior of axially compressed circular cylindrical shells", Journal of the Aeronautical Sciences, Vol. 21, 1954, pp. 329 - 335.

11. B. O. Almroth, "Post-buckling behavior of axially compressed circular cylinders", AIAA Journal, Vol. 1, 1963, pp. 630 - 633.

12. Nicholas J. Hoff, Wayne A. Madsen and J. Mayers, "Post-buckling equilibrium of axially compressed circular cylindrical shells", AIAA Journal, Vol. 4, No. 1, 1966, pp. 126 - 133.

13. Masiyi Uemura, "Post-buckling behavior of a circular cylindrical shell", Proc. of the 13th Japan National Congress for Applied Mechanics, 1963, pp. 76 - 85.

14. A. V. Pogorelov, "Post-buckling behavior of cylindrical shells", Part 1. Axial compression, Izdatel'stvo Khar'kovskogo Universiteta Khar'Kov, 1962, NASA TT F-90.

15. Y. Yoshimura, "On the mechanism of buckling of a circular cylindrical shell under axial compression", NASA TM 1390.

16. Robert M. Jones, "Toward a new snap-through buckling criterion for axially compressed circular cylindrical shells", AIAA Journal, Vol. 4, No. 9, 1966, pp. 1526 - 1530.

17. Theodore von Kármán and Hsue-Shen Tsien, "The buckling of spherical shells by external pressure", Journal of the Aeronautical Sciences, Vol. 7, No. 2, 1939, pp. 43 - 50.

18. Herman F. Michielsen, "The behavior of thin cylindrical shells after buckling under axial compression", Journal of the Aeronautical Sciences, Vol. 15, 1948, pp. 738 - 744.

19. D. M. A. Legget, "The buckling of thin cylindrical shells under axial compression", Lecture, read before the Sixth International Congress for Applied Mechanics, 1946.

20. D. M. A. Legget and R. P. N. Jones, "The behavior of a cylindrical shell under axial compression when the buckling load has been exceeded", Aeronautical Research Council, London, R and M 2190, August, 1942.

21. W. F. Thielemann, "On the post-buckling behavior of thin cylindrical shells", NASA TN D-1510, 1962, pp. 203 - 216.

22. V. V. Novozhilov, "Thin shell theory", revised 2nd edition, P. Noordhoff Ltd., Groningen - The Netherlands, p. 91.

23. H. L. Langhaar, "An invariant membrane stress function for shells", Transactions of ASME, Vol. 75, 1953, Journal of Applied Mechanics, pp. 178 - 182.

24. H. L. Langhaar and A. Boresi, "Buckling and post-buckling of elastic shells", NASA TN D-1510, 1962, pp. 115 - 133.

25. H. L. Cox, "The buckling of plates and shells", International Series of Monographs on Aeronautics and Astronautics, Vol. 4, The Macmillan Company, New York, 1963, p. 82.

26. C. H. Tsao, "Large displacement analysis of axially compressed circular cylindrical shells", AIAA Journal, Vol. 3, No. 2, 1965, pp. 351 - 353.

27. W. A. Madsen and N. J. Hoff, "The snap-through and post-buckling equilibrium behavior of circular cylindrical shells

under axial load", Stanford University, Stanford, California, SUDAER 227, April, 1965.

28. Hiroichi Ohira, "Local buckling theory of axially compressed cylinders", Proc. of the 11th Japan National Congress for Applied Mechanics, 1961, pp. 37 - 62.

29. N. J. Hoff, "Low buckling stresses of axially compressed circular cylindrical shells of finite length", Transactions of the ASME, Vol.87, 1965, Journal of Applied Mechanics, pp. 553 - 541.

30. N. J. Hoff and L. W. Rehfield, "Buckling of axially compressed circular cylindrical shells at stresses smaller than the classical critical value", Transactions of the ASME, Vol. 87, 1965, Journal of Applied Mechanics, pp. 542 - 546.

31. B. O. Almroth, A. M. C. Holmes and D. O. Brush, "An experimental study of the buckling of cylinders under axial compression", Proc. of the Society for Experimental Stress Analysis, Vol. 21, No. 2, 1964, pp. 62 - 70.

32. W. F. Thielemann, "New developments in the non-linear theories of buckling of thin cylindrical shells", Proc. of the Durand Centennial Conference, Pergamon Press, London, 1960, pp. 76 - 119.

33. J. S. Kennedy, "Piecewise nearly developable surfaces in the large deformation of very thin shells", Stanford University, Ph.D., 1960, Engineering Mechanics.

34. Octavio G. S. Ricardo, "A report on three series of experiments and the description of a simplified model of the thin wall cylinder and cone buckling mechanism", NASA TN D-1510, 1962, pp. 163 - 172.

35. H. L. Cox, op. cit., p. 102.

36. Hsue-Shen Tsien, "A theory for the buckling of thin shells", Journal of the Aeronautical Sciences, Vol. 9, No. 4, 1942, pp. 373 - 384.

37. Hsue-Shen Tsien, "Lower buckling loads in the non-linear buckling theory for thin shells", Ouart. Appl. Math., Vol. 5, pp. 236 - 237.

38. Y. C. Fung and E. E. Sechler, "Instability of thin elastic shells", Structural Mechanics, Proc. of the first symposium on naval structural mechanics, Pergamon Press, 1960, pp. 115 - 168.

39. Kh. M. Mushtari and K. Z. Galimov, "Non-linear theory of thin elastic shells", Academy of Sciences, USSR, Kazan' Branch, NASA TT F-62, pp. 231 - 232.